REPORT DOCUMENTATION PAGE

Public reporting burden for this collection of information is estimated to average 1 hour per response, including the time for reviewing instructions, searching existing data sources, gathering and maintaining the data needed, and completing and reviewing this collection of information. Send comments regarding this burden estimate or any other aspect of this collection of information, including suggestions for reducing this burden to Department of Defense, Washington Headquarters Services, Directorate for Information Operations and Reports (0704-0188), 1215 Jefferson Davis Highway, Suite 1204, Arlington, VA 22202-4302. Respondents should be aware that notwithstanding any other provision of law, no person shall be subject to any penalty for failing to comply with a collection of information if it does not display a currently valid OMB control number. **PLEASE DO NOT RETURN YOUR FORM TO THE ABOVE ADDRESS.**

1. REPORT DATE *(DD-MM-YYYY)* 17-02-2011	2. REPORT TYPE Technical Paper	3. DATES COVERED *(From - To)*

4. TITLE AND SUBTITLE

The Impact of Pore Structure on Densification Efficiency of 2-D Carbon-Carbon Composites and Its Relationship to Mechanical Properties

5a. CONTRACT NUMBER

5b. GRANT NUMBER

5c. PROGRAM ELEMENT NUMBER

6. AUTHOR(S)
David Daniel Swanson (AFRL/RZSM)

5d. PROJECT NUMBER

5f. WORK UNIT NUMBER
33SP0769

7. PERFORMING ORGANIZATION NAME(S) AND ADDRESS(ES)

Air Force Research Laboratory (AFMC)
AFRL/RZSM
9 Antares Rd.
Edwards AFB CA 93524-7401

8. PERFORMING ORGANIZATION REPORT NUMBER

AFRL-RZ-ED-TP-2011-036

9. SPONSORING / MONITORING AGENCY NAME(S) AND ADDRESS(ES)

Air Force Research Laboratory (AFMC)
AFRL/RZS
5 Pollux Drive
Edwards AFB CA 93524-7048

10. SPONSOR/MONITOR'S ACRONYM(S)

11. SPONSOR/MONITOR'S NUMBER(S)
AFRL-RZ-ED-TP-2011-036

12. DISTRIBUTION / AVAILABILITY STATEMENT

Distribution A: Approved for public release; distribution unlimited (PA #10777).

13. SUPPLEMENTARY NOTES
Master's Thesis for Cal State Pomona

14. ABSTRACT

The purpose of this study is to experimentally determine the efficiency and effectiveness of AFRL's *In-Situ* densification process for 2-D carbon-carbon composites. This method of densification intends to provide competitive thermal and mechanical properties based on minimal matrix porosity and above average skeletal density faster and cheaper than more standard liquid phase carbon-carbon composite densification. In order to validate this hypothesis, small sections of carbon-carbon composite panels were cut out at each stage of fabrication and tested for open porosity and skeletal density. These properties were determined using two proven methods of porosity testing: boiling water immersion and mercury porosimetry. At key stages of processing, mechanical properties were determined to assess the direct correlation between porosity characteristics and matrix strength. Results were gathered for several panels with the same processing conditions to determine possible variation during processing. Once the porosity characteristics and trends were understood for the entire *In-Situ* densification process, the data was correlated with the experimentally determined mechanical properties. The results show that the majority of matrix porosity originates during matrix carbonization, and three cycles of the *In-Situ* densification process can reduce porosity from 25% to 10% by volume with minimal processing time. Skeletal density values between 1.70 and 1.75 g/cc were also obtained. The results also show an increasing trend in the flexural strength, elastic modulus, and interlaminar tensile strength of the composite throughout densification. The fully densified composite demonstrated flexural strength above 23,000 psi and an elastic modulus above 9700 ksi. Also the interlaminar tensile strength of the composite increased from 230 psi after the first densification cycle to nearly 500 psi after the third cycle. The final composite with a known pore structure and high matrix density displays excellent mechanical properties and has tremendous application in the aerospace industry.

15. SUBJECT TERMS

16. SECURITY CLASSIFICATION OF:			17. LIMITATION OF ABSTRACT	18. NUMBER OF PAGES	19a. NAME OF RESPONSIBLE PERSON Maj Veasna Pel
a. REPORT Unclassified	b. ABSTRACT Unclassified	c. THIS PAGE Unclassified	SAR	139	19b. TELEPHONE NUMBER *(include area code)* N/A

The Impact of Pore Structure on Densification Efficiency of 2-D
Carbon-Carbon Composites and Its Relationship to
Mechanical Properties

An Independent Study Report
Presented to the
Faculty of
California State Polytechnic University, Pomona

In Partial Fulfillment
Of the Requirements for the Degree
Master of Science
In
Engineering

By

David Daniel Swanson

March 2011

Signature Page

Independent Study: The Impact of Pore Structure on Densification Efficiency of
                       2-D Carbon-Carbon Composites and Its Relationship to
                       Mechanical Properties

Author: David Daniel Swanson

Date Submitted: _____

Dr. Ali Ahmadi   _____
Ind. Study Committee Chair
Aerospace Engineering Dept.

Dr. Wes Hoffman   _____
Air Force Research Laboratory
Project Advisor

Dr. Steve Jones   _____
Allcomp Inc.

Acknowledgements

It is with my utmost gratitude that I would like to acknowledge the hard work and dedication of several individuals who greatly assisted me while working on this project. This thesis would not have been possible first of all without the assistance of my advisor and research supervisor, Dr. Wes Hoffman. Also I would like to thank Dr. Steve Jones who spent a great amount of time helping me further understand this research topic. I would also like to acknowledge and thank Allcomp, Inc. for supplying the materials for all the tests in this study. I am also very appreciative to all those working in the Material Applications Branch at the Air Force Research Laboratory at Edwards Air Force Base and everyone from Allcomp, Inc. who assisted in other ways throughout this effort.

-David Swanson

Abstract

The purpose of this study is to experimentally determine the efficiency and effectiveness of AFRL's *In-Situ* densification process for 2-D carbon-carbon composites. This method of densification intends to provide competitive thermal and mechanical properties based on minimal matrix porosity and above average skeletal density faster and cheaper than more standard liquid phase carbon-carbon composite densification. In order to validate this hypothesis, small sections of carbon-carbon composite panels were cut out at each stage of fabrication and tested for open porosity and skeletal density. These properties were determined using two proven methods of porosity testing: boiling water immersion and mercury porosimetry. At key stages of processing, mechanical properties were determined to assess the direct correlation between porosity characteristics and matrix strength. Results were gathered for several panels with the same processing conditions to determine possible variation during processing. Once the porosity characteristics and trends were understood for the entire *In-Situ* densification process, the data was correlated with the experimentally determined mechanical properties. The results show that the majority of matrix porosity originates during matrix carbonization, and three cycles of the *In-Situ* densification process can reduce porosity from 25% to 10% by volume with minimal processing time. Skeletal density values between 1.70 and 1.75 g/cc were also obtained. The results also show an increasing trend in the flexural strength, elastic modulus, and interlaminar tensile strength of the composite throughout densification. The fully densified composite demonstrated flexural strength above 23,000 psi and an elastic modulus above 9700 ksi. Also the interlaminar tensile strength of the composite increased from 230 psi after the first densification cycle to nearly 500 psi after the third cycle. The final composite with a known pore structure and high matrix density displays excellent mechanical properties and has tremendous application in the aerospace industry.

Table of Contents

List of Figures

Appendix A

Appendix B

Appendix C

Appendix D

List of Tables

Appendix C

Appendix D

List of Equations

List of Abbreviations

2-D	Two Dimensional
3-D	Three Dimensional
AFRL	Air Force Research Laboratory
C	Celsius
cc	Cubic Centimeters
CVD	Chemical Vapor Deposition
LoPIC	Low Pressure-Impregnation-Carbonization
g	Grams
H_2O	Water
Hg	Mercury
HiPIC	High Pressure-Impregnation-Carbonization
HT	Heat Treatment
ksi	Thousand Pounds per Square Inch
mL	Milliliter
nm	Nanometer
psi	Pounds per Square Inch
SEM	Scanning Electron Microscopy
mm	Millimeter
μm	Micrometer

1. Introduction

1.1 History of Carbon-Carbon Composites

As technology advances in the aerospace industry, progress is often limited by the materials available. Hypersonic vehicles must withstand extreme temperatures for longer periods of time, launch vehicles must be lighter to increase range and efficiency, and commercial airlines are fighting to stay in business by keeping costs low. Composite materials provide the answer to all of these difficult and complex problems. They are lighter than most metals, and thus have very high specific strength, and in addition they can provide a tailored mix of properties for a specific need. As the demand for these materials grows, new and efficient methods of fabrication are being developed to bring costs down, making composites readily available for many different uses.

Composite materials are generally broken down into four different categories: polymer matrix composites, metal matrix composites, ceramic matrix composites, and carbon-carbon composites [18]. Each of these different materials have advantages and unique properties, but the high strength and exceptional thermal stability of carbon-carbon composites make them ideal for structural aerospace applications [3,5,18].

Carbon-carbon composites can withstand temperatures well above 3000° C in inert environments [5,18], and they will not fracture when subjected to sudden heating and cooling. Because of these unique attributes, they are extremely valuable for the aerospace industry, specifically high temperature applications, such as hypersonic vehicle leading edges, heat shielding for atmospheric re-entry, rocket nozzles, and exit cones [5,18].

These composites are also very light weight and have extremely low density when compared to metals with similar performance. The densities of these composites range from 1.5 g/cc to almost 2 g/cc. They are also used for high temperature insulation, requiring even lower density values. Aluminum, which is quickly being surpassed by composites as the most popular material for aircraft skin, has a density of 2.7 g/cc. Titanium alloys which can provide very high strength compared to other metals can be as dense as 4.4 g/cc. High strength composites, specifically carbon-carbon, are very effective and light weight substitutes for high strength, durable metals [18].

Another benefit of carbon-carbon composites is their exceptional mechanical properties. The fiber reinforcement provides higher strength than most ceramic materials while also protecting them from brittle fracture. Carbon-carbon composites also have a very high fracture toughness which causes them to be very resistant to crack propagation while their high fatigue tolerance and resistance to creep give these composites an almost infinite service life [18]. However, carbon-carbon composite performance at high temperatures is the most important mechanical property. They cannot only maintain their exceptional strength and stiffness in inert environments to temperatures in excess of 3000° C, but their properties will actually improve.

The thermal properties of carbon-carbon composites are also advantageous in many applications. Some carbonaceous materials have very high thermal conductivity, which allows them to dissipate heat efficiently. However, this property is dependent on the orientation of the fibers, as the conductivity values are much higher in the fiber direction. For this reason these composites can also be designed as heat shields with good insulating properties [18].

Carbon-carbon composites have two main weaknesses. The first is their poor oxidation resistance [7]. They are not able to maintain strength or thermal stability when exposed to harsh oxidative environments for long periods of time [18]. Because of this they require oxidation resistant coatings unless used only in inert environments. This is an unfortunate problem because creating and applying these coatings adds more time and expense to the fabrication process.

The second weakness is delamination of the various layers in applications requiring 2-D composites. This is caused by interlaminar tensile and shear stresses. Diagrams of delamination due to tensile and shear stresses are shown below.
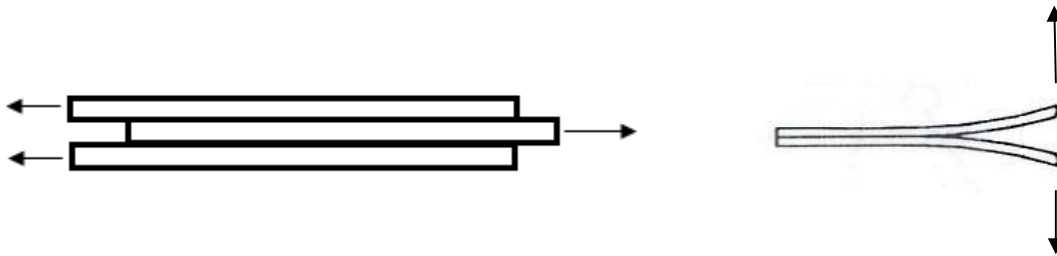
Figure 1: Delamination of composite layers due to tensile and shear stresses.

This results from the lack of fiber support in all directions. The properties perpendicular to the fibers in a 2-D composite are entirely controlled by the matrix material [2,7]. This material while able to provide rigidity, holding the fibers in place has poor strength when not reinforced [18]. While fiber strength can easily exceed that of high strength metals, 2-D composites will often delaminate from stresses of 100-300 psi. As a result when high stress is applied in the direction perpendicular to the fibers, the composite will delaminate and break apart. Strengthening the matrix material by eliminating impurities and voids is one of the main goals of this study and can greatly improve interlaminar properties [2,4,9].

1.2 Carbon-Carbon Composite Fabrication and Processing

A carbon-carbon composite, as the name suggests, requires that both of its main components consist of carbon. These components are the reinforcing carbon fibers and the carbon matrix material. The first step in the fabrication of a carbon-carbon composite is to generate a preform of carbon fibers. The preform is simply defined as the shape and distribution of the reinforcement in the composite, or how the fibers are arranged [3]. There are a wide variety of carbon fiber architectures from unidirectional preforms to an almost unlimited number of orientations. Of course, as the preform becomes more and more complex, the manufacturing becomes more costly and more time consuming. Because of this, the simplest preforms are ideal if the application permits [8].

The two most common arrangements of fibers are 2-dimensional and 3-dimensional preforms, with some instances of unidirectional as well as 4-D or more. Examples of these different types of composites are shown below.

1-D   2-D   3-D   n-D
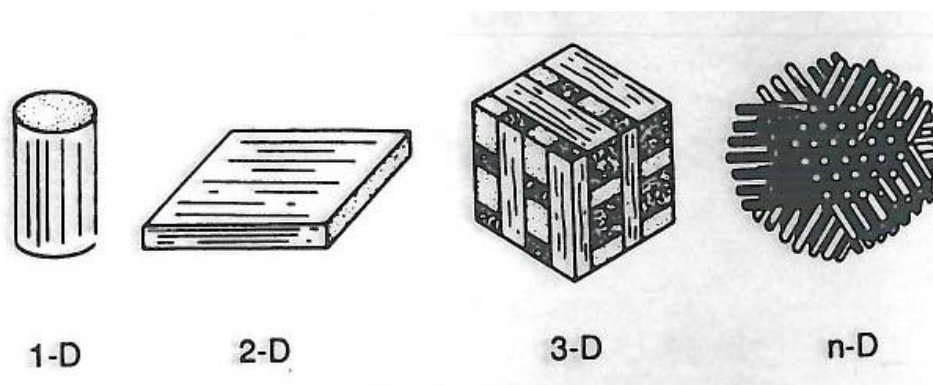
Figure 2: Examples of different fiber orientations [3].

Uniaxial or unidirectional composites are preferred in some cases for excellent reinforcement in a single direction along the fibers, and the properties in that direction will be

very consistent and predictable. They can also be used for high thermal conductivity in one

direction. 2-D composites are more often preferred because they provide stable properties in two

directions which are desired for most applications, such as structural panels, disc brakes, rotors,

and beams. One of the biggest problems with both unidirectional and 2-D composite structures

is the very low strength in the direction perpendicular to the fibers. Because there are no

reinforcing components in this direction, the interlaminar properties are governed solely by the

matrix material as was mentioned previously. Despite this disadvantage 2-D composites are still

widely used; however, their use is limited to applications where they will not see severe

interlaminar stress. This problem can be solved by creating 3-D structures, but this involves

much more complex fabrication methods [8]. Below are figures of special 3-D fabric

architecture, which help to eliminate interlaminar strength problems.
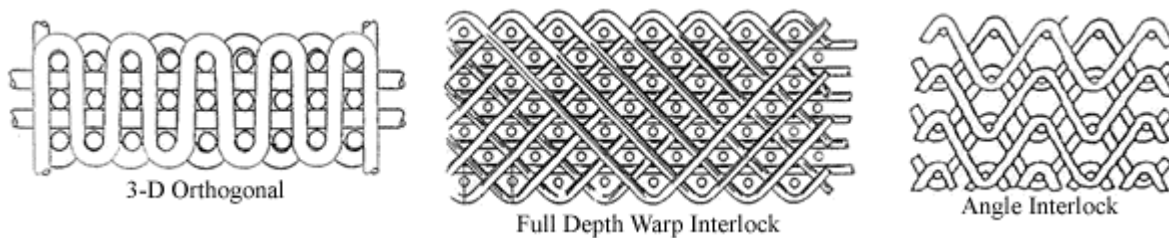
Figure 3: Different types of 3-D fiber architectures for complex shapes minimizing interlaminar strength problems [22].

In 2-D composite fabrication, which is the focus of this study, the fibers are woven

together on a plane to create a flat fabric with the fibers oriented in only two directions.

Common types of weaves include plain weaves, twill weaves, and satin weaves. These different

types of weaves are shown below in Figure 4.
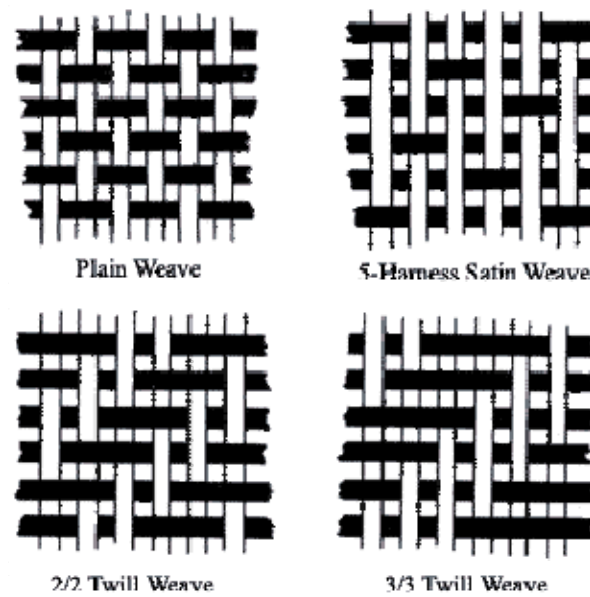
Figure 4: Comparison of common 2-D fabric weaves for composite construction [22].

A plain weave consists of a simple mesh of fiber bundles following a consistent pattern in two perpendicular directions. Each bundle overlaps the adjacent bundle in the perpendicular direction without skipping more than one bundle. The satin weave is slightly more complex. Each fiber bundle skips a certain number of perpendicular bundles before weaving back into the fabric. This results in a smoother surface and is more conducive to molding and shaping for specific structural applications [8].

Once the 2-D fiber weave is chosen, initial matrix material is usually added to the fabric to allow for better layer consolidation and eventually to add rigidity. This is called pre-impregnation, or prepregging. The fabric is then cut, stacked, and consolidated to create the preform. For carbon-carbon composites the initial matrix material is some type of hydrocarbon which can be broken down at high temperatures leaving just carbon. This can be a thermosetting resin with a relatively high carbon yield when heated, or a thermoplastic pitch [3].

Thermosetting resins are very easy to work with because they have low viscosities before curing allowing them to easily coat the fabric laminates. The matrix precursor must have a viscosity which is low enough to easily wick into the fabric, yet it must also give a high enough carbon yield. Finding a balance between these two qualities is very important and affects the type of precursor chosen [10]. In some instances epoxy is chosen over phenolic resin because of its excellent adhesion to the fiber reinforcement and its small amount of shrinkage at higher temperatures. However, phenolic resin specifically is known to have a carbon yield greater than other resins, and it can also withstand higher temperatures. In addition to these benefits, phenolic resin is also inexpensive [6]. For these reasons phenolic resin is an ideal prepreg material for carbon-carbon composites prior to densification. The char yield after carbonization is usually less than most pitches, but the ease of manufacturing often compensates for this disadvantage [3,5].

Pitch is often used as a densification matrix precursor, but can also be added to dry fabric as well. It can be applied as a prepreg or as a dry powder for hot press consolidation. Examples of composites requiring pitch for the prepreg include those with very high thermal conductivity requirements, or very high performance, expensive composites often used in high stress environments. Pitch in its most generic form comes from the distillation of either coal tar or petroleum. It contains many different types of hydrocarbons, many of which have not been identified [2]. Because these various compounds have a wide variety of molecular composition and a range of molecular weights, certain thermal properties vary over a large range of temperatures, and are difficult to predict [8]. Pitch can be synthesized, resulting in a much more pure and stable substance, which is also easier to work with. This type of pitch can also generate much less off gassing emissions, causing less of an effect on the composite structure during

processing [14]. When heated, causing a specific thermal reaction to occur, a mesophase can form. This result depends on the specific temperatures and the exact type of pitch being used, but it can retain properties of both a solid and a liquid. This liquid crystal material can flow like a semi-viscous liquid, yet it can retain the structural stability of a solid due to its crystal structure [8,11]. The carbon yield of mesophase can reach as high as 90% [11].

The process of prepregging can be done by several different methods. It can be done mechanically on a large scale or more simply by coating the fabric by means of a brush or a roller. The fabric is typically prepregged before it is cut to its specified dimensions. It is laid out and coated with a substance usually containing some type of resin and a binder mixed with a solvent. Once the fabric is prepregged, it is either left out to air dry or heated to expedite the process. The prepregged fabric is then cut to the required size.

Once the fabric is prepregged and dried, it is stacked and consolidated. For a 2-D composite, this is typically done on a hot press or in an autoclave. The temperature is increased to allow the prepregged fabric plies to bond to one another, and pressure is applied to ensure effective consolidation of the layers. Alternatives to these standard methods of consolidation include vacuum bagging or inserting the fabric into a tool. Both of these methods are usually for complex shapes and require specially made parts. The method of vacuum bagging involves applying a vacuum over the prepregged fabric while it is placed onto a mold. The plies are then consolidated, and the preform maintains its shape. Alternatively, a special tool can be made to constrain the fabric for consolidation.

For certain applications, the fabric is not prepregged. A dry preform can be placed into a pressure chamber along with excess pitch. The pitch becomes less viscous when heated and is able to be forced into the preform with pressure. As the pitch decomposes and is carbonized, the

off-gassing hydrogen is released out of the chamber [18]. Powder prepreg substances can be used as well and can be sprinkled into the preform in between the plies. This can then be heated and consolidated either in a hot press for a 2-D panel, or heated in an oven with applied pressure.

The consolidated preform is then heated at a low temperature of about 100°-150° C to cure and harden the matrix, allowing the composite to maintain its shape. Following the initial curing there are a series of heat treatments at incrementally increasing temperatures. First the cured composite is post-cured to further stabilize the matrix, usually at slightly higher temperatures between 200° C and 250° C. The next step is pyrolysis or carbonization. The composite is brought up to a temperature where the precursor matrix material will begin to breakdown only leaving its carbon backbone. This usually occurs at temperatures <1000º C. The heating rate for carbonization is very slow and is usually done over several increments of increasing temperature in order to minimize damage to the composite. A final heat treatment is then accomplished to restructure and densify the matrix material [3]. This usually occurs between 1800º C and 2400º C depending on the matrix material. When these temperatures are reached, the molecules can realign, forming a graphite-like structure. This process, known as graphitization, can improve several different properties of the composite, such as thermal and electrical conductivity, stiffness, modulus of elasticity, and others.

During matrix carbonization, the matrix material becomes denser as a result of gas evolution and shrinkage, and for a 2-D panel, the overall composite thickness will decrease. However, the composite cannot shrink in the fiber direction. Because the composite size and shape are restrained by the fiber bundles, as the matrix carbonizes and shrinks in size, it begins to separate and crack, opening up voids. Due to the formation of large open pores, the matrix can

then be further densified with the addition of more matrix material, optimizing the properties and performance of the composite [12,19].

1.3 Composite Densification

There are two main types of composite densification methods. The first is gas infiltration, also known as chemical vapor deposition (CVD), and the second is liquid impregnation, which can be done at low or high pressures. These liquid phase densification methods are referred to as LoPIC and HiPIC: low and high pressure-impregnation-carbonization [3,18].

1.3.1 Chemical Vapor Deposition (CVD)

Chemical vapor deposition is accomplished by "cracking" a hydrocarbon gas inside a fiber preform. The preform is first put inside a chamber and placed under a vacuum (typically millitorr range). The temperature is increased to approximately 1100° C. The chamber is then brought up to, and maintained at, 5-25 Torr using a hydrocarbon gas. Gas is continuously pumped into the chamber, depositing carbon within the pores of the composite. The efficiency of this method depends greatly on what precursor gas is chosen, the geometry of the composite, and the process parameters such as the temperature and pressure. Two to four cycles are usually required, and surface machining is often necessary to re-open surface porosity between cycles. This process is also very wasteful in terms of gas quantity in order to reach an acceptable carbon yield. It can take up to 650 hours to reach the required density [18].

1.3.2 Liquid Phase Densification

The second densification method, liquid impregnation, is accomplished using liquid precursor materials, which must be inserted into the preform often requiring pressure. The first type of liquid impregnation is LoPIC. This process can be done using either resin or pitch; however, for carbon-carbon composites LoPIC is usually done with pitch and uses pressures around 1500 psi. Densification by LoPIC is often done by submerging the composite in a resin or pitch bath, sealing the tank, and then applying external pressure forcing the liquid to fill the voids in the matrix. This method is often used on thicker parts due to its ability to force matrix material deep beyond the surface.

A similar method to LoPIC is pitch pot densification with a long soaking time. This is done at low pressures of about 150 psi, but can be very time consuming. This method is often used on thinner parts because there is very little pressure involved. The composite is then carbonized and heat-treated at high temperatures. This process is repeated until the required density is reached [18].

The high pressure variation to the liquid phase densification method, or HiPIC, is used to create very high density carbon-carbon composites. For this process pitch is applied to the preform and relies on higher pressures to force the viscous liquid into the part. The temperatures are raised to allow the pitch to flow more smoothly, but this process often requires pressures between 10 and 15 ksi [18]. As the pressure forces the pitch into the part, the temperature is raised further allowing the pitch to break down leaving carbon within the pores of the composite. The higher the pressure applied during this process, the higher the carbon yield. Usually about 4-5 HiPIC densification cycles are needed to reach the maximum density for carbon-carbon composite applications [3].

Each variation of liquid phase processing can be very costly and time consuming. Due to the rapid emission of volatile gases, if a sample is heated too quickly, the off-gassing can cause swelling and expansion within the part. This can distort the original shape, fracture the composite, or even push out matrix material, resulting in large needle-shaped pores. As a result, the heating rate in most liquid phase carbon-carbon composite fabrication methods is very slow to allow emissions to safely escape and pores to effectively be filled. These issues in addition to the numerous cycles needed to reach sufficient density create a very expensive and lengthy process [14].

1.3.3 *In-Situ* Densification Variation

A variation of the standard liquid phase process is the *In-Situ* carbon-carbon composite densification process. Developed by the Air Force Research Laboratory at Edwards Air Force Base and currently being licensed exclusively by Allcomp, Inc., located in City of Industry, CA, the *In-Situ* process seeks to solve some of the biggest problems associated with current composite development, i.e. fabrication time and cost. A standard high pressure impregnation process can take between three to six months to finish all the required densification cycles. Also because of the high pressure equipment involved, this process can become very expensive. As a result, much of the high performance, high density carbon-carbon composite demand comes only from government defense programs and large aerospace corporations [14]. With some critical changes in the manufacturing process, the *In-Situ* procedure can decrease these drawbacks.

The main difference between the *In-Situ* process and the standard pressure-impregnation-carbonization is how the precursor matrix material is placed in the preform. Because of the high

viscosity of pitch, elevated temperature and pressure are typically required to force it into the part, as is the case with pitch pot, LoPIC, and HiPIC densification methods. The *In-Situ* process uses a pre-pitch hydrocarbon feedstock plus a catalyst, which due to their surface tension and wettability are drawn into the composite. By raising the temperature to initiate a reaction, this feedstock is converted to pitch once it is already in the part. It is then carbonized. The precursor substances that are initially added to the preform are polyaromatic hydrocarbons, such as naphthalene, along with a catalyst, such as aluminum chloride. When these substances melt and wick into the part, a reaction occurs and mesophase pitch results. This process requires no external pressure to completely fill the composite with pitch. Several cycles are still required to maximize matrix density; however, cycle times are relatively short resulting in a processing time of only a few weeks, and the required equipment is inexpensive.

The main goal of densification is to eliminate open pores and cracks within the carbon matrix and preform. Because the *In-Situ* process converts the precursor material to pitch already within the part, new pores and micro cracks can form from gasses escaping during densification in an inconsistent pattern. This problem is magnified because there is no pressure applied to continually force material into opening voids. Therefore the resulting porosity of the composite becomes a very serious issue affecting the overall efficiency of the process. In standard liquid phase processing this problem can be partially avoided because elevated pressure helps keep escaping gas bubbles smaller. In order to create optimum pore structure and allow for maximum densification within the *In-Situ* process, each stage of the process must be carefully considered.

1.4 Previous Research

The study of the fabrication of carbon-carbon composites has been ongoing for four decades and has included research into various aspects of the process. There are extensive reference materials covering everything from types of carbon fibers and their different advantages [3,6,18] to advanced oxidation resistant coatings for application in harsh environments [3,8]. There is also literature describing densification methods, which will typically include the final density results of the composite for comparison to the competition [12,19,20]. General explanations of typical composite densification methods, such as CVD, LoPIC, and HiPIC will be mentioned in almost every book on carbon-carbon composites [3,18], but literature focusing on unique variations to the densification process is not as common. This is often due to patents and licenses held for certain procedures. There are a few reports written concerning the *In-Situ* densification process, but all relevant data have come out of the same materials group at the Air Force Research Lab where the process was developed.

Densification of carbon-carbon composites is often looked at as one process. Initial data are given and then it is compared to final results after a certain number of cycles. In some cases the efficiency of each cycle is broken down showing a trend of increasing density and the retention of more carbon matrix material [12]. Research has modeled the decrease in porosity over several densification cycles, demonstrating general efficiency of pitch densification [14,19]. This type of research is very valuable to this study as it gives a baseline for comparison. Pore size distributions are easily found in literature as well. Improvements are easily seen in distribution graphs when comparing a densified sample to an undensified sample [15,16].

The study of porosity measurement techniques is an entirely separate field, and often targets different materials other than fabricated composites. Extensive local research has been

done at the Propulsion Directorate of the Air Force Research Lab on carbon-carbon composites comparing several prominent porosity measurement techniques including x-ray, mercury porosimetry, water immersion, and others [20]. However, this research has not covered samples part way through a densification process. There are also ASTM standards for many different types of porosity and density test methods focusing on many different types of porous materials [17,20], such as concrete, plastics, rubbers, and laminated materials.

The shortcomings in the previous research are not with one of these individual topics, but rather with combining these topics into a concise analysis of carbon-carbon composite densification. This current study attempts to analyze the carbon-carbon composite densification efficiency of a unique method based on decreasing open porosity and increasing skeletal density. This study also supplies detailed analysis of the effect of pitch densification and heat treatment of the composite at each step of the process, so that a much better understanding of overall trends can be achieved. The thorough evaluation of each step in a densification process by multiple test methods is lacking in literature currently available.

Correlations of composite porosity and matrix strength have been well-documented in many sources. This is one area where there is much confidence. There is a general increasing trend in matrix strength when voids are filled and density increases [2]. This study intends to expand on this research by comparing the results of two types of mechanical tests and determining possible changes in the correlation at different times in the densification process.

1.5 Porosity Test Methods

There are various methods to determine porosity. These include but are not limited to X-ray, vacuum immersion, water immersion, gas pycnometry, scanning-tunneling microscopy, scanning electron microscopy, adsorption and desorption of gasses, mercury porosimetry, and others. For this study, water immersion and mercury porosimetry were chosen.

1.5.1 Water Immersion

Water immersion, specifically boiling water immersion, is a very simple but effective method of determining the percentage of open void space within a composite sample. In fact the test method simplicity and inexpensive equipment were among the main reasons for choosing this method of obtaining porosity and skeletal density. The data are determined by first weighing a dry sample, and then immersing it in water. Once the sample is completely saturated, it is weighed while submerged to determine the "wet weight". This is a measure of its skeletal density, or "true" density. This density is then compared with the bulk density measured at the beginning of the test, and the amount of open porosity within the sample is determined [16,17]. The equation that compares dry weight to wet weight resulting in skeletal density of the sample is shown below:

$$\frac{W_{dry}}{W_{dry} - W_{wet}} * \rho_{water} = \rho_{skeletal} \qquad \textbf{(Equ. 1)}$$

This provides the density of the actual material present, excluding open voids and air pockets. From this point the porosity percentage can be calculated using the following equation:

$$\frac{\rho_{skeletal} - \rho_{bulk}}{\rho_{skeletal}} * 100 = \% \; porosity \quad \textbf{(Equ. 2)}$$

From these two simple equations much insight can be gained concerning the matrix material of the carbon-carbon composite sample [17]. There are also certain downfalls associated with this porosity test method. Because no external pressure is applied, it is often assumed that the water does not always reach the smallest pores. This disadvantage was ignored for this study, as past internal research has shown that the results are comparable to other proven methods for this type of material [20]. Another disadvantage with boiling water immersion is the inability to reach any closed porosity. Certain methods which utilize highly advanced x-ray and microscopy procedures are capable of getting accurate open and closed porosity percentages from a sample, whereas water immersion cannot. However, for this study the methods capable of determining such thorough porosity results were not options based on available equipment and expertise. Rather assumptions were made concerning the small effect that closed porosity likely had on this material and its properties.

1.5.2 Mercury Porosimetry

The second test method chosen for this study was mercury porosimetry. This is usually the method of choice when total pore distribution is desired. It is capable of analyzing the entire range of pore sizes above 3 nm [1,20]. Advantages of this test method include the fact that it is a relatively simple process, the equipment is available for testing, and it is not very time consuming. There have been several documented porosity test comparisons which show the close correlation between mercury porosimetry and other proven test methods. This method should be very effective in verifying the accuracy of the water immersion results, and also it will

provide other porosity related measurements which cannot be easily determined by other

techniques [20].

Mercury porosimetry not only determines porosity of a substance but also porosity

related parameters such as average pore-size, pore distribution, and total pore volume. These

results are determined by the intrusion of a non-wetting fluid, such as mercury, which is forced

into the part by high external pressure. Porosity data can be determined because there is a

specific relationship between the pressure applied to a non-wetting fluid and the pore-size that

the fluid is able to fill. This relationship is based on the governing law of liquid being forced

into small spaces. The proportionality equation, known as the Washburn equation, is shown

below:

$$D = \left(\frac{1}{P}\right) 4\gamma \cos(\theta) \quad \textbf{(Equ. 3)}$$

where D = pore diameter, P = applied pressure, γ = surface tension of mercury, and θ = contact

angle between the mercury and the sample. Although an assumption of this relationship is that

pore shape is cylindrical, the porosimeter provides average porosity data which are still accurate

and reliable for as an average over the entire sample [16]. The precision and accuracy of pore

data are determined by how well the device can detect small changes in the level of mercury as it

is forced into the tiny void space within the sample. The particular penetrometer (sample holder)

used for this application can detect changes of 0.1 microliters of mercury resulting in very

accurate results [1,20].

1.6 Mechanical Test Methods

Composite materials can be tested for mechanical properties in a variety of different ways. The method is chosen based on the specific property desired. Mechanical properties encompass any structural characteristic of the material on a microscopic and macroscopic level which determines how it will behave under an applied load. These characteristics include tensile strength, compressive strength, shear strength, hardness, toughness, elasticity, plasticity, brittleness and many more. The desired characteristics of the carbon-carbon composites used in this study were those most closely related to the properties of the matrix material.

1.6.1 Flexure Tests

Tensile tests in which the sample is pulled apart in the direction of the fibers until failure occurs are very common tests, but the results are solely dependent on the strength of the fibers. Flexure tests, such as three and four point bend tests, also rely greatly on the strength of the fibers; however, the matrix material also plays a large role in how effectively the load is distributed to the fibers. For this reason the four point bend test was chosen as a method of testing mechanical properties to determine their correlation to matrix porosity.

The two most important results obtained by this test are the flexural strength and the elastic modulus. The characteristics of the matrix play a large role in both of these properties, which can also have a large effect on the overall performance of the composite.

The flexural strength equation takes into account the dimension of the fixture and the dimensions of the sample so the final result can be compared to others with different dimensions

and test methods. It also takes into account the maximum observed load resulting in the flexural strength at failure. The equation is shown below,

$$S = \frac{PL}{bd^2} \quad \textbf{(Equ. 4)}$$

where S = Flexural Strength, L = Support Span, b = width of beam, and d = depth of the beam.

Elastic Modulus is obtained by the same flexure test. However, the equation takes into account the slope of the elastic region in the stress vs. strain curve. The equation for elastic modulus is shown below,

$$E = \frac{0.21L^3 m}{bd^3} \quad \textbf{(Equ.5)}$$

where E = elastic Modulus, m = slope of initial linear portion of stress vs. strain curve, b = width of beam, and d = depth of beam.

In order to determine flexural strength, the two common test methods are four point bend and three point bend. The three point bend test is fairly accurate, but the single point load creates a stress concentration where the load is applied. Because of this the sample will often break too soon at the point of contact with the load fixture, resulting in inaccurate measurements. Four point bend applies the load at two points, which evenly distributes the stress throughout the sample and reduces the severity of any stress concentrations. For this reason the four point bend test method was chosen for this study. Below are two diagrams demonstrating the different test fixtures for the three and four point bend tests.
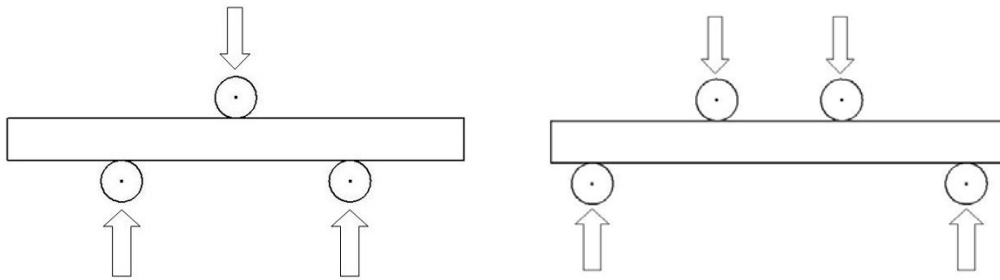
Figure 5: Diagrams of three and four point bend tests.

1.6.2 Interlaminar Tensile Tests

A second mechanical test method chosen for this study was the interlaminar tensile test. Because the composites in question are 2-D, the fibers are woven together in a fabric with no fiber reinforcement between the fabric layers. This means that strength of the bond between these layers is determined solely by the matrix strength and the quality of the bond that it makes with the fibers. These interlaminar, or flatwise, tensile tests were conducted to determine the strength of the composite matrix between plies. This is one of the most critical weaknesses of 2-D composites and is greatly influenced by matrix porosity and density. This test was chosen to determine the correlation between the porosity of the composite and the strength of the carbon matrix.

This test is conducted by inserting the composite flatwise between to tensile fixtures, pulling the composite apart, and measuring the load at failure. The following equation is used to determine the maximum interlaminar tensile strength:

$$S = \frac{P}{A} \quad \textbf{(Equ.6)}$$

where S = interlaminar strength, P = max load applied, A = cross sectional area. Typically, the

data acquisition program can also yield load vs. deflection curves. The maximum deflection at

the point where the composite delaminates correlates with the brittleness and stiffness of the

matrix. The figure below shows a diagram of the interlaminar tensile test.
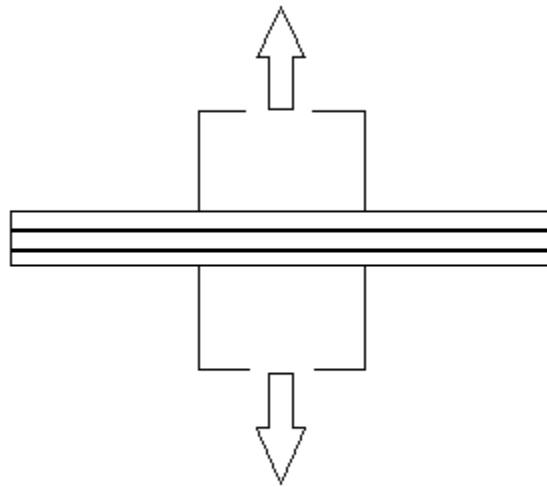
Figure 6: Diagram of interlaminar tensile test.

2. Experimental Procedures

This study of the porosity of carbon-carbon composites and the efficiency of the *In-Situ* densification process was conducted in two sections. The first section, Task 1, focused on the densification process specifically. A 2-D carbon-carbon composite panel was densified according to the AFRL *In-Situ* process described previously, and porosity tests were conducted throughout densification. Samples were tested after each of three densification cycles by pitch impregnation as well as after three heat treatment cycles which preceded each densification. This resulted in six steps throughout the densification process after which samples were tested. The purpose of these tests was to determine the skeletal density, porosity percentage, and pore-size distribution at each stage of densification as well as any trends that may be apparent.

Task II expanded beyond Task I by analyzing panels earlier in the fabrication process. Two panels were tested immediately following curing to determine the preliminary porosity characteristics. As the panels reached the densification stages, porosity tests using water immersion and mercury porosimetry were repeated to verify Task 1 testing. Also flexure tests and interlaminar tensile strength tests were conducted at crucial points in the fabrication process to determine the correlation between matrix porosity and mechanical properties of the composite. Porosity testing in Task 2 occurred after the same six densification steps as in Task 1 but also after two preliminary steps prior to densification. The mechanical tests were conducted following the second and third heat treatment and the third pitch impregnation cycle during densification.

2.1 Materials Used

The panels to be tested in this study all began from 2-D carbon fiber preforms. The preforms consisted of a five harness satin weave made of T300 carbon fibers. The material chosen to pre-impregnate, or prepreg, the 2-D fabric was phenolic resin. Task 1 focused on an already fabricated 12" X 12" panel prepregged by Allcomp's standard process of painting the fabric with resin and heating the stacked fabric under constant load once they dried. Task 2 focused on two 12" X 12" panels that were prepregged commercially by JD Lincoln's mass production process. Once these panels were prepregged with phenolic resin and carbonized, they were densified with a pitch matrix according to the AFRL *In-Situ* method, adding strength, and densifying the composite.

2.2 Analysis Equipment

Several pieces of equipment were used throughout this study for porosity tests, mechanical tests, material fabrication, optical microscopy, and other purposes as well. Once panels were fabricated, they were cut into sections for various tests using a standard floor mounted band-saw. Samples were weighed on several occasions before and after testing using several different sized Mettler DeltaRange lab balances accurate to one milligram. Porosity measurements were obtained by mercury porosimetry using a Micromeritics Autopore IV Porosimeter. Boiling water immersion porosity tests utilized a Precision Scientific vacuum oven, glass beakers, glass stir bars, small metal wire, distilled water, one IR 6100 infrared stirring hot plate, and one 1000 watt Corning stirring hot plate. Both flexure and interlaminar tensile tests were conducted using a Tinius Olsen H100K-S 100 kN tensile test machine. Custom

fixtures were used to mount the samples to the machine, a 10 kN load cell was used to measure

the resistance, and an MTS compression extensometer was used to measure mid-span deflection

of the flexure samples. In order to photograph the surface to visualize the porosity, small

samples were mounted in epoxy and polished to a high gloss. Sanding was done using a Buehler

Ecomet 3 variable speed grinder-polisher. Microstructure pictures were then obtained using a

Leica MEF4M optical microscope and a Diagnostic Instruments Spot Flex camera.

2.3 Processing Parameters and Sample Preparation

Panel 12656-4 tested in Task 1 was received after it had been carbonized and

initially heat-treated. Prior to this, the resin impregnated preform was cured at about 200° C to

ensure that it held its shape. The cured preform was then post-cured by heating in a furnace at a

slightly higher temperature than the initial cure.   At this point the temperature was raised

progressively higher until carbonization of the resin was complete. The panel was then heat-

treated to 1650° C to further convert the matrix material that was already present within the

composite. This also caused matrix shrinking and cracking, which opened up further pore space

to be filled later [12,19]. These initial processing steps were done at another location, and were

not part of the analysis and testing for Task 1.

The panel was then ready for densification. At this point all additional processing was

performed by Allcomp at their production facility at the Air Force Research Lab at Edwards Air

Force Base. Due to the proprietary nature of this process, details will not be given. In general,

three densification cycles by pitch impregnation were performed within a 20" reactor according

to the *In-Situ* process using a hydrocarbon feedstock and a catalyst. Two additional heat

treatments were done in between the three impregnation steps to further densify the matrix. All

heat treatment cycles took place in various environmentally controlled ovens.

In order to test the panel, a one square inch section was cut out and removed at each stage

of the process. Each square was then tested and compared to each of the other sections. Once

these tests were conducted, trends could be generated, and the results could show the

effectiveness of each densification cycle. The first section was cut out immediately after the

panel was received after its initial heat treatment. There were then three cycles of densification

by pitch impregnation, separated by two additional heat treatments. This process resulted in

cutting out six square sections. Each section will be divided into pieces for each type of porosity

test. The layout is shown in the figure below:
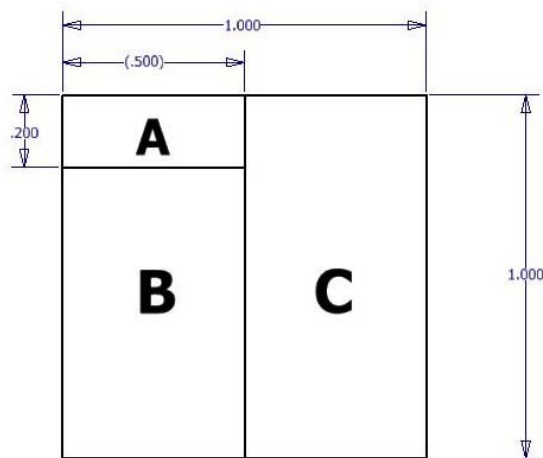
Figure 7: 1" X 1" test specimen cut from carbon-carbon panel at each stage of processing.

Section A was used for microstructural analysis by optical microscopy, section C was used for water immersion followed by Hg porosimetry, and section B was used for back-up water immersion and additional Hg porosimetry.

Panels 12680 and 12681 tested in Task 2 were received after the prepreg and cure. All the subsequent carbonization and densification steps for each panel were also performed by Allcomp at their production facility. Post cure, carbonization, and high temperature heat treatment followed the general temperature requirements for typical carbon-carbon processing, although the temperature requirement never exceeded 1650° C. At this point three densification cycles occurred in the same manner as in Task 1.

The two 12" X 12" panels were divided up into small sections, similar to Task 1, but starting earlier in the process after the composite was cured. Small pieces were cut out for porosity tests, flexure tests, and interlaminar tensile tests. The layout of the Task 2 panels is shown in Figure 8 below. These pieces were periodically removed from the panel following the appropriate stage of processing.
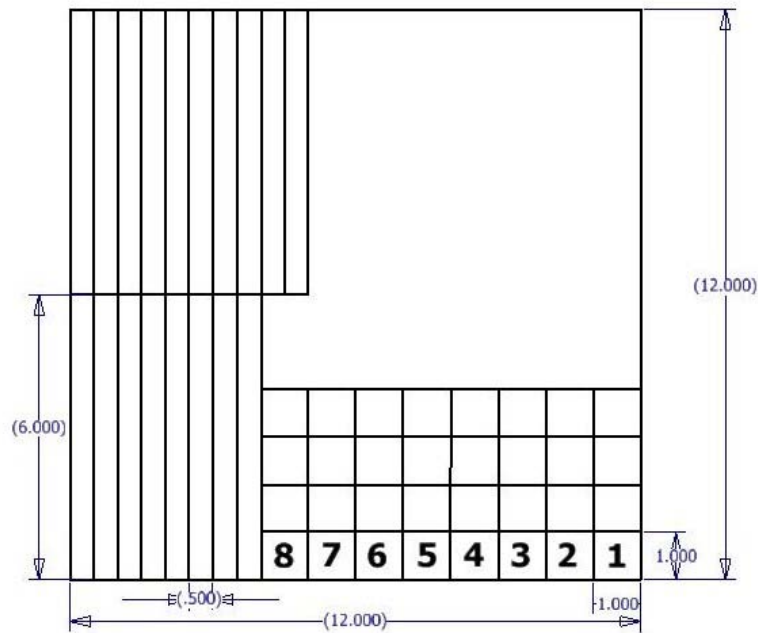
Figure 8: 12" X 12" carbon-carbon composite panel sectioned for porosity, flexure, and interlaminar tensile tests.

The squares labeled 1 through 8 in the figure above were used for porosity testing and were further divided similarly to the squares in Figure 7. The 6" beams were used for flexure tests and these were cut out at the three critical points during processing. The remainder of 1" X 1" squares were used for interlaminar tensile tests and were also cut out at the three critical points during processing. The remainder of the panel was used for additional testing and further study after densification was complete.

2.4 Porosity Test Procedures

Two tests were chosen in order to determine open porosity percentage by volume and skeletal density of the composite samples. These were boiling water immersion and mercury

porosimetry. The first step in the water immersion process was to dry out the sample completely. This was done to obtain an accurate dry weight of the sample without any moisture on the surface or in the pores. The samples were first put into dry, empty beakers, which were then placed in a vacuum oven set at 110° C and left there overnight to dry. The next day the samples were removed from the oven, and their weights were recorded. At this point the beakers were filled with water, and the samples were suspended in the middle of the beaker by a wire. This can be seen below in Figure 9. The beakers were then set on a hot plate and brought to a boil. The samples remained in boiling water for 4 hours. After this was completed, the burner was turned off, and the water was allowed to cool while the samples remained submerged. This took place overnight for approximately 20-24 hours [17].
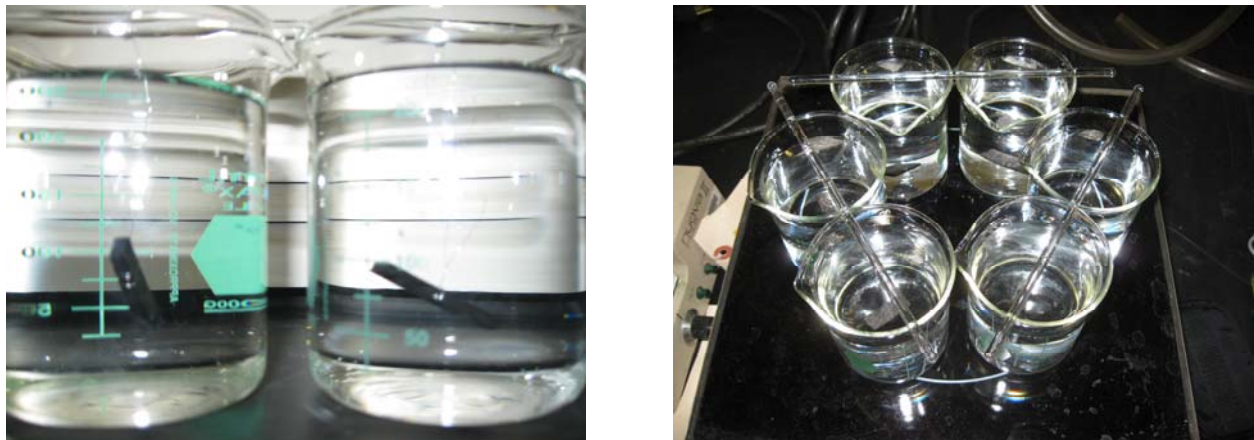
Figure 9: Photos of a water immersion porosity test being conducted. Composite samples suspended in water (left), and beakers containing samples on hot plate (right).

At this point the samples were considered fully saturated, they were removed from the wires, and their weights were measured while suspended in water. A scale with a hook and special harness hanging underneath it was used for this measurement. Once this weight was obtained, analysis could begin, and Equations 1 and 2 were used.

In order to verify the results from water immersion and to expand upon the porosity analysis, mercury porosimetry was chosen as the second porosity test method. From the 2-D composite panel, a small section was cut using a band-saw with dimensions similar to those used for water immersion. Each sample was first dried in a vacuum oven for several hours and then weighed. The sample was then put into a sample container called a penetrometer, which is comprised of a cup to hold the sample connected to a precision-bore, glass stem with a known internal volume. The penetrometer was then weighed before it was connected to the porosimeter. Standard procedures were then followed as are laid out in the porosimeter manual [1].

Once the penetrometer was sealed, it was placed into the porosimeter for low pressure mercury intrusion. The penetrometer was evacuated to remove all air and moisture, and then it was filled with mercury. At this point high pressure is not yet applied, so no mercury is forced into the sample; however, the large outer pores may begin to fill. The penetrometer was then transferred to the chamber within the porosimeter for high pressure analysis. As the pressure increased, the mercury in the stem of the penetrometer was forced into the sample, filling its pores. The porosimeter that was used for these tests is capable of reaching 60,000 psi, and at that pressure nearly all of the open pores within the sample are filled [1]. Based on the level of mercury in the stem of the penetrometer, and the pressure applied, the device can calculate many aspects of a sample's porosity.

2.5 Mechanical Test Procedures

The two types of mechanical tests conducted during Task 2 were Four point bend and

interlaminar tensile tests. Samples were cut from panels 12680 and 12681 at three different

times throughout the densification process in order to assess the correlation between composite

strength and matrix porosity. The samples were cut out after the second heat treatment, after the

third heat treatment, and after the third pitch impregnation step during panel densification. The

specific procedures for each test are described in detail below.

2.5.1 Four Point Bend Procedures

Five samples were cut from each panel at each of the three cycles previously mentioned

to ensure accurate and precise results. The rectangular pieces were 6" long and 0.5" wide and

are shown below in Figure 10. These were then placed in four point bend fixtures and standard

procedures described below were followed. Figure 11 is a picture of the load fixture alongside a

picture of a sample being tested by the four point bend method.

Figure 10: Rectangular beams cut out of composite panels for four point bend tests.
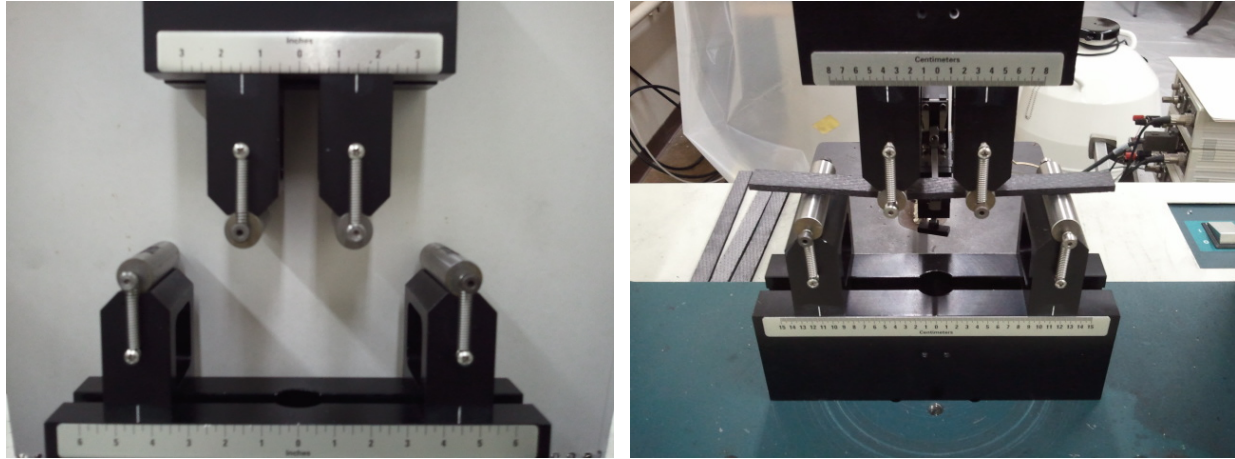
Figure 11: Four point bend fixture (left) and a sample undergoing four point bend test (right).

The specific procedures for the four point bend tests were taken from ASTM standard D-6272-02. The support span to sample depth ratio for laminated materials such as carbon-carbon composites was set at 32. The two load fixtures were then placed at intervals of L/3, where L = support span, in order to evenly distribute the load across the beam. The crosshead rate, which is the speed at which the upper four point bend fixture moves toward the sample, was set to 0.25 in/min in accordance with standard test procedures. In order to monitor the maximum deflection at the center of the beam, an extensometer was used. It was placed directly between the two load fixtures in order to monitor the displacement, which was not provided by the data acquisition program. The extensometer was calibrated before each test to ensure accuracy.

2.5.2 Interlaminar Tensile Test Procedures

The specific procedures for the interlaminar tensile tests were taken from ASTM standard C 297-04. A special load fixture was designed to attach to a metal mount which was then glued to the top and bottom of the composite. The samples to be tested were cut into 1" diameter cylinders, and glued to the mounts as shown in Figure 12.

Figure 12: Custom sample mounts for interlaminar tensile tests.

There is an extensive procedure to follow to ensure a controlled test for accurate results. First the surfaces of the fixtures, which will be bonded to each sample, are thoroughly cleaned. The samples are then machined resulting in a circular cross section with a diameter of exactly one inch. The primer and adhesive were then added to the surface of the each fixture. The particular adhesive used for this application was Hysol EA 9309-3NA, which has high peel strength and is designed for composite bonding. Once the sample is pressed onto the fixture, it is placed in an oven so the adhesive can cure. The samples remained in the oven for one hour at 180° F. The fixtures mounted in the oven are shown above in Figure 12.

The custom mounts, which were bonded to each sample, were then placed in a load fixture designed for this type of test. The entire load fixture is comprised of a load cell and a custom, flexible connector, which attaches to the sample mounts. The fixture has a pivot joint in

its center to ensure that the forces are acting vertically on the sample. Any side forces can

significantly affect the data. The load fixture is shown below in Figure 13.

Figure 13: Custom designed load fixture for interlaminar tensile tests.

The crosshead was set at a rate of 0.005 in/min in accordance with standard test

procedures. A data acquisition program was used to monitor the applied load and the crosshead

displacement. The load at the time of failure was then used to determine the maximum

interlaminar tensile stress.

3. Task 1 Results and Analysis

The purpose of this first set of testing was to determine the current porosity and density characteristics of a 2-dimensional carbon-carbon composite panel fabricated by AFRL's *In-Situ* process, and to determine the effectiveness of each densification cycle for overall porosity improvement. The Task 1 porosity tests were conducted throughout three densification cycles of the composite panel's fabrication. Three cycles were expected to be adequate, as had been seen by comparable densification methods [14]. Because each subsequent densification cycle results in a smaller improvement than the last, and each cycle requires more time and more money, the improvement from too many additional cycles is not worth the cost [19]. Each densification cycle was preceded by a heat treatment cycle to prepare the sample for the addition of pitch.

The first sample to be tested was cut immediately following the first heat treatment to 1650° C prior to the first densification cycle, as was described in the experimental procedures section of this report. This square was labeled "Post HT (1)". The second piece was cut from the panel after the first pitch impregnation. This square was labeled "Post Pitch (1)". The table below shows the six samples cut from panel 12656-4 along with naming convention for each sample.

Table 1: Task 1 densification cycles and sample nomenclature.

Cycle #*	Processing Step	Sample Name
1	Heat Treatment	Post HT (1)
2	Pitch Impregnation	Post Pitch (1)
3	Heat Treatment	Post HT (2)
4	Pitch Impregnation	Post Pitch (2)
5	Heat Treatment	Post HT (3)
6	Pitch Impregnation	Post Pitch (3)

*This numbering system is used in all graphs displaying results throughout densification.

The results of porosity measurements at the end of each heat treatment and at the end of each pitch impregnation should demonstrate the overall hypothesized trend of decreasing porosity and increasing skeletal density. This initial porosity study should also determine if three densification cycles are adequate to surpass the industry standard regarding porosity within a 2-D carbon-carbon composite panel.

3.1 Water Immersion Results

Each sample was tested two to three times to ensure accurate data. The results of skeletal density and porosity percentage of panel 12656-4 were averaged and are displayed in Table 2, shown below.

Table 2: Porosity and skeletal density results from water immersion.

Cycle #	Panel	Sample	Bulk Density (g/cc)	Skeletal Density (g/cc)	% Porosity
1	12656-4	Post HT (1)	1.32	1.66	20.62
2	12656-4	Post Pitch (1)	1.40	1.67	16.23
3	12656-4	Post HT (2)	1.42	1.69	16.18
4	12656-4	Post Pitch (2)	1.50	1.69	10.96
5	12656-4	Post HT (3)	1.46	1.71	14.18
6	12656-4	Post Pitch (3)	1.53	1.71	10.33

These results were analyzed by first looking at the trends of the density and porosity values throughout the densification cycles of panel 12656-4. It is important to understand how the bulk and skeletal density and porosity values change over the course of these six stages so the effectiveness of each stage can be determined, and the efficiency of processing can be assessed. Below are graphs of the general trends of density and porosity as the panel was densified.
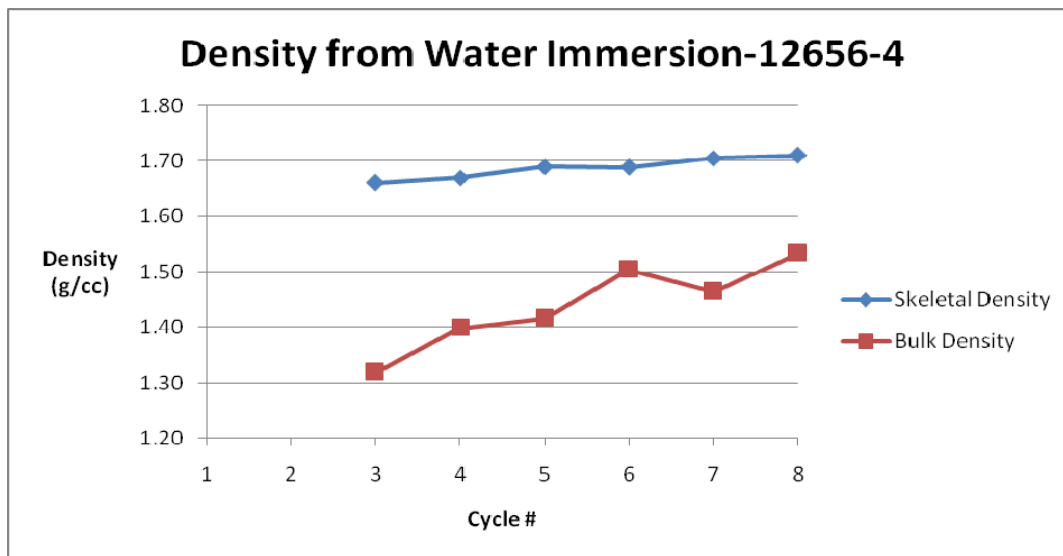
Figure 14: Graph of the density trends from water immersion over 3 densification cycles of panel 12656-4.
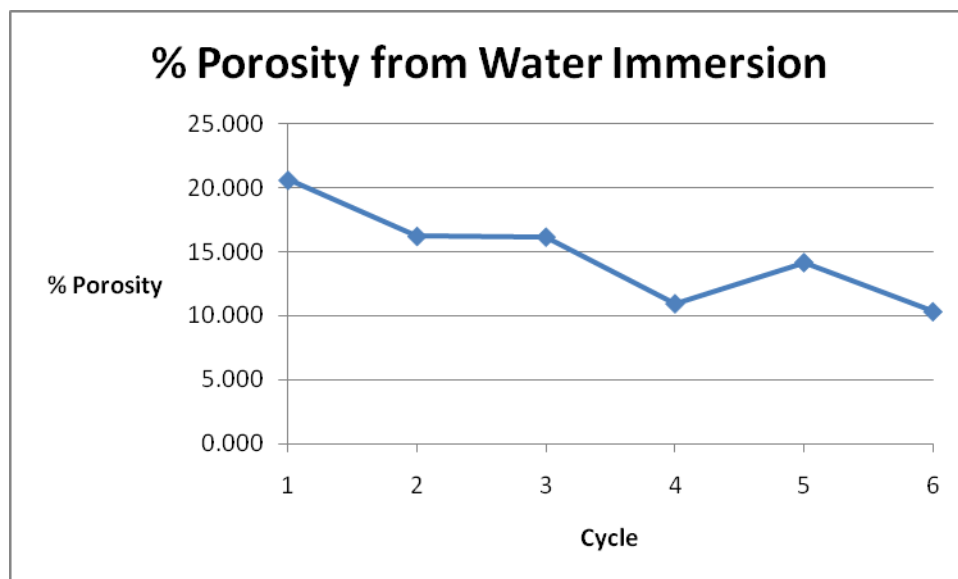
Figure 15: Graph of the porosity percentage trend from water immersion over 3 densification cycles of panel 12656-4.

In Figure 14 the trend of the bulk and skeletal densities for panel 12656-4 are shown. The overall trend is increasing which is desired, and this initially confirms the success of the

densification process. The amount that the skeletal density increases is small, but because skeletal density does not take into account open porosity, this is to be expected. Skeletal density only takes into account the material present as well as the closed porosity. The carbon matrix left from the phenolic based precursor will yield a certain skeletal density. As pores are filled with matrix from pitch densification, the skeletal density of this new material is averaged together with the old. Pitch will yield a higher skeletal density than the carbonized phenolic; therefore, when pitch fills open porosity, overall skeletal density should increase slightly.

The bulk density increases as well. Bulk density measures the total weight of the sample compared with its bulk volume. As a result, the bulk density measurement does include open porosity. Therefore, as porosity decreases, bulk density should increase similarly. This is seen in the graph above.

The other observation that was taken from the skeletal density graph is the changing rate of increase for each cycle. The heat treatment cycles, 3 and 5 on the graph, show a greater rate of increase. This has been seen in the past and was expected for this test [19]. As the carbon matrix is heated to such a high temperature, it restructures and densifies further, leaving only the dense char residue and additional voids. During pitch impregnation, cycles 2, 4, and 6, voids are being filled with matrix material, drastically increasing bulk density. Heat treatment cycles will have a lower rate of increase due to the formation of more open porosity. Skeletal density may stay the same or even decrease over a heat treatment cycle because closed porosity can also form.

These same concepts apply to the analysis of the porosity graph as well, which is shown in Figure 15. This graph represents the overall percent of the bulk volume that is void space. Because these results were obtained from water immersion, the graph only represents the open

pores where water could reach, and not the completely enclosed air pockets within the matrix. The immediate observation is that the porosity is decreasing. This shows that the overall densification process is working, and the improvement is significant. The porosity is around 20% at the beginning of the first densification cycle, and by the end of the third cycle, it is 10%. Due to this 50% decrease in porosity, the corresponding properties of the composite are expected to improve dramatically, and this will be discussed in greater detail in later sections of this paper.

Another observation that can be made from the porosity results is the varying rate of change of the porosity percentage. During pitch impregnation, cycles 2, 4, and 6, the rate that the porosity decreases is much greater. During the heat treatment cycles, 3 and 5, the porosity either stays close to the same or actually increases slightly. These are both reasonable and expected results. Material is added during pitch impregnation, and porosity forms when the matrix is densified during heat treatment. We see this process occurring in the porosity graph in Figure 15, and this explanation describes why the graph is not a straight line [19].

Once porosity data were obtained for each sample, optical microscopy was used to verify the data and to better understand the types and characteristics of pores present at each stage of densification. This microstructural analysis is beneficial because the porosity can be visualized. It shows the type of porosity present, such as large open pores, micro-cracks, or a combination of the two, their shape and size, as well as where in the matrix they are forming.

A small piece was cut from each of the 1 square inch samples. These were then mounted in epoxy with a cross-section of the composite visible from the bottom of the mount. Each sample was polished using up to 1600 grit sand paper and then viewed under a microscope at various magnifications to better understand the porosity characteristics.

Figure 16 below is a cross-section of sample 12656-4 Post HT (1) magnified at 50x. The fiber bundles and carbon matrix are clearly distinguishable as are the large pores throughout the matrix. The widths of these oval-shaped pores are above 300 μm in some cases. This explains how the overall porosity of this composite can be approximately 20% by volume. In addition to the large pores, micro-cracks are visible throughout the matrix. Figure 17 is a cross section of sample 12656-4 Post Pitch (1) also magnified at 50x. As pitch impregnates the matrix, some of the voids begin to fill, as seen by the lighter color material in the photo.
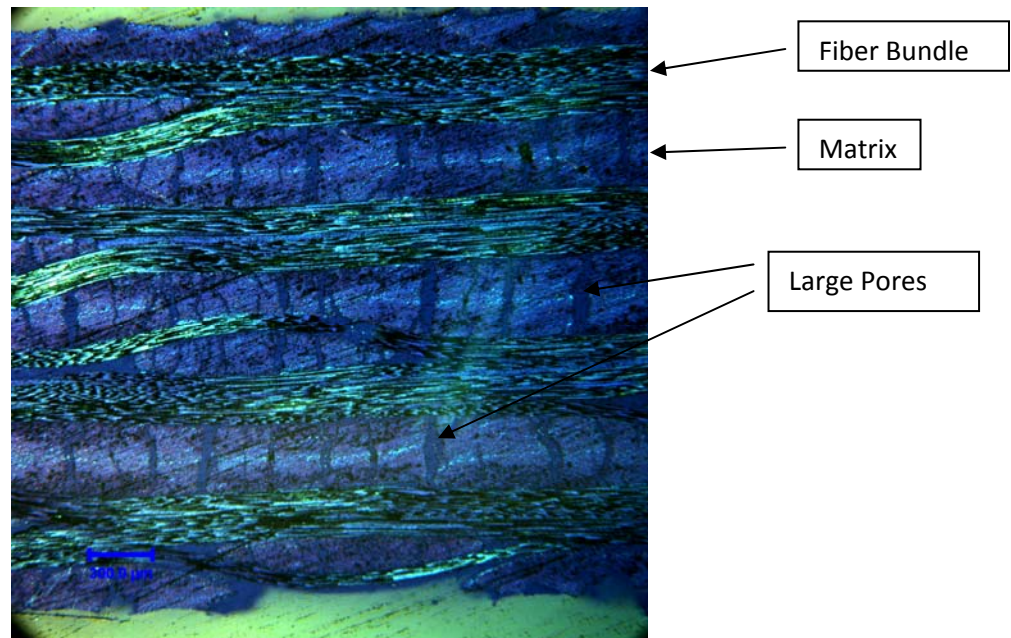
Figure 16: Cross section of panel 12656-4 after the first heat treatment. This photo was taken at 50x magnification.
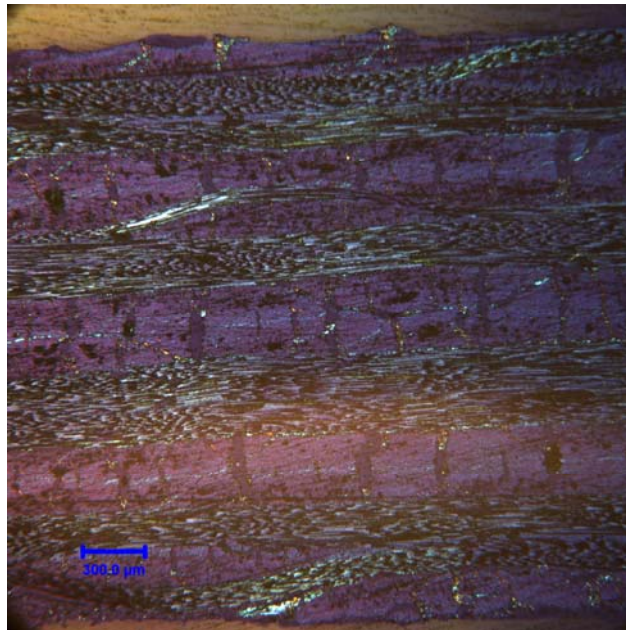
Figure 17: Cross section of panel 12656-4 after the first pitch impregnation cycle. This photo was taken at 50x magnification.

The figure below shows a similar photo taken after the final densification cycle. In this sample the porosity has been cut in half, and this is apparent in the photo. The majority of the large pores are between 100-200 μm, and they are fewer in number as well. These photos help to verify the data found by the initial porosity tests.
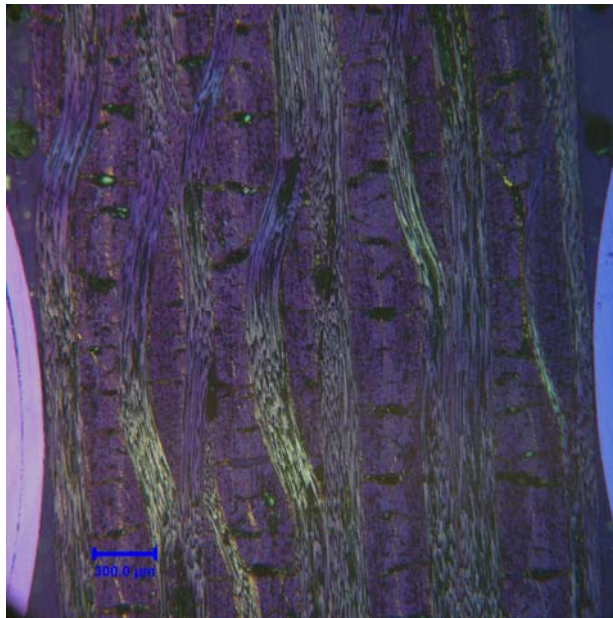
Figure 18: Cross section of panel 12656-4 after the final densification cycle. This photo was taken at 50x magnification.

3.2 Mercury Porosimetry Results

Porosimetry data were gathered for the same set of samples from panel 12656-4 that was tested using water immersion. The results were averaged together and are shown in the table below.

Table 3: Porosity results from mercury porosimetry tests.

Cycle #	Panel	Sample	% Porosity
1	12656-4	Post HT (1)	22.40
2	12656-4	Post Pitch (1)	15.96
3	12656-4	Post HT (2)	15.93
4	12656-4	Post Pitch (2)	13.08
5	12656-4	Post HT (3)	14.82
6	12656-4	Post Pitch (3)	9.10

These results were analyzed to determine if the trends matched the results from the water immersion. The graphs are shown below. Most of the results are directly in line with the water immersion despite some small variation. Figure 19 shows the trend in the porosity percentage as was determined by mercury porosimetry.
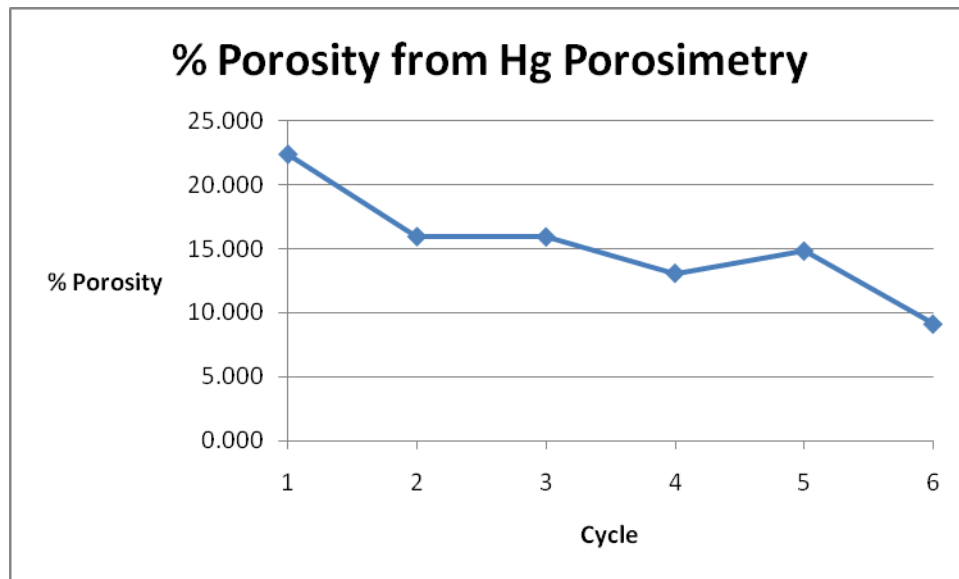
Figure 19: Graph of the porosity trend from mercury porosimetry over 3 densification cycles of panel 12656-4.

The porosity trend correlated very well with that found by water immersion. There was some variation to note, but the mercury porosimetry tests successfully verified the accuracy of the water immersion tests. Below is a graph showing the consistency of the two different test methods.
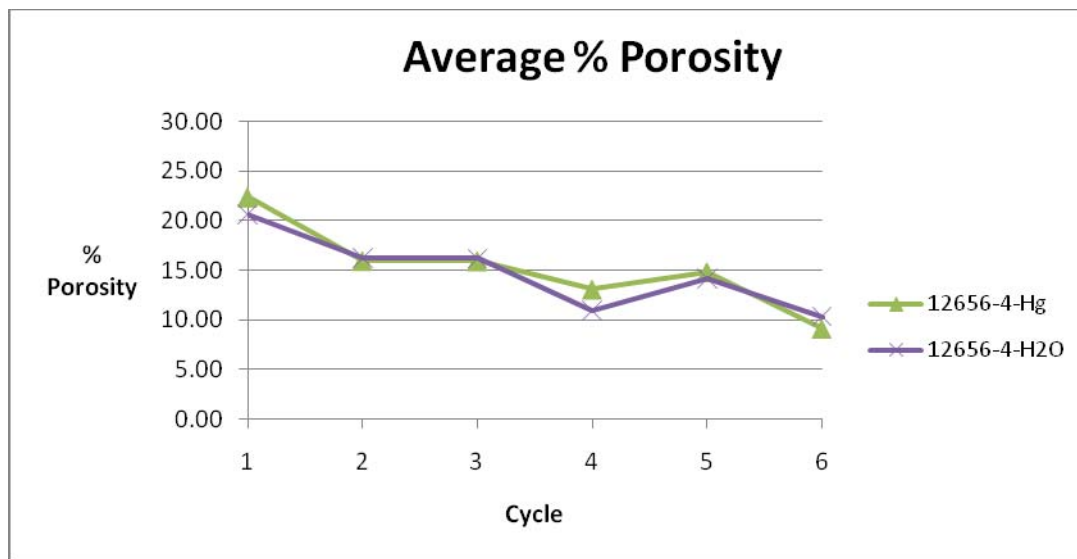
Figure 20: Comparison graph of porosity data of panel 12656-4 obtained by water immersion and mercury porosimetry.

Both porosity test methods show a similar trend. The porosity decreases overall from the first to the third densification cycle, and the rate of decrease is greatest during the pitch cycles. The mercury porosimeter does not show as much of a decrease during the second pitch impregnation, cycle 4, which is the greatest point of deviation between the two methods, almost 2%.

3.3 Explanation of Variation

Below is a table showing the variation between the two test methods. These percentages were found by using water immersion as a base line for porosity, and the percentages represent the amount that the mercury porosimeter deviated.

Table 4: Differences found between water immersion and mercury porosimetry with calculated percent variation.

Cycle #	Sample	H2O Porosity	Hg Porosity	Difference	Variation (%)
1	Post 1650 C (1)	20.62	22.40	1.78	8.64
2	Post Pitch (1)	16.23	15.96	0.27	1.67
3	Post 1650 C (2)	16.18	15.93	0.25	1.52
4	Post Pitch (2)	10.96	13.08	2.12	19.38
5	Post 1650 C (3)	14.18	14.82	0.64	4.54
6	Post Pitch (3)	10.33	9.10	1.23	11.89
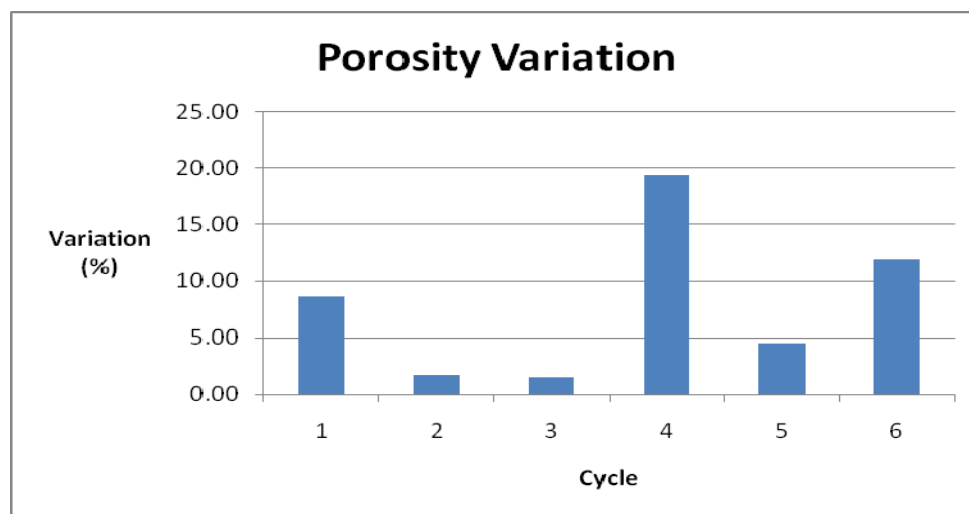
Figure 21: Variation between mercury porosimetry and water immersion porosity tests for each densification cycle of panel 12656-4.

There are two different likely explanations as to the sources of the variation between the mercury porosimetry and water immersion. One likely reason for the variation is the side effect of the high pressure employed by mercury porosimetry. Because the pressure reaches 60,000 psi, it is possible that some of the closed porosity was opened. This would increase the porosity percentage found by mercury porosimetry. This is one explanation for the high porosity seen after the second pitch cycle [20]. Also, this is most likely to happen after pitch is added prior to the next heat treatment when the new matrix material is weakest.

Another explanation is small variations throughout a panel. In order to save time and because mercury porosimetry destroys each sample, porosimetry cannot always be conducted using the exact same piece of the panel as water immersion or additional porosimeter tests. Throughout a densified carbon-carbon composite panel, there will be variation in terms of porosity and how much each cycle improves properties. This can account for some small difference between water immersion and porosimetry; however, the overall trends and characteristics should be approximately the same. Based on the comparison graph in Figure 20, these possible sources of variation should be taken into consideration.

3.4 Pore-Size Distribution

In order to better understand and characterize the pore structure and distribution in the composite over these three densification cycles, graphs were produced correlating pore-size with the intrusion levels of mercury. The first set of pore-size distribution graphs in Figure 22 shows pore-size as it relates to incremental intrusion. Each point on the graph represents another measurement of the change in the level of mercury recorded by the porosimeter. These intrusion volumes also correlate to an average pore-size, which allows the approximate amount and size of the pores to be determined. When these graphs are compared to each other, the success of each cycle can be seen because the level of incremental intrusion decreases as pores are filled. The graphs representing all three densification cycles are shown together to illustrate the progression of the pore distribution throughout processing [9,15,16].
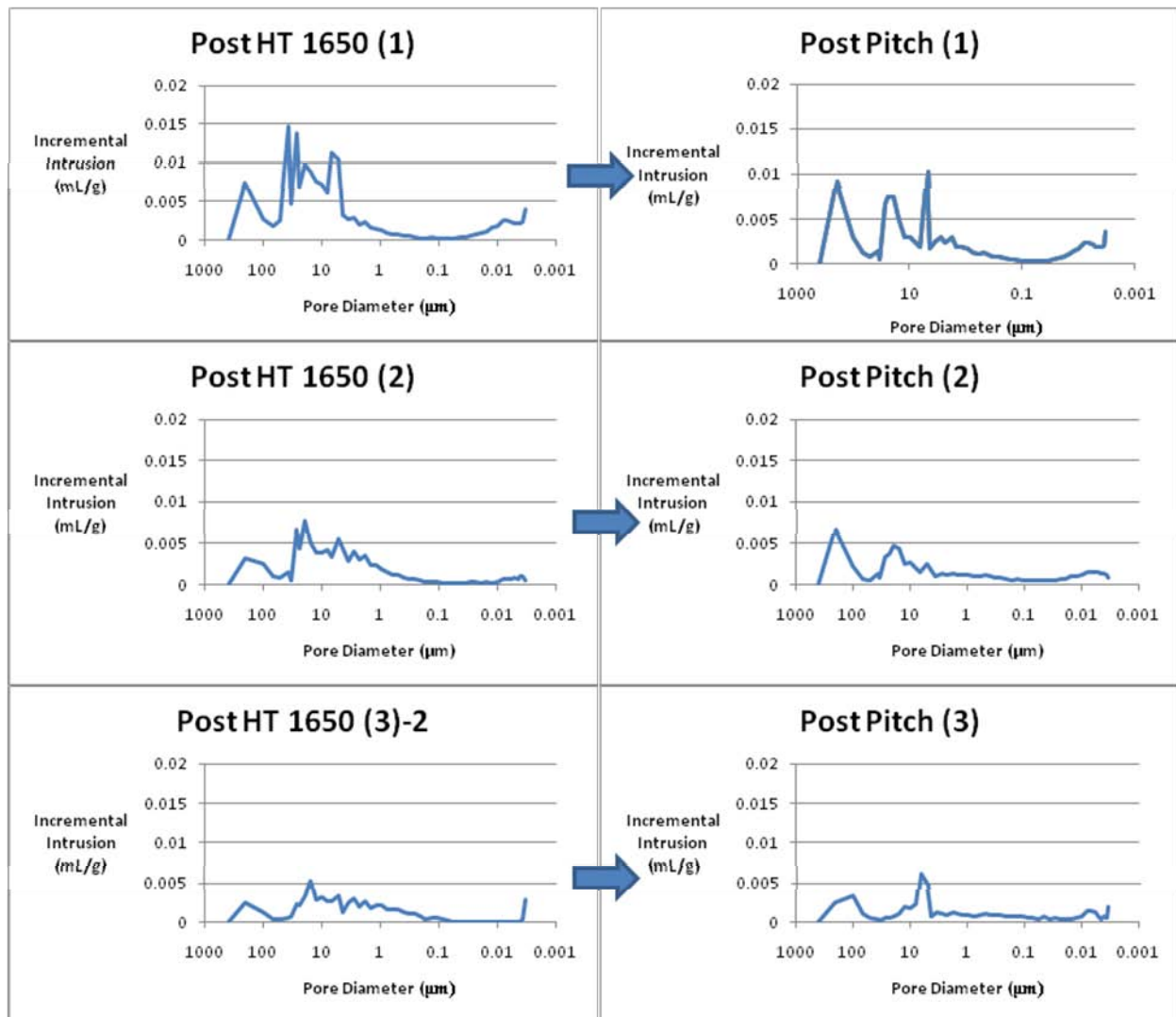
Figure 22: Pore-size distribution for each densification cycle of panel 12656-4. These graphs display the incremental intrusion of mercury corresponding to pore-size.

Each peak on the graphs shown above represents pores of a certain size being filled by the incremental intrusion of mercury. As peaks of the same pore size decrease in size, it means that those pores are slowly being filled throughout the densification process. This results in less porosity of the same size; therefore, the peak becomes lower. As peaks move to the right throughout the graphs, large pores are being partially filled, which results in more pores of a

smaller size. Large peaks are noted and are easily seen shrinking. The small pores remain at very similar levels in almost every stage of densification. This is because the pitch impregnation is not effectively filling all the small pores. Also, more small pores are opened during heat treatment, so the smaller pore levels are generally staying the same.

It is noted that some large peaks arise in the middle of densification that were not present on earlier cycles. One example is the first large peak on Post Pitch (1). There are multiple reasons why this may occur. First of all, these are different parts taken from the same panel throughout densification as described in the previous error explanation. Using different pieces of the panel can result in some variation in terms of porosity. Although a pitch impregnation cycle may generally decrease large open porosity throughout the entire panel, each cycle does not reach all pores, even large ones. There may be some large pores that were not filled by Post Pitch (1) that were only present in the specific sample placed into the porosimeter. Because the porosimeter destroys each sample that it analyzes, the same sample cannot be tested, densified, and tested again. The second possible reason is that the heat treatment cycles restructure the pore distribution. When the matrix is brought to high temperatures the crystal structure partially changes, and new cracks can form. This can also account for new peaks in the distribution graphs above. In addition to heat treatment, the mercury porosimeter can also restructure the pore distribution by breaking open closed pores. This would cause the distribution curves to display certain porosity characteristics that were not present in the part before it was put into the machine for testing. This can also account for large peaks arising after pitch is added. They may not have been large pores until the mercury broke open smaller pores and closed porosity.

The second set of porosity distribution curves are shown below in Figure 23. These graphs represent the cumulative intrusion of mercury as opposed to the incremental intrusion.

The general shape of each graph shows that large pores are filled initially, and this is where the largest change in the level of mercury occurs. As the graphs level off in the small pore range, much less mercury is being forced into the sample. The trend is easily seen throughout the densification process. The height of the curve slowly decreases representing less and less porosity, specifically large porosity. Also the curve shifts slightly over from the left to the right. This represents the largest pores being completely filled by the subsequent densification cycle, and are, therefore, not present in the next graph.
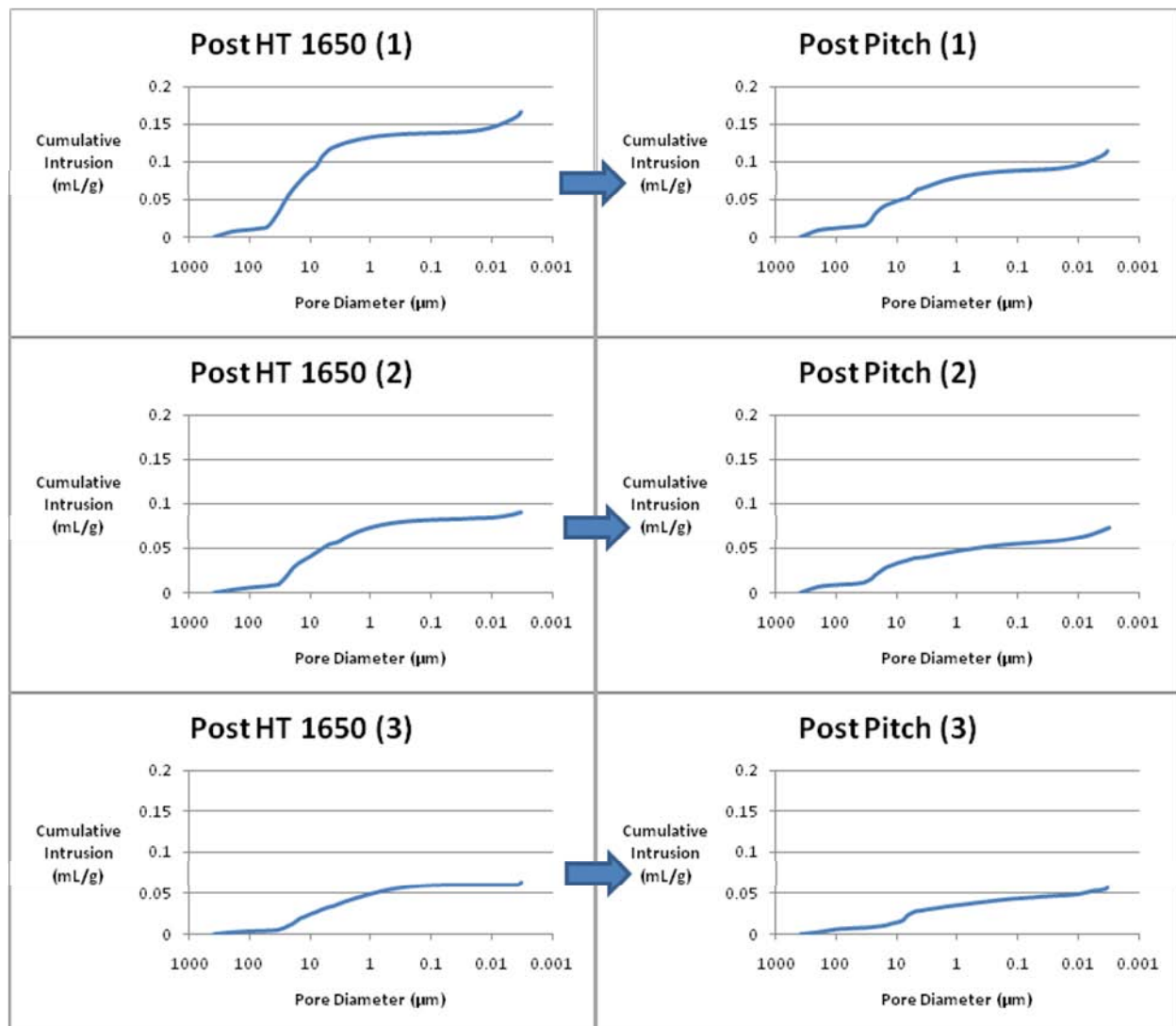
Figure 23: Additional pore-size distribution plots for each denisification cycle of panel 12656-4. These graphs represent the cumulative intrusion of mercury corresponding to pore-size.

3.5 Comparison to Standard Fabrication Methods

Analysis was also done within Task 1 on similar carbon-carbon composite panels, some of which were fabricated by a more traditional liquid phase process as opposed to *In-Situ* densification. The performance of some of these composites has been proven and accepted in the past, and they are a good representation of the industry standard for carbon-carbon panels. They have been included to compare porosity results and to help determine the effectiveness of this alternate method of fabrication.

The different panels and their fabrication methods are summarized in the table below, listing the sample name, the prepreg material, and the densification method.

Table 5: Sample names and fabrication methods of additional carbon-carbon panels used for comparison.

Panel	Prepreg	Densification
41	Phenolic Resin	Pitch Pot
12656-3	Phenolic Resin	Pitch Pot
12473	Phenolic Resin	*In-Situ*
12656-4	Phenolic Resin	*In-Situ*
H5-3	Hot Pressed Pitch	*In-Situ*

The first of these additional panels was 41. This panel was entirely fabricated by FMC, another company located in Tucson, AZ. This panel represents a typical mid-grade, commercially available, 2-D, carbon-carbon composite. The fabrication method used for panel

41 was pitch pot densification. It was initially prepregged with phenolic resin and cured, but for densification, it was dunked into a pot of A240 coal-tar pitch. The pitch was heated up to reduce the viscosity, and the part was immersed and soaked until the pitch successfully wicked into the panel. This is another fairly simple way to densify a thin 2-D composite, but the performance of the resulting composite often suffers.

The next panel was 12656-3. This panel was fabricated using Allcomp's standard prepregged fabric; however, it was densified at FMC with A240 coal-tar pitch and the simple pitch pot method described above. This panel was designed at the same time as 12656-4 to compare the two different densification methodologies.

The third panel for comparison was 12473. This was considered the baseline for the Allcomp *In-Situ* fabrication method in the past when the method was newly created. The process has since been refined in certain ways, and the porosity results must be compared.

The final panel for comparison was H5-3. This panel was fabricated by Allcomp, Inc. and was designed for thermal applications, for which the desired property is good thermal conductivity. For this panel the pore structure is not as relevant as long as the density of the matrix is sufficient. To achieve these results, AR synthetic mesophase pitch was used as the initial matrix precursor by being placed between the plies in powder form and hot pressed together. Starting with pitch as the matrix precursor typically will improve density faster than phenolic resin because the carbon yield from pitch is often higher. The results for this panel are show high porosity and also a relatively low skeletal density. This is likely due to a side-effect of the unusual preform used for this panel or the manner in which the pitch was applied.

Below is a table summarizing the porosity results of these additional panels tested by water immersion.

Table 6: Porosity results of additional panels tested by water immersion.

Sample	Skeletal Density (g/cc)	% Porosity
12656-3	1.691	11.319
12473	1.676	12.340
H5-3	1.698	18.919
41	1.725	14.874
12656-4	1.711	10.326

According to these results there is a variety of porosity values, but they are all between 10% and 20% by volume. The skeletal density has some slight variation as well, but is essentially the same for all samples, about 1.7 g/cc. The porosity values are very close for 12656-3, 12656-4, and 12473. The latter two are both densified according to the *In-Situ* method, but 12656-4 has slightly less porosity demonstrating the success of the refined process. 12656-3, which was densified using the pitch pot method has very similar porosity. This shows that the *In-Situ* method is able to yield porosity characteristics similar to other common methods of densification. This combined with low cost and fast processing time make the *In-Situ* densification method very advantageous to carbon-carbon development.

These results show the effectiveness of the *In-Situ* densification process, which after three cycles produced a panel with porosity of approximately 10% and a density of 1.71 g/cc. These numbers are slightly more desirable but very close to several comparable panels. Based on the results above, the *In-Situ* densification method is highly effective, especially due to the ease and efficiency of processing.

Below is a picture taken under the microscope of the cross section of panel 12656-3. There appears to be many small cracks that have been filled in, which is represented by the light colored material throughout the matrix.
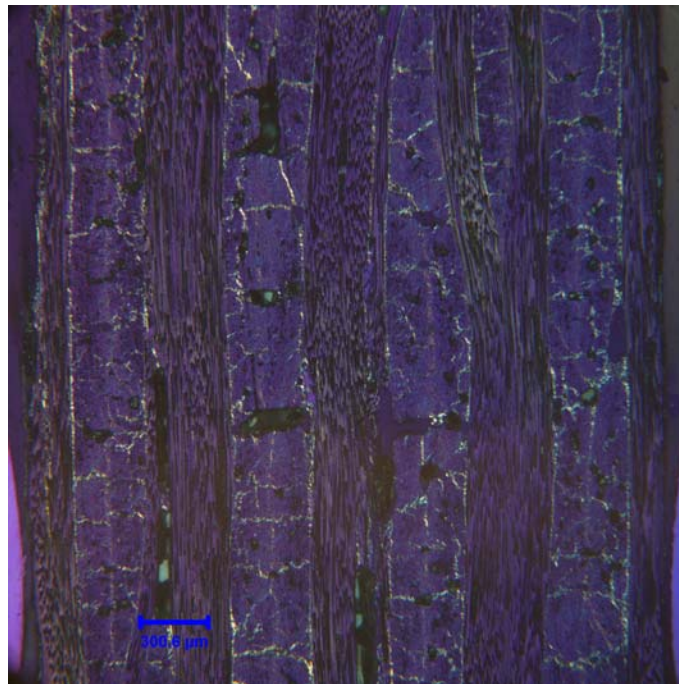
Figure 24: Cross section of panel 12656-3 after densification. This photo was taken at 50x magnification.

It is apparent that most of the small cracking has been filled within the matrix of panel 12656-3. This filling process has undoubtedly improved the overall porosity of the composite. However, there are several large voids in the matrix different from the standard pattern of oval pores which contribute to the similar porosity percentage. Below in Figure 25 the image is shown again at 100x beside 12656-4. The black arrows point out the large voids along side of the fiber bundles, which were not filled in with pitch during densification.
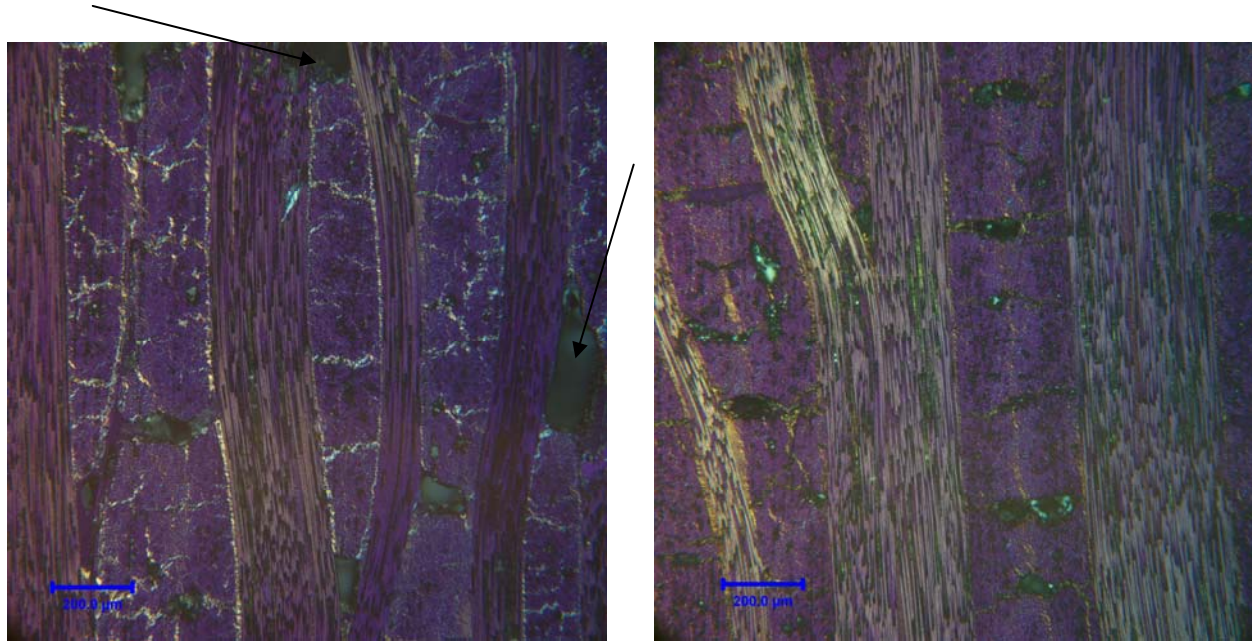
Figure 25: Cross section photos taken at 100x magnification. Panel 12656-3 after densification (left), and panel 12656-4 after densification (right).

Panel 12656-4 has less small cracking, but a more common pattern of 200 μm oval shaped pores. It is interesting how the pattern of porosity within each of these samples is very different due to the different styles of processing, but the porosity and density values were measured to be approximately the same. Due to the common pattern of porosity within 12656-4 from *In-Situ* densification, further study of the pore structure at different stages of processing may lead to accurate prediction and improvement of overall porosity. Microstructure pictures of all the comparable panels are shown in Appendix A.

4. Task 1 Conclusions

Task 1 porosity testing was very successful overall. Porosity and skeletal density results were initially obtained by water immersion tests throughout each densification cycle for panel 12656-4. These test successfully showed the increasing trend of skeletal density and the decreasing trend of open porosity throughout densification. The results were then compared to additional panels fabricated by different methods. Panel 12656-4 by its last densification cycle reached similar skeletal density of 1.7 g/cc and a surprisingly low porosity of approximately 10%. These results validate the effectiveness of the *In-Situ* densification method for carbon-carbon composite fabrication by reaching the desired density and porosity after three densification cycles.

These results were also verified by mercury porosimetry. The porosity values were found to be very similar, and they follow the same trend as that found by water immersion. The pore-size distribution graphs show that each densification cycle is partially filling large voids causing a larger number of smaller pores in each subsequent measurement. However, overall porosity percentage was reduced throughout each cycle. There was a small amount of variation that was noted when comparing the trends in porosity found by the two different test methods. The first likely explanation for this is variation throughout a large composite panel. The different tests use different samples due to the destructive nature of the porosimeter, so variation in porosity may be noted. This will be further tested in Task 2 by creating multiple panels for redundant testing and repeatability. The second likely explanation is inconsistent results from the porosimeter due to side effects from the high pressure. Because the pressure reaches 60,000 psi, it is possible that the structure of the composite fractures, opening up some of the closed porosity. This would

cause the open porosity to appear greater because closed porosity may be included in the measurement. It is likely that this would happen following a pitch cycle before the new matrix material is hardened by heat treatment. The results of Task 2 will be carefully analyzed to determine if this type of 2-D carbon-carbon composite samples is vulnerable to that amount of pressure.

Task 1 demonstrated many characteristics and results of the *In-Situ* densification method; however, there is much more to be tested. The magnified image in Figure 6 of Panel 12656-4 during the first densification cycle shows that large voids are already present in the matrix at this point in processing. If the cause of this initial porosity can be determined, research efforts can be focused on decreasing the percentage of porosity before densification begins. Task 2 among other things will address when these pores are being formed during fabrication. Once this is determined, the *In-Situ* densification method will be adjusted and will produce panels with a more notable improvement of properties. Task 2 will also attempt to verify the hypothesized correlation between decreasing porosity and increasing strength and stiffness of the matrix and the overall composite. Once Task 2 is completed, the results will be analyzed along with the results from Task 1, and this new method of carbon-carbon composite densification will be better understood and able to be optimized.

5. Task 2 Results and Analysis

The purpose of the second task of this study was to specifically determine the characteristics of the initial pore formation prior to heat-treat and densification cycles in order to better optimize the process. This was done by evaluating the porosity at each stage of processing as well as the corresponding mechanical properties following key densification cycles. The panels for Task 2 were sectioned and tested after they were initially cured. This was two steps earlier in the fabrication process than in Task 1. Sections were also tested at each subsequent stage of processing including the three densification cycles and three heat treatment cycles, which were analyzed during Task 1. By repeating the porosity tests during the same three densification cycles, the results from Task 1 could be verified, and the trends could be identified and compared. In addition mechanical tests were performed at three key stages of processing to assess the correlation of overall porosity and matrix strength.

Water immersion and mercury porosimetry tests were conducted at each of the eight stages analyzed during Task 2. Mechanical testing was conducted at three stages spread throughout the later parts of processing. Below is a table displaying the cycle number, the name of each sample and the corresponding tests that were conducted for panels 12680 and 12681.

Table 7: Testing plan and nomenclature for each processing step during Task 2 for panels 12680 and 12681.

Cycle #*	Processing Step	Sample Name	Porosity Test 1	Porosity Test 2	Mechanical Testing
1	Cure	Post Cure	Water Immersion	Hg Porosimetry	
2	Carbonization	Post Carb	Water Immersion	Hg Porosimetry	
3	Heat Treatment	Post HT (1)	Water Immersion	Hg Porosimetry	
4	Pitch Impregnation	Post Pitch (1)	Water Immersion	Hg Porosimetry	
5	Heat Treatment	Post HT (2)	Water Immersion	Hg Porosimetry	Flexure/ILS
6	Pitch Impregnation	Post Pitch (2)	Water Immersion	Hg Porosimetry	
7	Heat Treatment	Post HT (3)	Water Immersion	Hg Porosimetry	Flexure/ILS
8	Pitch Impregnation	Post Pitch (3)	Water Immersion	Hg Porosimetry	Flexure/ILS

*Cycles 3-8 corresponded to the 6 densification steps in Task 1. Cycles 1-2 were prior to densification. These Cycle numbers were used in all graphs during Task 2.

5.1 Water Immersion Results

Water immersion tests were conducted in the same manner as in Task 1. Samples were immersed in boiling water for several hours and then allowed to cool over night. The weights of the samples were taken once fully saturated in water and compared to the dry weight. Using Equations 1 and 2 from Task 1, skeletal density and the open porosity percentage were obtained. The results of the Task 2 water immersion tests are shown below. Table 8 shows the skeletal density and porosity percentage results for Panel 12680, Table 9 shows the same results for Panel 12681, and Table 10 shows the results for both panels averaged together.

Table 8: Porosity and skeletal density results from water immersion for Panel 12680.

| Sample	Cycle	Bulk Density (g/cc)	Skeletal Density (g/cc)	% Porosity
12680	Post Cure	1.46	1.56	5.97
12680	Post Carb	1.32	1.76	25.63
12680	Post HT (1)	1.32	1.67	20.36
12680	Post Pitch (1)	1.4	1.67	15.34
12680	Post HT (2)	1.41	1.67	15.57
12680	Post Pitch (2)	1.49	1.72	13.91
12680	Post HT (3)	1.49	1.70	12.53
12680	Post Pitch (3)	1.51	1.70	11.82

Table 9: Porosity and skeletal density results from water immersion for Panel 12681.

Sample	Cycle	Bulk Density (g/cc)	Skeletal Density (g/cc)	% Porosity
12681	Post Cure	1.49	1.54	3.14
12681	Post Carb	1.36	1.76	23.08
12681	Post HT (1)	1.36	1.67	18.22
12681	Post Pitch (1)	1.41	1.67	15.45
12681	Post HT (2)	1.43	1.68	14.78
12681	Post Pitch (2)	1.50	1.69	11.33
12681	Post HT (3)	1.49	1.70	12.47
12681	Post Pitch (3)	1.52	1.70	10.61

Table 10: Average porosity and skeletal density results from water immersion for Panels 12680 and 12681.

| Sample	Cycle	Bulk Density (g/cc)	Skeletal Density (g/cc)	% Porosity
average	Post Cure	1.48	1.55	4.56
average	Post Carb	1.34	1.76	24.35
average	Post HT (1)	1.34	1.67	19.29
average	Post Pitch (1)	1.40	1.67	15.39
average	Post HT (2)	1.42	1.68	15.18
average	Post Pitch (2)	1.49	1.71	12.62
average	Post HT (3)	1.49	1.70	12.49
average	Post Pitch (3)	1.51	1.70	11.22

These results show the porosity of the panels throughout three densification and heat treatment cycles in the same manner as in Task 1, and also the two processing steps before densification began. The first stage that was analyzed was initial curing. Because only mild heat is applied, the matrix polymerizes but does not begin to densify and crack. This results in very low porosity. The results above indicate this fact for each panel. In both cases, the porosity is less than 6%. However, the skeletal density is also very low, and, as a result, the mechanical properties of the matrix would be very poor. The following steps of the process attempt to greatly improve the thermal and mechanical properties of the panels [2,3,18]. The Figure below shows an image of the cross section of panel 12680 after it has been cured.
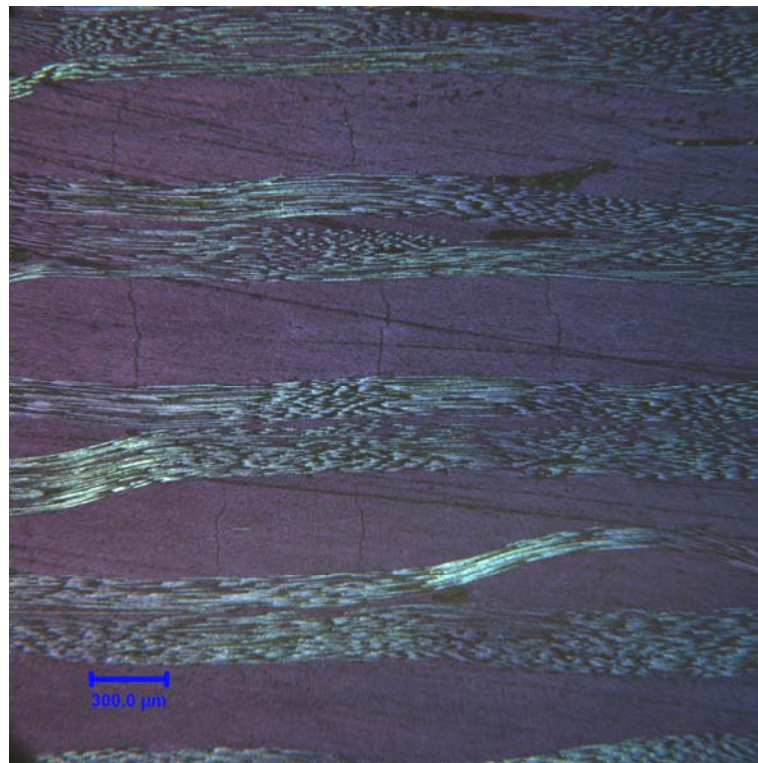
Figure 26: Cross section of panel 12680 following its initial cure taken at 50x magnification.

As the picture indicates there are very few cracks or voids in the matrix. This is also verified from the bulk density results. After the composite is cured, the bulk density is very close to the skeletal density. This means that there is very little porosity at this point in the process.

The second step in the process is the post cure followed by carbonization, which are done together to save time. This is a very long heating process which slowly takes the composite to about 1000° C. During this step the matrix carbonizes, causing it to densify and shrink drastically. However, because the carbon fibers do not shrink with the matrix, the result is huge voids and cracks forming within the matrix [19]. If the matrix shrinks uniformly in the thickness direction, the entire composite can actually shrink. This would be ideal because the matrix would not need to crack form open porosity. However, this shrinkage of the composite is very limited, especially later in the densification process. The material becomes much denser, but the newly formed voids cause the porosity to remain high. In Tables 8, 9, and 10 above, the panels were noted to have porosity levels near 25% following the carbonization step. This is illustrated very clearly in the figure below, showing the cross section of the same panel, 12680, following carbonization.
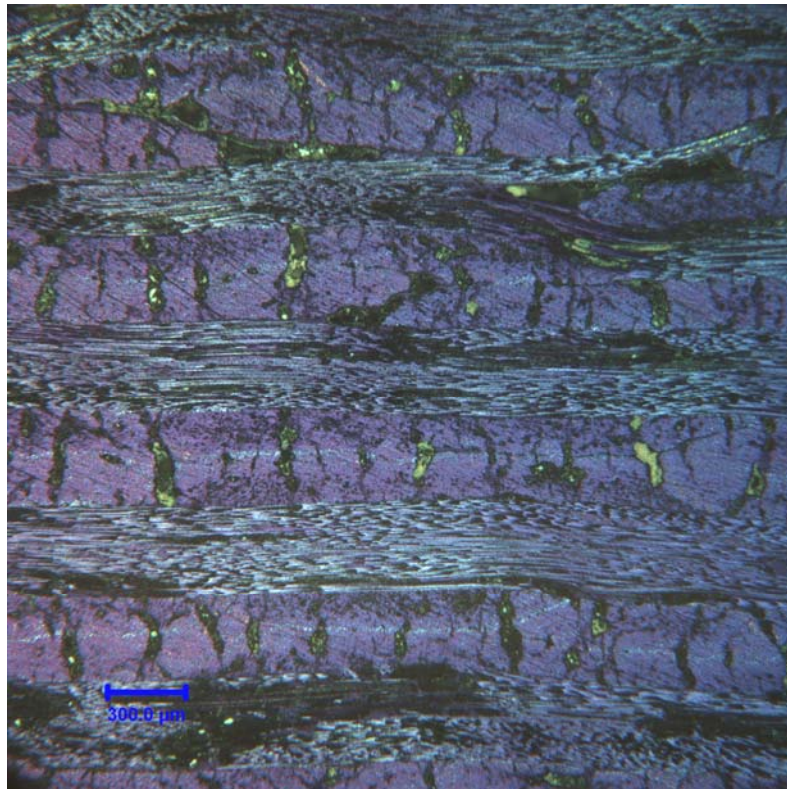
Figure 27: Cross section of panel 12680 following carbonization at 50x magnification. (Note: the yellow color is from the epoxy mount holding the sample in place).

These results show that the large oval-shaped pores are initially created during carbonization of the prepreg. This will most likely be an area of great emphasis during future studies. In addition to the formation of cracks and voids, the prepreg matrix material has drastically changed here. It has carbonized resulting in a material with a much higher skeletal density. According to the results above the density increased from 1.55 g/cc to about 1.76 g/cc. Also the thickness of the panel decreased from about 0.157 in to about 0.142 in. The bulk density decreased from about 1.46 g/cc to about 1.32 g/cc due to the formation of open porosity. The decrease in composite thickness minimized this effect; however, there is still a significant decrease in bulk density.

Once carbonization was completed, the densification process could begin. This consisted of the same three heat treatment and pitch impregnation cycles performed and analyzed in Task 1. The first stage of densification was the first high temperature heat treatment. During this stage the skeletal density and the porosity decreased. Bulk density remained the same, which means that essentially no material was lost due to off-gassing. Initially an increase in porosity was expected due to further matrix shrinkage and cracking, but the data do not support this hypothesis. After further analysis of the results, a different explanation was proposed.

A substance found within the carbonized matrix (proprietary information, details left out) has a tendency to fuse and sinter together at elevated temperatures. Because the particles within the pores can join together, the pore structure can drastically change. Below is a comparison between the cross section photos of panel 12680 after carbonization and after heat treatment.
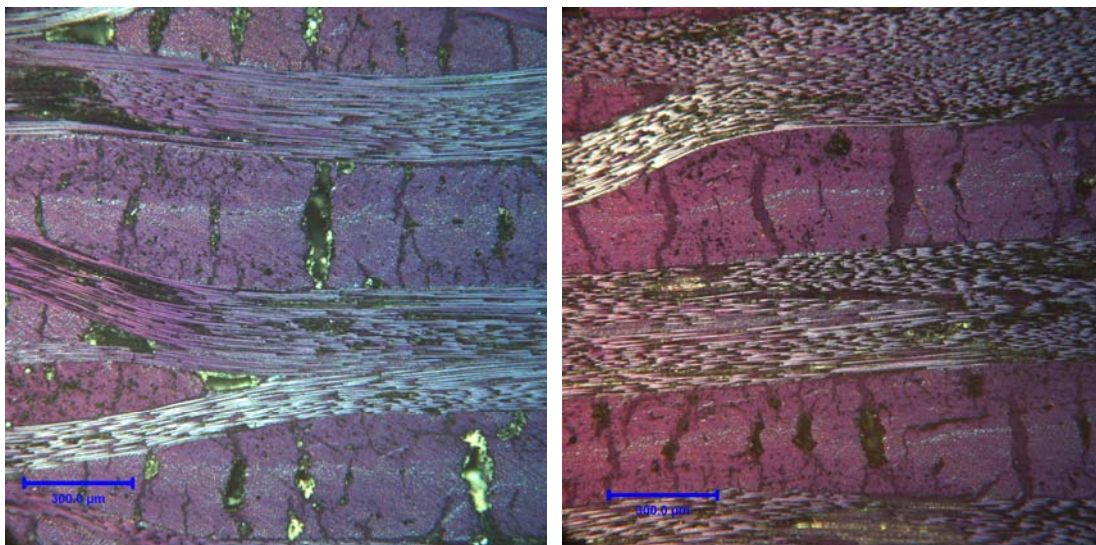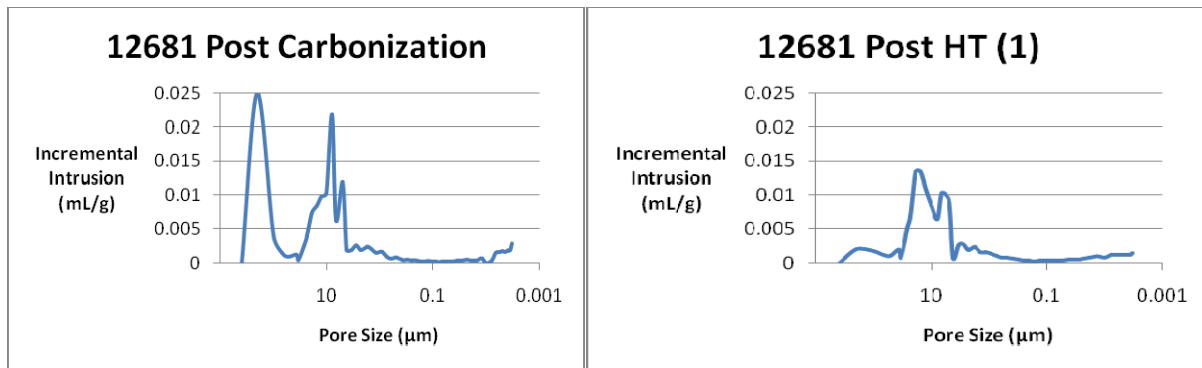
Figure 28: Comparison of pore size between carbonization (left) and heat treatment (right) both at 100x magnification.

The carbonized sample on the left has very large and deep pores. The depth is noted by the yellow epoxy mount visible through the large open pores. The heat-treated sample on the

right also has some large oval pores, but significantly smaller than those after carbonization. This change in pore size is also shown below with a comparison of the pore-size distribution before and after heat treatment. The distributions at each stage of processing will be analyzed in depth later in this report, but it is necessary to note this now.

Figure 29: Pore-size distribution comparison of panel 12681 before and after the first heat treatment.

As the pore-size distribution graphs show, after carbonization there is a significant volume of pore space created by large pores of about 100 µm. After the first heat treatment to 1650° C there is much less open porosity, and the average pore diameter is about 10 µm. From this distribution data and the microscope images, the experimentally measured porosity and skeletal density values have been verified. The initial conclusion that was made for this case was that the matrix did in fact shrink, but instead of additional cracking, the result was that the entire composite thickness decreased in the direction not controlled by fiber reinforcement. However, the thicknesses were compared before and after heat treatment, and there was a negligible decrease from about 3.6 mm to 3.5 mm. Below is a graph showing the change in composite thickness over the entire process.
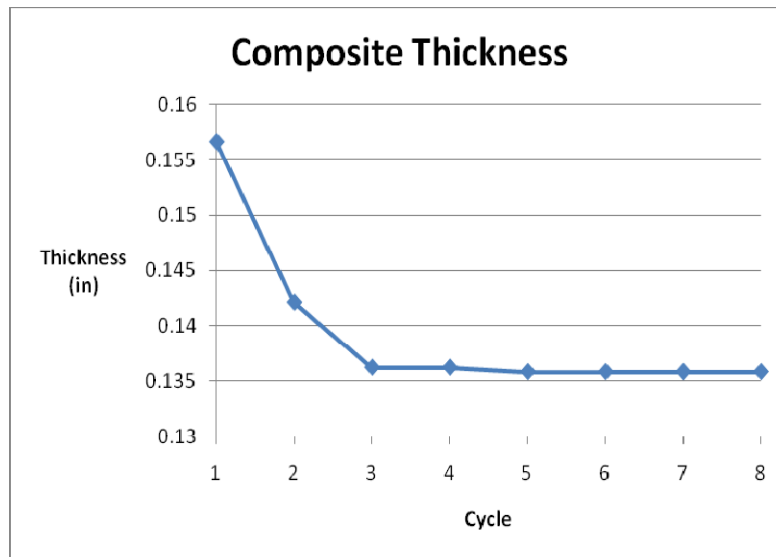
Figure 30: Graph of changing composite thickness as the matrix material densifies for panel 12680.

The overall changing size of the composite must be taken into account when analyzing changes in porosity and density. In the case of Panel 12680 shown above, the matrix shrinks a significant amount during carbonization, a very small amount during the first heat treatment, and essentially no more thoughout the process. The approximate 3% reduction in composite thickness during the first heat treatment is not a valid explanation for the reduction in both porosity and density.

Because the composite thickness decreased such a small amount, other possibilities were investigated as to the overall effect of the first heat treatment. As the the pore structure changed due to the temperature during heat treatment, closed porosity was created. Also the entrance size of open the pores decreased. Closed porosity greatly affects skeletal density, as opposed to open porosity, so this accounts for the decrease in skeletal density as well as the decrease in open porosity. Unfortunately, our methods of porosity analysis cannot determine closed porosity

[1,20]. This behavior during the first heat treatment is very unique, and it does not occur during the second and third heat treatments. The behavior during these processing steps is noted below as well as the overall trend in porosity and density. Also additional microstructure photographs of samples from Task 2 are shown in Appendix B.

At this point, the results of Task 2 are very consistent with the results from Task 1. Below is a graph showing the trend in porosity throughout processing for panels 12680 and 12681.
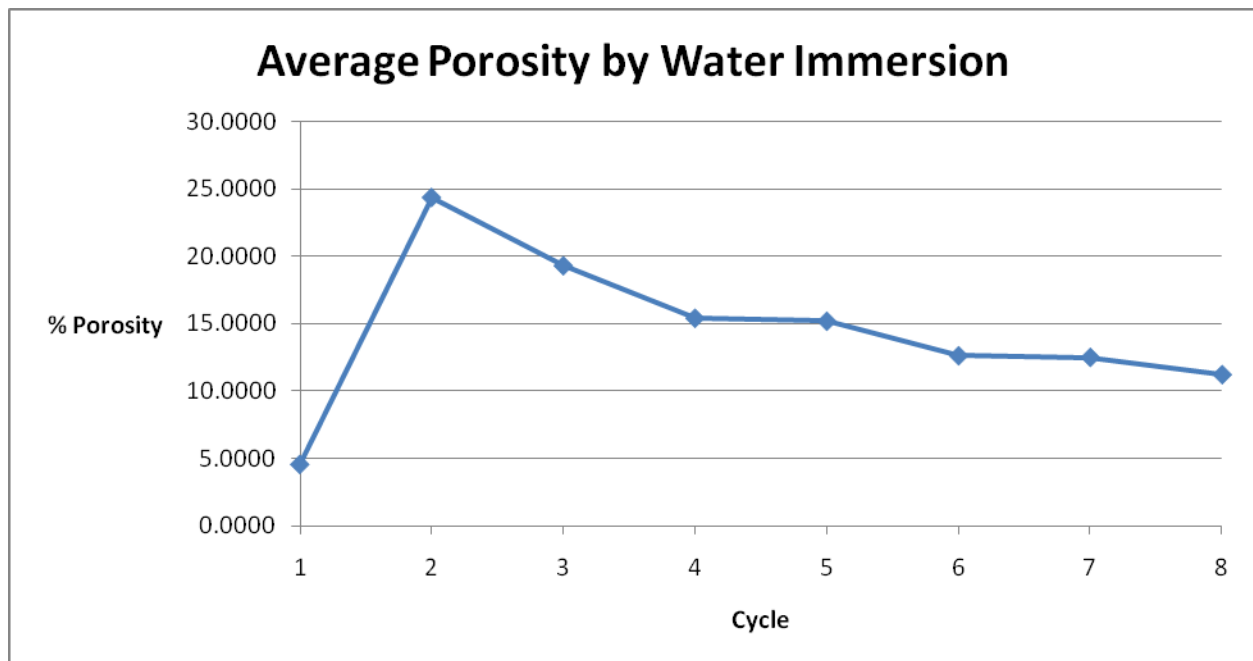

Figure 31: Average open porosity for Panels 12680 and 12681 determined by boiling water immersion.

As was discussed above the porosity begins very low following curing, and it then jumps to 25% following carbonization. Once it is taken to high temperature during heat treatment, the matrix restructures and the porosity decreases to around 20%. At this point the trend is

compared to that found during Task 1 of this study. As is expected there is a steady decrease in porosity ending up near 10%. However, this line does not have a constant slope. This is because the porosity tends to decrease noticeably when the matrix is impregnated with pitch. The pitch is added precisely for that purpose, to fill the voids left from the heat treatment. The porosity decrease is noted in the graph at cycles 4, 6, and 8 when pitch is being added. During the heat treatment steps, the matrix further densifies, but more voids are opened due to matrix shrinking. As a result, the porosity rate of decrease is much greater during the pitch impregnation cycles. The heat treatment steps are noted in the graph above at cycles 5 and 7. Cycle 3 is the first heat treatment, but the porosity decreases at a greater rate than the subsequent heat treatments. This first heat treatment yielded unique results, and possible explanations for this difference were stated above.

The trend of decreasing porosity during densification during Task 2 shown above is very similar to that in Task 1. In the graph below the trend found during Task 1 is added into the graph above so that the consistency can be observed.
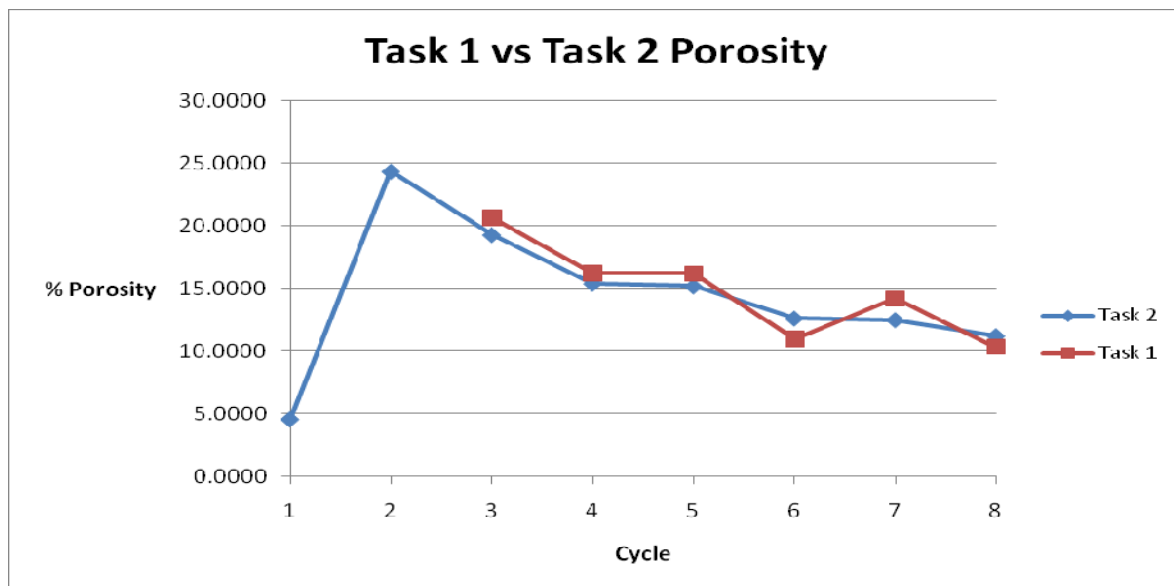
Figure 32: Porosity results from Task 1 and Task 2 found by boiling water immersion.

The panel tested in Task 1 and the panels tested in Task 2 were densified using the same method, and the results correlate very closely. There are small differences noted in the graph above, but the trend is consistent. The trends from panels 12680 and 12681 were also compared to further investigate the amount of porosity variation between panels. Below is a graph comparing these two panels.
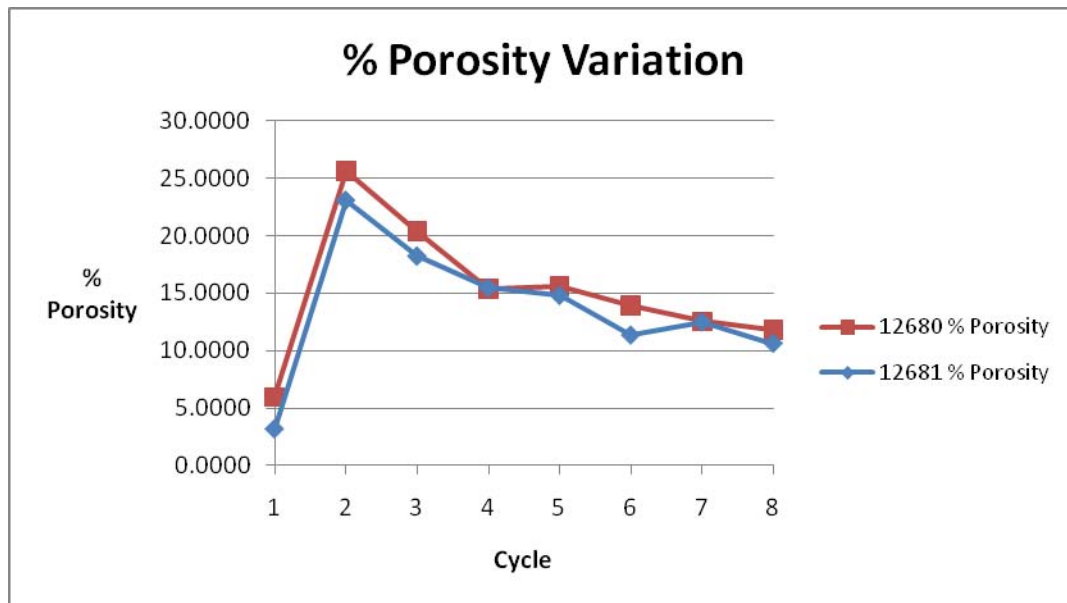

Figure 33: Porosity variation between panels 12680 and 12681.

As is shown by the graph, the trends are very consistent between the two panels. There are minor differences in porosity values, but overall they behave in the same manner. The location with the most variation is the second pitch cycle followed by the final heat treatment, cycles 6 and 7. Based on the specific pore shapes and sizes, pitch impregnation can be more or less successful at times. The second pitch cycle for panel 12681 was very successful and decreased the porosity by about 4%. However, when a large amount of pitch wicks into the

voids in the matrix, the following heat treatment will also be more effective as it densifies the

new material and opens up more porosity. This is why the porosity comes back up to about 12%.

      The water immersion results also yielded skeletal density values which behaved similarly

to what was expected from Task 1. Below is a graph showing the overall trend in skeletal

density compared to bulk density.
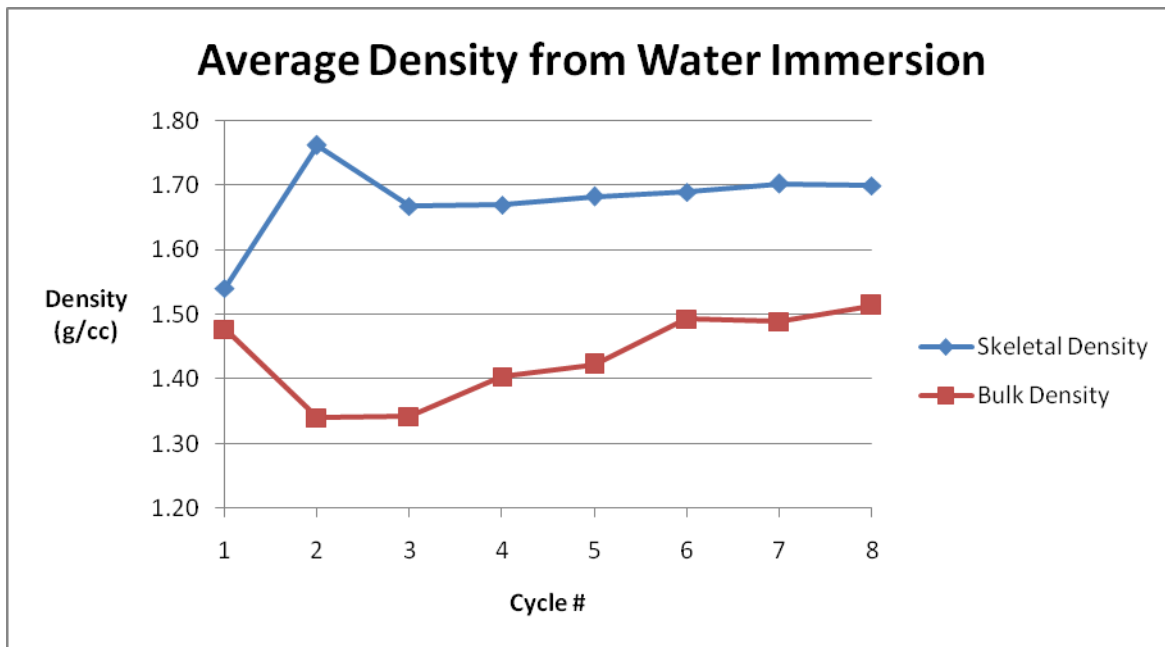
Figure 34: Average density for panels 12680 and 12681 determined by boiling water immersion.

      The inital two points in this graph behave just as was discussed above. After the panel

was cured, there was very little porosity, but the density was also very low. The skeletal density

jumped up once the matrix was carbonized to above 1.75 g/cc; however, it was still very porous

with a low bulk density, and the composite lacked the structure for ideal properties. The matrix

was restructured during the first heat treatment, which brought the density value back down to

what was expected based on Task 1. At this point the trend continued consistently with what had

been seen previously. Below is a graph of the skeletal density values from Task 1 compared to

those from Task 2. Also Figure 36 compares the variation in densities between Panels 12680
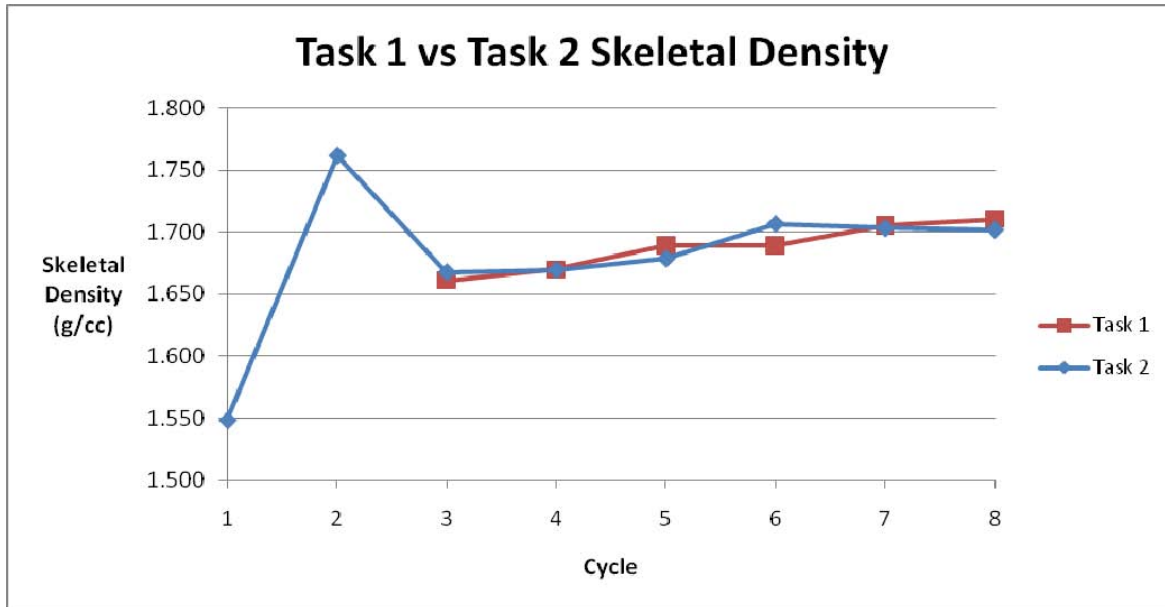
and 12681.

Figure 35: Skeletal density results from Task 1 and Task 2 found by boiling water immersion.
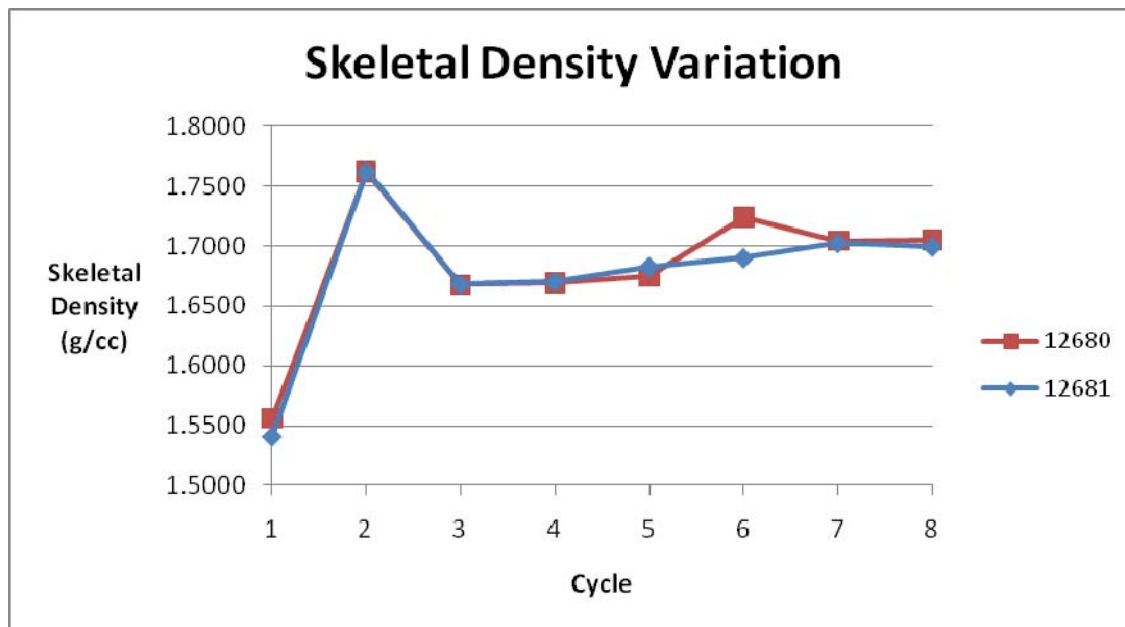
Figure 36: Skeletal density variation between panels 12680 and 12681.

The skeletal density trends are very consistent between Task 1 and Task 2. The effectiveness of each densification cycle will vary somewhat for each panel as is seen most clearly at cycles 6 and 7. Figure 32 shows a similar difference in the porosity values between the same cycles. However, these differences are relatively small, and the overall increase in density is consistent between the Task 1 and Task 2 panels. The variation is also minor between the two panels from Task 2. This correlation is shown above in Figure 36. This graph also shows some strange results during the second pitch cycle and final heat treatment. The issue appears to be from panel 12680. Based on the data, the success of the second pitch impregnation cycle was above average. The skeletal density spiked to about 1.73. Also there was significant weight gain as is seen by the bulk density change in Figure 34. If a large amount of pitch is able to penetrate the open porosity during the pitch impregnation cycle, the following heat treatment should also greatly affect the new matrix material. This is also shown in the Figure 36 above. The final heat treatment densified the new pitch that successfully impregnated the composite. This restructured the matrix, and the density came back down significantly taking into account additional formation of open and closed porosity.

The final pitch densification yielded similar porosity and density results as was seen during Task 1. Water immersion found porosity levels around 10% and skeletal density just over 1.711 g/cc. This verifies a drastic improvement throughout densification; however, the overall goal is to be able to optimize these values, further minimizing porosity and maximizing skeletal density. Below is a microstructure photo of a sample from panel 12680 after final densification. This picture illustrates how the large oval shaped pores have significantly decreased in size from the beginning of densification. For more Task 2 microstructure photographs, see Appendix B.
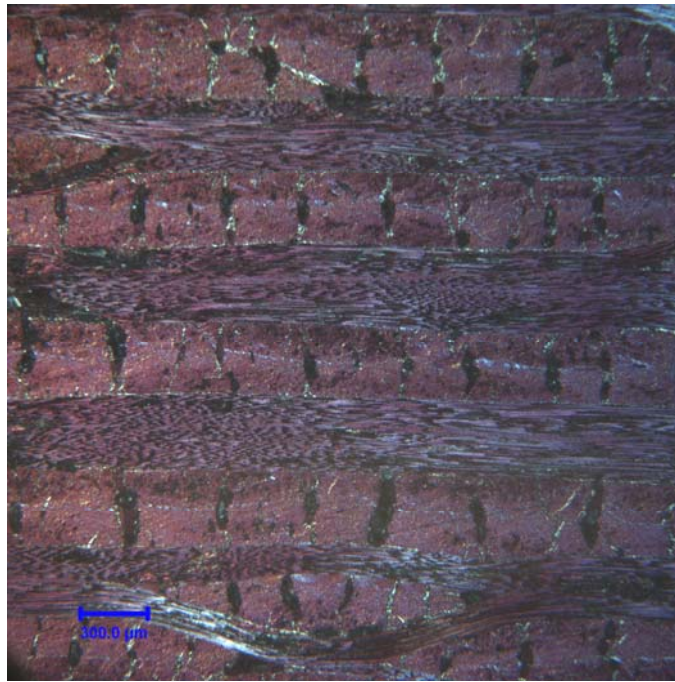
Figure 37: Panel 12680, Post Pitch (3) at 50x magnification.

5.2 Mercury Porosimetry Results

The Task 2 panels were evaluated at each stage of fabrication and densification by the

mercury porosimeter as well as by boiling water immersion. This was done for verification of

the water immersion results, but also to obtain pore-size distribution graphs, which can only be

obtained by this method [1,20]. During Task 1 the porosimeter resulted in similar trends as was

seen by water immersion, verifying the overall behavior of the composite during densification.

However, some differences were also noted. It was concluded that the porosimeter values can be

less consistent due to several extra variables that must be taken into account. These include, but

are not limited to, the size of the sample compared to the size of the penetrometer, the ability of

the high pressure to open up closed porosity that the water immersion method does not account

for, and other inherent possibilities of error within the porosimeter [1,20]. However, the

porosimeter can still yield overall trend data resulting in valid conclusions for the composite

densification process.

The porosity results from the mercury porosimeter are displayed in the tables below. The

same porosimeter from Task 1 was used for Task 2, and all the settings and procedures remained

the same as well.

Table 11: Porosity results from Hg porosimetry for Panel 12680.

Panel	Sample	% Porosity
12680	Post Cure	8.48
12680	Post Carb	33.11
12680	Post HT (1)	18.95
12680	Post Pitch (1)	14.95
12680	Post HT (2)	12.62
12680	Post Pitch (2)	13.01
12680	Post HT (3)	10.72
12680	Post Pitch (3)	11.22

**Table 12: Porosity results from Hg porosimetry for Panel 12681.**

Panel	Sample	% Porosity
12681	Post Cure	7.62
12681	Post Carb	22.86
12681	Post HT (1)	18.52
12681	Post Pitch (1)	18.32
12681	Post HT (2)	14.73
12681	Post Pitch (2)	14.36
12681	Post HT (3)	13.18
12681	Post Pitch (3)	8.70

Table 13: Average porosity results from Hg porosimetry for Panels 12680 and 12681.

Panel	Sample	% Porosity
average	Post Cure	8.05
average	Post Carb	27.98
average	Post HT (1)	18.73
average	Post Pitch (1)	16.63
average	Post HT (2)	13.67
average	Post Pitch (2)	13.69
average	Post HT (3)	11.95
average	Post Pitch (3)	9.96

The mercury porosimetry results show similar porosity trends for the first two steps of processing. Once the panels are cured the open porosity values are very low. The porosimeter values are greater than those given by water immersion, around 8%. It is understandable that the mercury porosimeter would yield higher porosity values when the matrix is weakest because the extreme pressure will more easily break open the closed porosity. The closed porosity within the cured matrix could easily account for 3%-4% increase in overall porosity as was observed in this case.

Similar to what was seen previously, the porosity spikes after the matrix is carbonized yielding porosity values above 22% and as high as 30% for panel 12680. From this point, a similar change in porosity occurs after the first heat treatment step. The porosity decreases with very little change in sample thickness. This is very consistent with the data gathered from water immersion analyzed previously. Below is a graph showing the trend of open porosity throughout processing found by mercury porosimetry for panels 12680 and 12681.
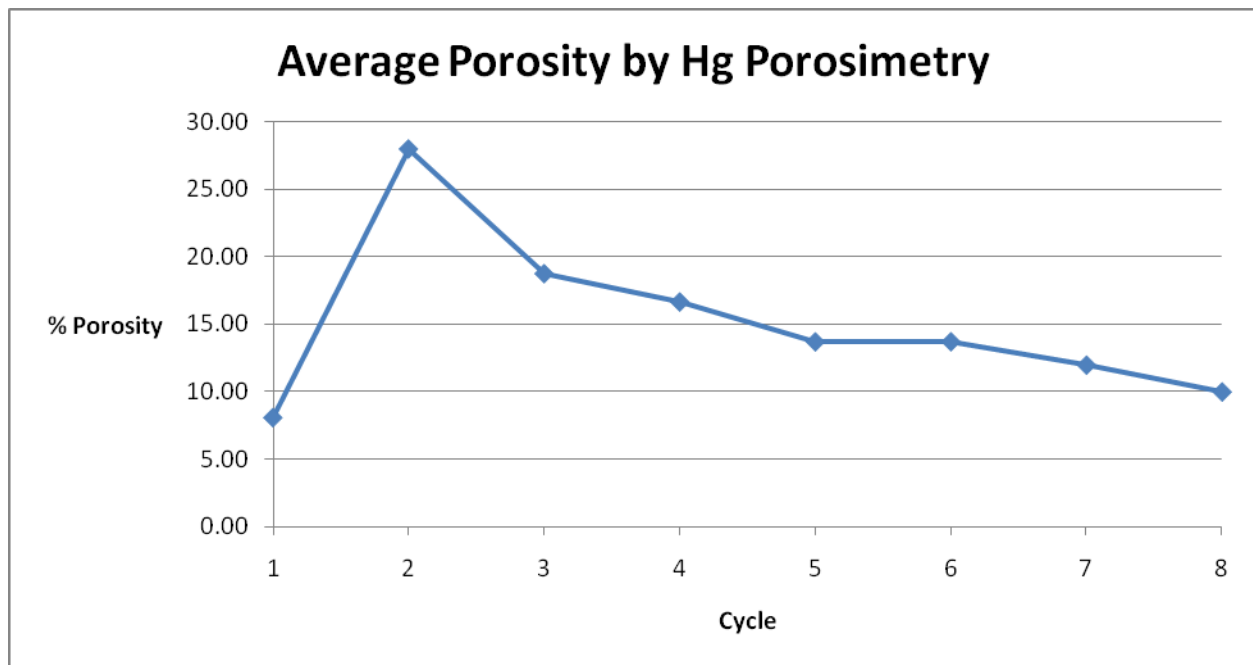
Figure 38: Average porosity for Panels 12680 and 12681 determined by mercury porosimetry.

This graph displays similar results for the first three steps in processing and a decreasing overall trend. Also the final resulting porosity is similar when measured by both water immersion and mercury porosimetry. However, the rate at which the porosity decreases for each heat treatment and each pitch impregnation cycle varies between the two porosity test methods. Below is a graph comparing both methods of porosity testing.
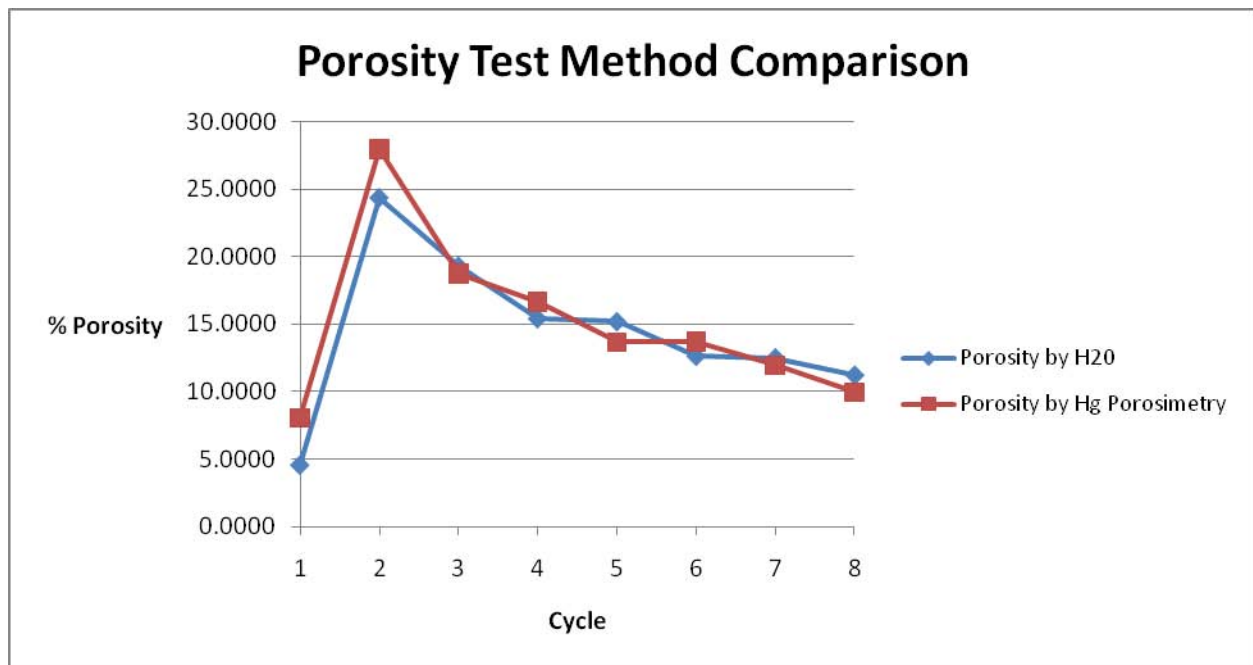
Figure 39: Comparison of the porosity trends found by water immersion and Hg porosimetry.

5.3 Explanation of Variation

This odd trend as measured by the mercury porosimeter is not verified by the water immersion test method, and it is also not what was expected based on the common understanding of carbon matrix behavior at high temperatures during heat treatment. Below are a graph and table showing the variation found between the water immersion tests and the mercury porosimetry for Task 2.

Table 14: Differences found between water immersion and mercury porosimetry with calculated variation.

Cycle #	Sample	H2O Porosity	Hg Porosity	Difference	Variation (%)
1	Post Cure	5.97	7.62	1.65	27.64
2	Post Carb	24.35	27.98	3.63	14.91
3	Post HT (1)	19.29	18.73	0.55	2.87
4	Post Pitch (1)	15.39	16.63	1.24	8.05
5	Post HT (2)	15.18	13.67	1.50	9.90
6	Post Pitch (2)	12.62	13.69	1.07	8.45
7	Post HT (3)	12.50	11.95	0.55	4.37
8	Post Pitch (3)	11.22	9.96	1.26	11.23
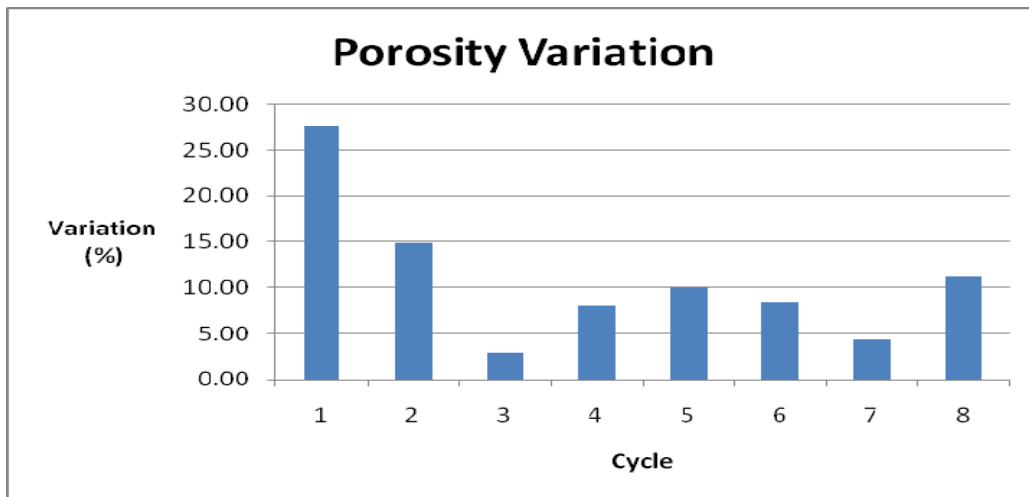
Figure 40: Variation percentage between mercury porosimetry and water immersion porosity tests for Task 2.

The most interesting feature of this variation is the location of the greatest difference during the densification process. The mercury porosimeter does not show a decrease in porosity following pitch impregnation; however, there may be a reasonable explanation for this unusual data. As has been noted previously, it is suspected that the high pressure from the mercury porosimeter can break open some of the closed porosity, which the water immersion cannot measure. This is most likely to happen when the matrix is at its weakest point, which would

occur directly after pitch is added before the subsequent heat treatment cycle. Once the matrix is heat-treated it hardens further and would be more resistant to breaking open at high applied pressure.

Hypothetical data were determined assuming the following scenario. If high pressure from the mercury porosimeter broke open closed porosity and included that in its porosity measurement, this would most likely occur at cycles 4 and 6 on the graph above, which are the second and third pitch impregnation steps, when the new additionsto the matrix are weakest. When comparing water immersion to mercury porosimetry, the only porosity that can be compared is open porosity because that is all that water immersion can measure. To account for this, 2%-3% porosity was subtracted from the porosimeter measurement at cycles 4 and 6 to account for a small amount of closed porosity which opened up during testing. Once this subtraction was made, the new adjusted data were graphed. This is shown below in Figure 41.
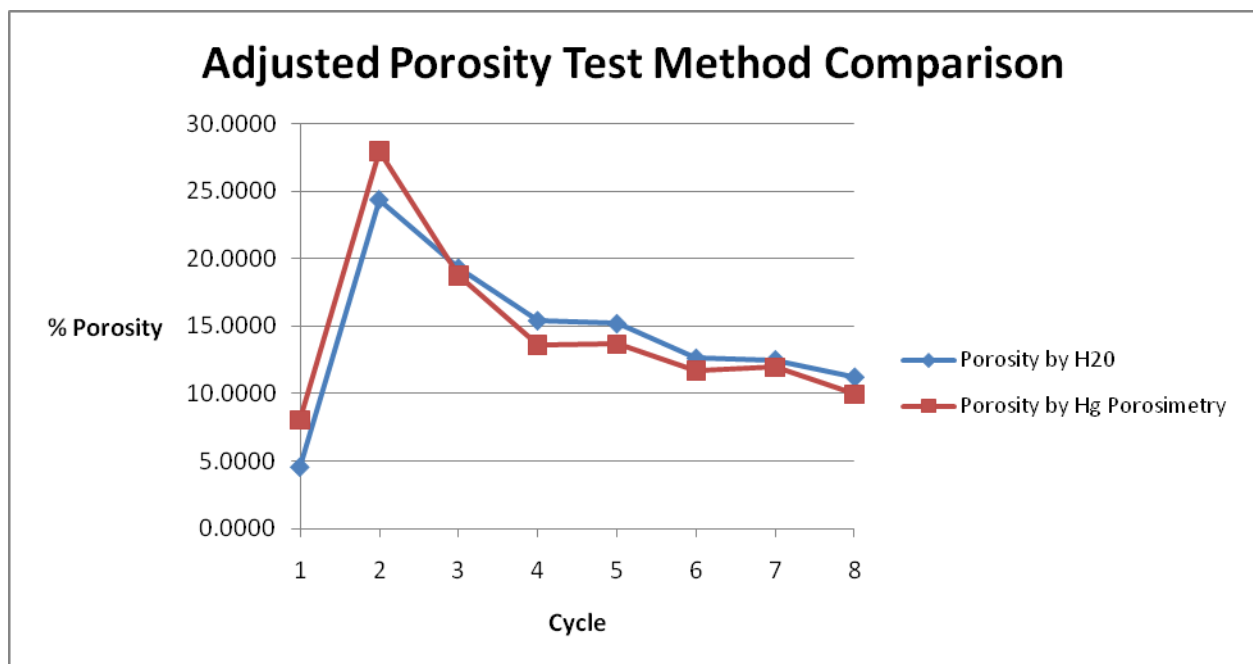
Figure 41: Porosity comparison of water immersion and mercury porosimetry adjusted for possible closed porosity measured by the porosimeter.

Once this adjustment is made, only open porosity is being compared, and there is a better sense of the consistency between the two test methods. This also changes the basic trend in the porosimeter data. There is now a greater decrease in porosity after pitch is added to the matrix, and no decrease when the sample is heat-treated. The overall porosimeter data are slightly less than the water immersion, which is understandable as well. The mercury is forced into the part by pressure up to 60,000 psi. It is likely that mercury can reach very small pores that the water cannot penetrate. This could account for the small difference in overall porosity throughout the graph.

5.4 Pore-Size Distribution

A similar analysis of pore-size distribution was conducted for Task 2 just as was done during Task 1. These data were gathered during the porosimetry tests on the same samples at each stage of the fabrication process. As in Task 1 the first set of distribution curves represents the incremental distribution of mercury. Each peak is a measured amount of mercury which successfully fills pores of a certain size. This pore-size is measured on the horizontal axis of each graph. The incremental pore-size distribution graphs for panels 12680 and 12681 are shown in Figures 42 and 43 below.
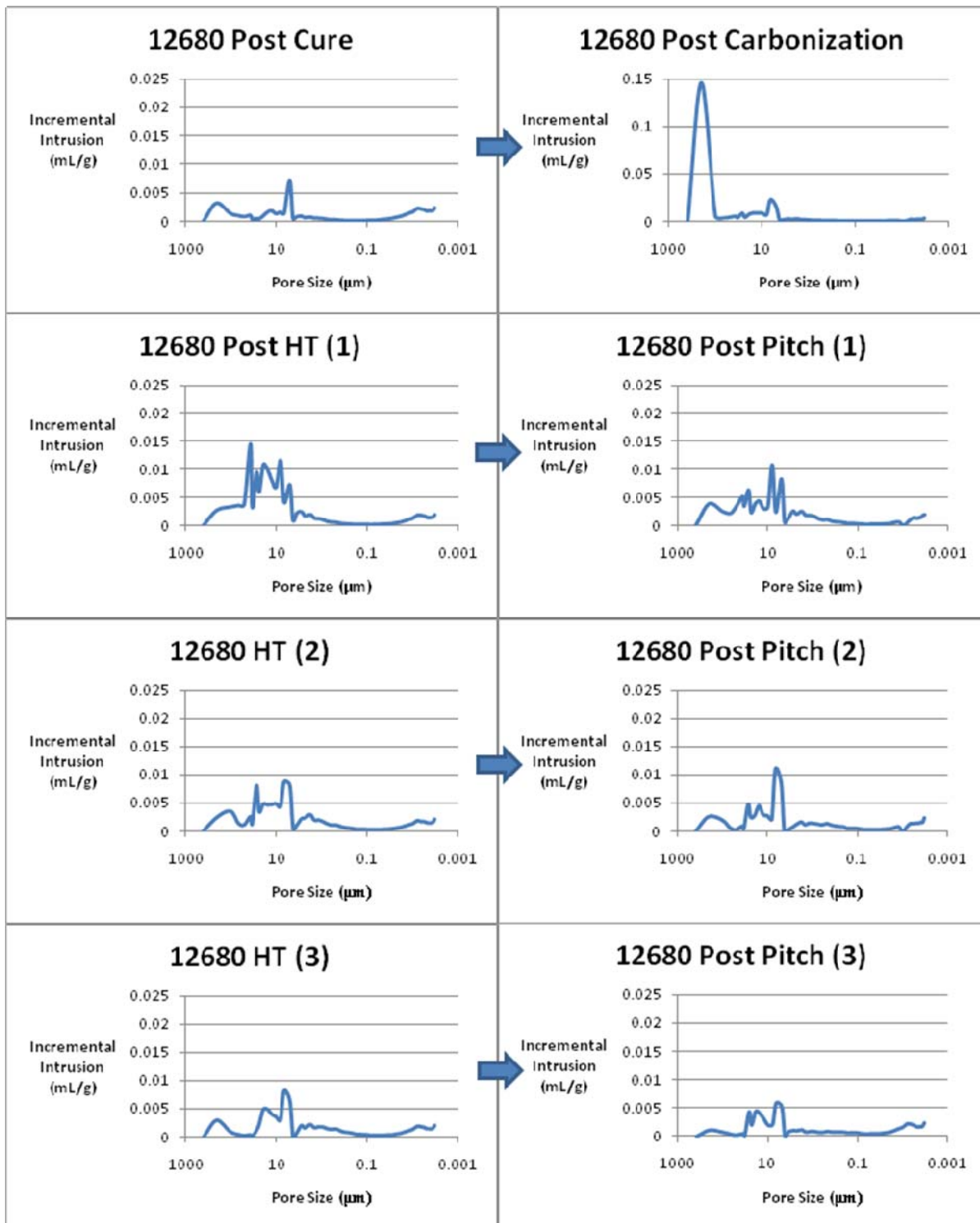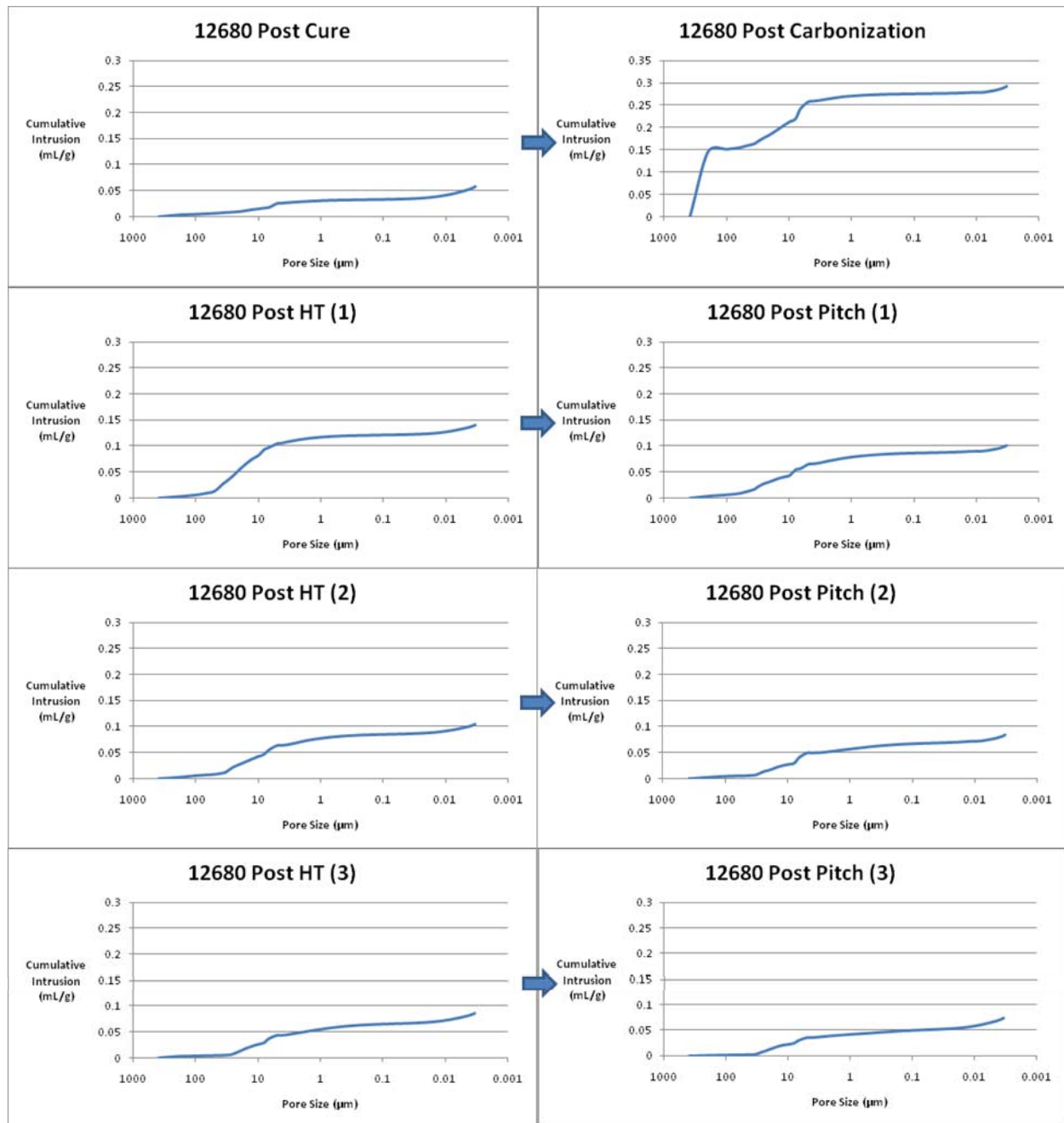
Figure 42: Pore-size distribution for each densification cycle of panel 12680. These graphs display the incremental intrusion of mercury corresponding to pore-size.
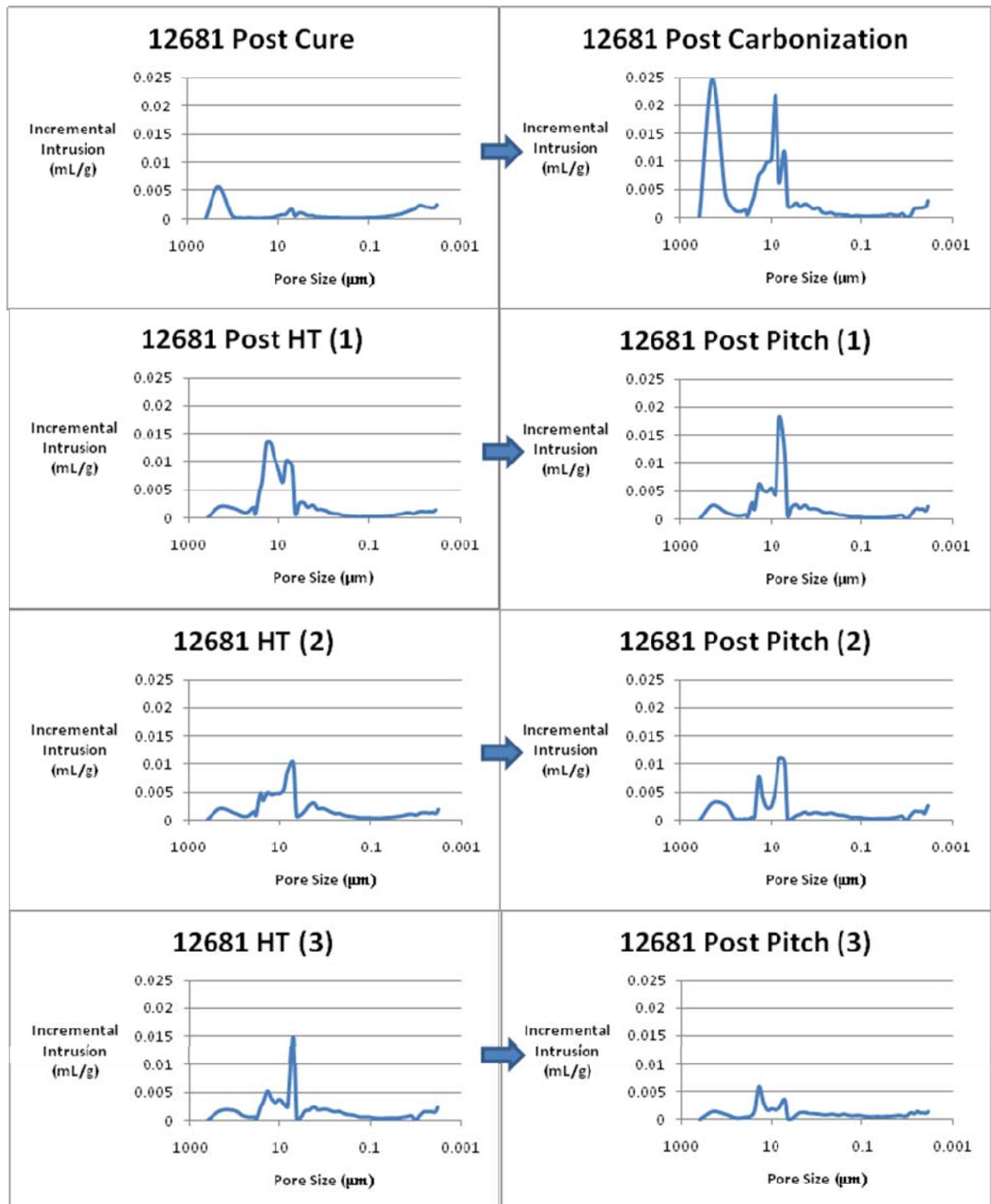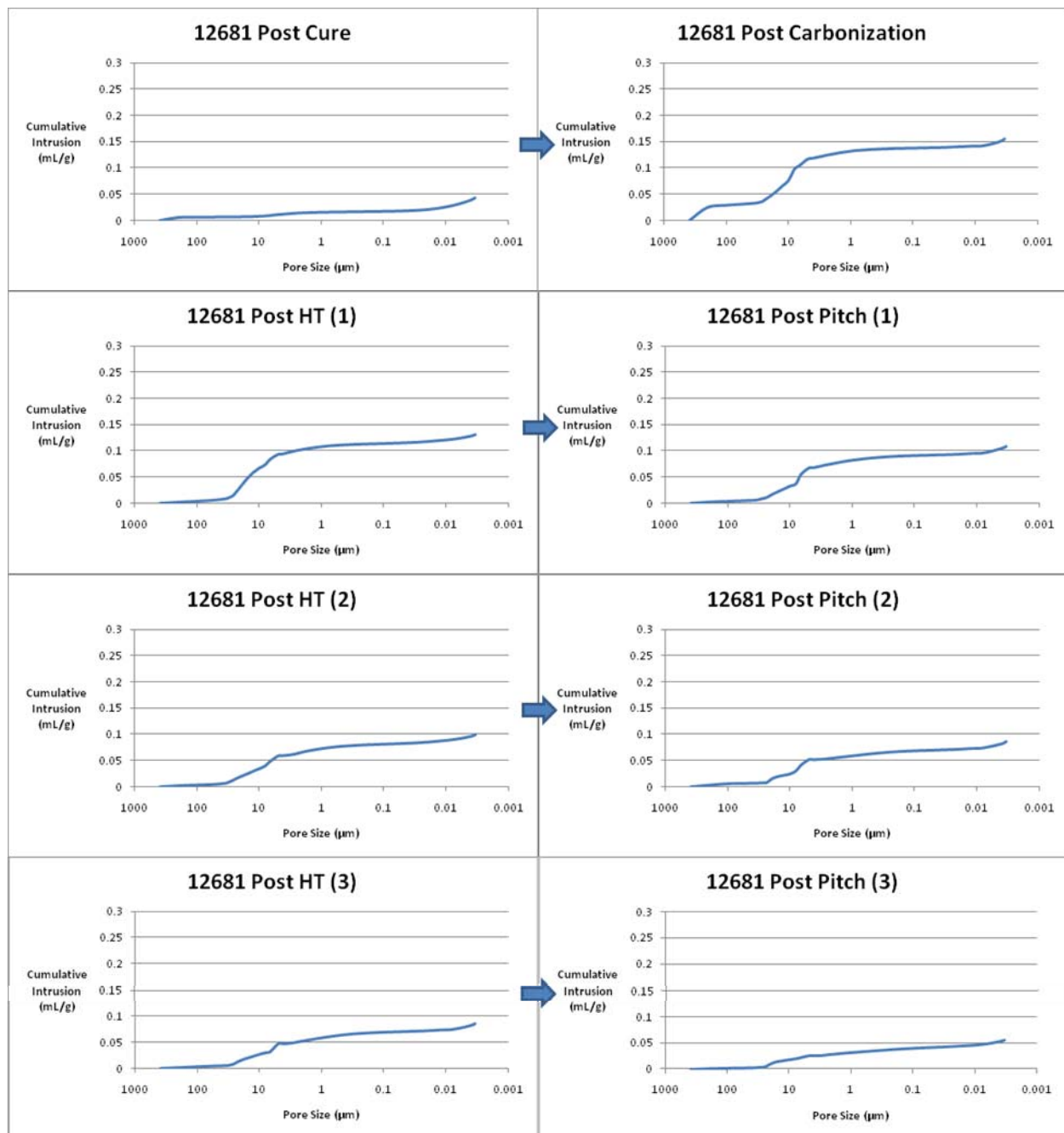
Figure 43: Pore-size distribution for each densification cycle of panel 12680. These graphs display the incremental intrusion of mercury corresponding to pore-size.

The graphs above demonstrate the decrease of open porosity throughout densification. They also show the results of carbonization on the cured phenolic composite. As is seen in the first plot, there is very little porosity in the composite after it is cured. This is represented by the very small peaks. The situation is drastically different after carbonization, however. The first large peak represents the large open pores between 100 μm and 1000 μm in diameter. Once the samples are heat-treated and the matrix restructures, the porosity comes back down to a reasonable level. At this point the trends are similar to what was seen in Task 1. Large peaks are reduced in size and peaks also shift to the right as pores are partially filled, increasing the number of smaller pores.

The second set of distribution curves shown below in Figures 44 and 45 represent the cumulative distribution of mercury as it successfully penetrates the open porosity. The horizontal axis still represents the sizes of the pores being filled, but the vertical axis shows the overall amount of mercury entering the sample.

Figure 44: Additional pore-size distribution plots for each denisification cycle of panel 12680. These graphs represent the cumulative intrusion of mercury corresponding to pore-size.

Figure 45: Additional pore-size distribution plots for each denisification cycle of panel 12681. These graphs represent the cumulative intrusion of mercury corresponding to pore-size.

The graphs above show the same results from a different perspective. It is important to note the overall height of each graph. This represents the total amount of mercury which penetrated the pores of each sample. As the porosity decreases throughout processing, the curve slightly shifts down and to the right. The lower curve represents less mercury filling pores, or in other words, less pore space for the mercury to fill. When the curve moves to the right, it signifies that the large pores are decreasing in size due to pitch densification.

One interesting feature noted on both types of distribution graphs is the small jump at the very end of the curve. The incremental distributions show the curves almost touching the horizontal axis, but at the end they increase again. The cumulative distributions show the curves almost leveling out, which means no more mercury is able to enter the sample pore space, but then there is a small jump in intrusion volume at the very end. This means that once the pressure reaches a certain amount, approximately 40,000 psi-60,000 psi, more mercury is able to be forced into the sample. Below the same type of distribution curve is plotted with pressure instead of pore size. One sample from panel 12680 was chosen as an example.
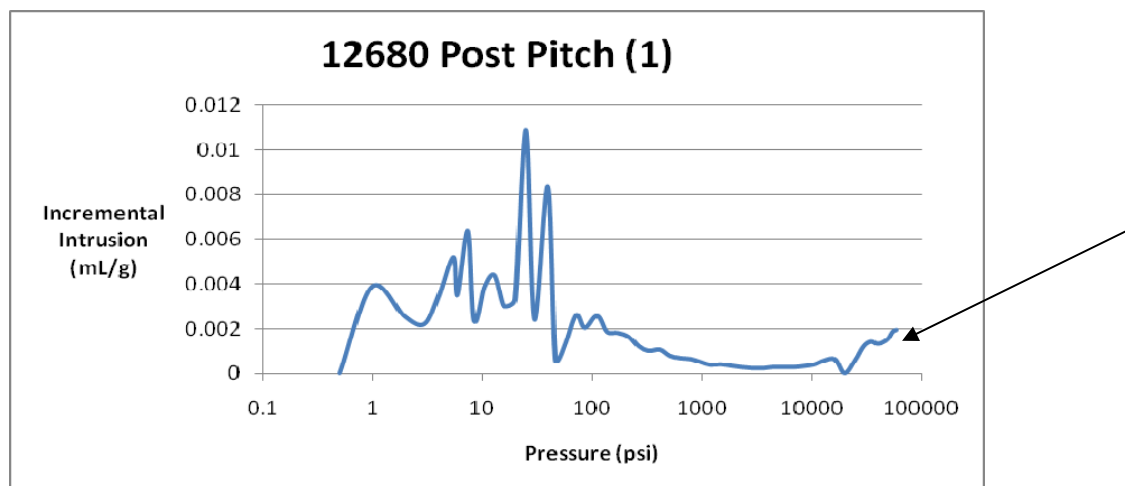
Figure 46: Incremental intrusion of mercury vs pressure for 12680 Post Pitch (1).
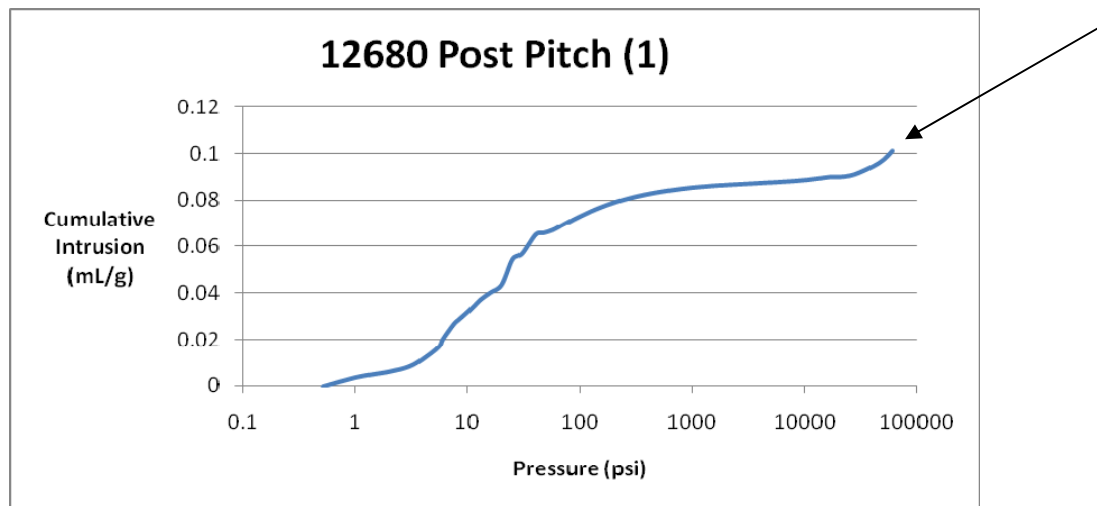
**Figure 47: Cumulative intrusion of mercury vs pressure for 12680 Post Pitch (1).**

There are two conclusions to draw from these data. The first possibility is that once the pressure is high enough, mercury can finally reach the smallest open porosity, which couldn't be reached previously. The second possibility is that once the pressure is high enough, the matrix structure fractures and closed porosity is opened. Based on this data and the comparison of water immersion and porosimeter results, it is likely that the small jump in mercury intrusion is partially due to both of these scenarios.

5.5 Flexure Test Results

Because flexural properties are affected by both the strength of the fibers and the matrix density and porosity, it is expected that the flexural strength and elastic modulus will improve as the porosity decreases and the density increases. Below is a table showing the change in Flexural Strength and Elastic Modulus from the second heat treatment to the end of densification. These same results are illustrated by the graphs in Figure 48.

Table 15: Summary of results from four point bend tests for panels 12680 and 12681.

Flexural Strength Average (psi)			
Sample	**HT(2)**	**HT(3)**	**PP(3)**
12680	19478.336	19894.810	21988.540
12681	20898.037	23895.434	23213.214
Average	**20188.186**	**21895.122**	**22600.877**
Modulus Average (psi)			
Sample	**HT(2)**	**HT(3)**	**PP(3)**
12680	8122787.877	8071267.008	9192285.460
12681	9097522.992	9808792.302	9740125.375
Average	**8610155.435**	**8940029.655**	**9466205.417**
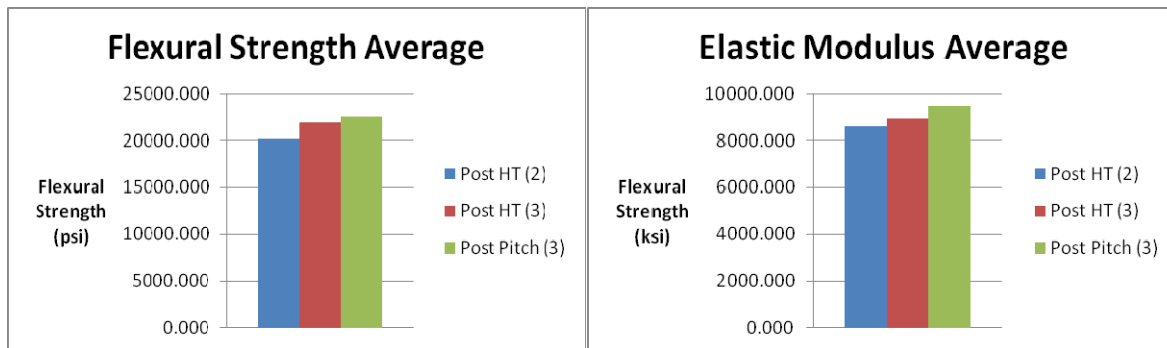
Figure 48: Steady increase in both flexural strength and elastic modulus from HT (2) to Post Pitch (3).

It was expected that the increase in flexural strength would correlate very closely with the overall increase in matrix density. Because of this, flexural strength may increase during a heat treatment cycle as well as a pitch impregnation cycle. As the matrix densifies, both due to heat treatment and the filling of voids, the strength will go up. As the matrix densifies, the load is transferred more effectively to each bundle of fibers, evenly distributing the stress throughout the composite. The average flexural strength is observed to increase more between Post HT (2) and Post HT (3), and less between Post HT (3) and Post Pitch (3). This is seen above in Figure 48.

Both heat treatment and the addition of pitch occur between the first two columns of the graph

resulting in a considerable increase in strength; however, there is less of an increase between the

second and third columns, where there is only the addition of pitch and no further heat treatment.

Throughout this densification process the elastic modulus should also increase slightly.

Both the overall density of the matrix and the structure of the matrix porosity will affect the

elastic behavior of the composite. As the sample becomes more dense and brittle, the elastic

modulus should increase. As the pores are filled in, the matrix becomes more resistant to cracks

forming, which can also increase the modulus of elasticity. As the graph above shows, the

elastic modulus increases throughout the densification cycles.

Panels 12680 and 12681 yielded very similar results. Figure 49 below shows the force at

the breaking point for both panels after the second heat treatment. The red and blue dots

represent the moment when the beam broke under load. The horizontal axis represents the

corresponding mid-span deflection of the beam while the vertical axis represents the load acting

on the beam. The lines represent the average progression of deflection as the load increased.

The force-deflection curves for each individual sample can be found in Appendix C. In each

instance the force deflection curve behaves linearly until failure occurs. From the slope of this

elastic region, the modulus is determined using Equ. 5. Figures 50 and 51 show the same graphs

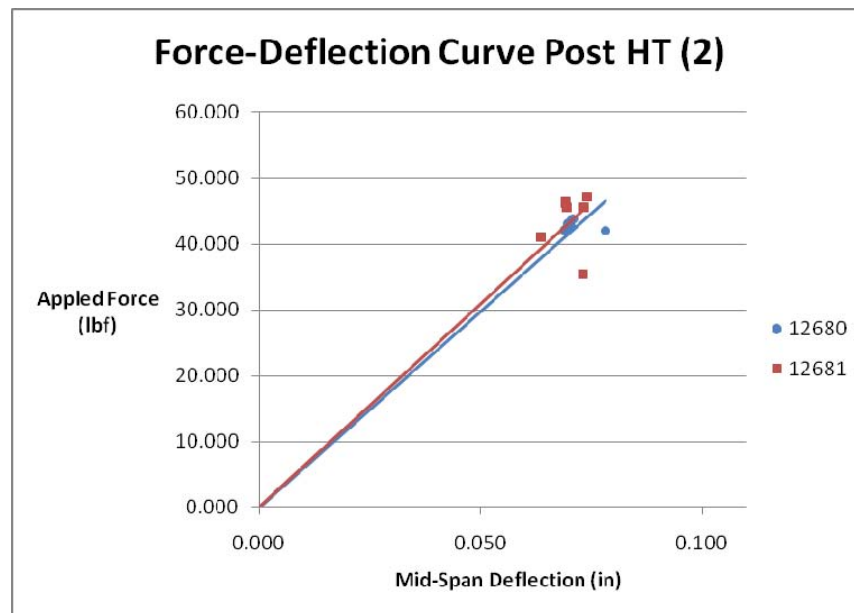for both panels following the third heat treatment and final pitch densification.

Figure 49: Force-deflection curve for both panels following the second heat treatment.
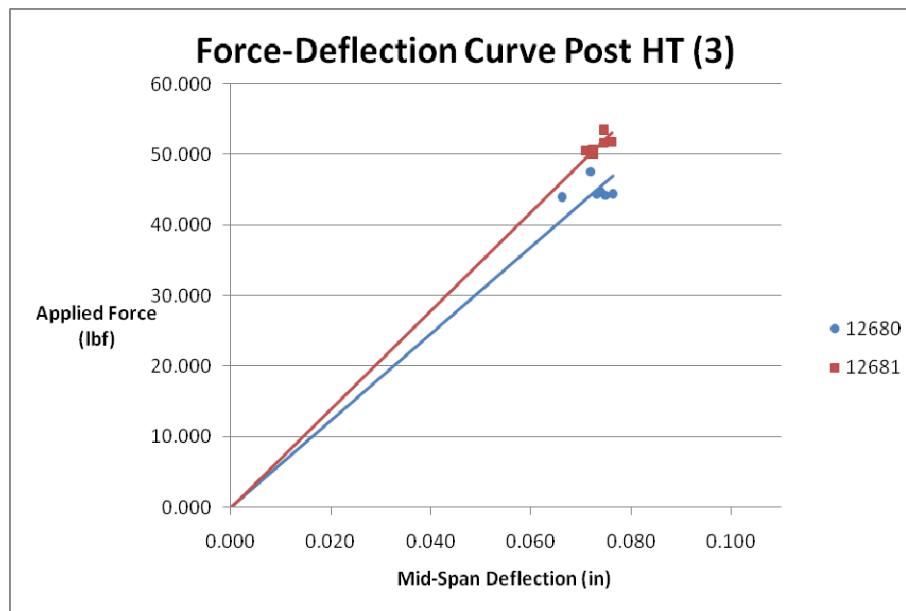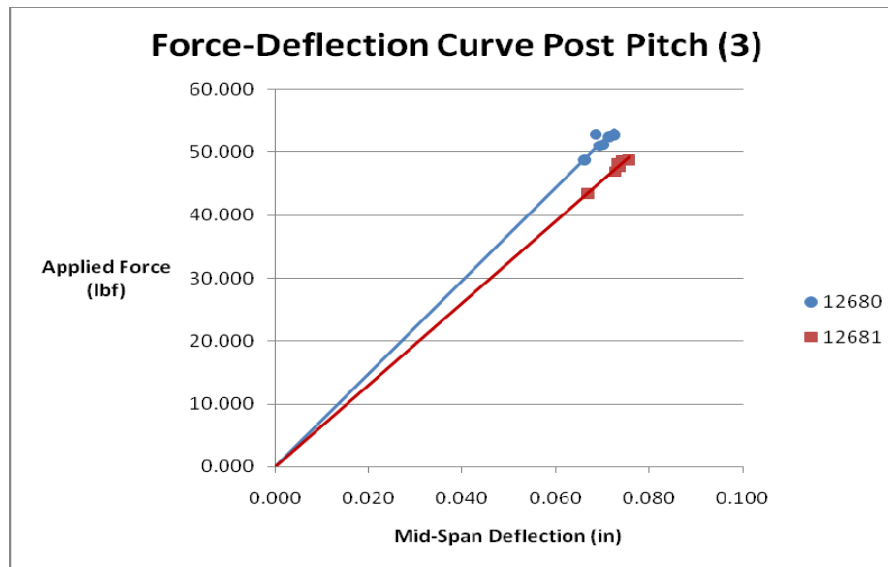

Figure 50: Force-deflection curve for both panels following the third heat treatment.

Figure 51: Force-deflection curve for both panels following the third pitch impregnation.
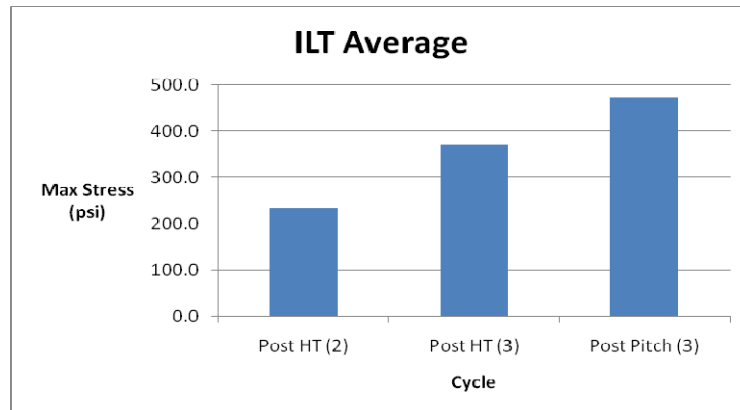
5.6 Interlaminar Tensile Test Results

Interlaminar tensile test were conducted at the same times during processing as the flexure tests. The goal was to observe the trend of interlaminar strength throughout densification. Below is a table summarizing the results for two different panels over three different cycles.

Table 16: Interlaminar tensile test results for panels 12680 and 12681.

ILT Average Stress (psi)			
Panel	HT(2)	HT(3)	PP(3)
12680	289.627	309.819	463.782
12681	178.256	430.339	479.241
Average	**233.942**	**370.079**	**471.512**

The graph below visualizes the consistent increasing trend between the different cycles. The first set of tests were conducted after the second heat treatment. One pitch densification

cycle follows this as well as a third heat treatment. At this point the second set of samples was tested. One pitch densification cycle followed this heat treatment, and then the third set of samples was tested.

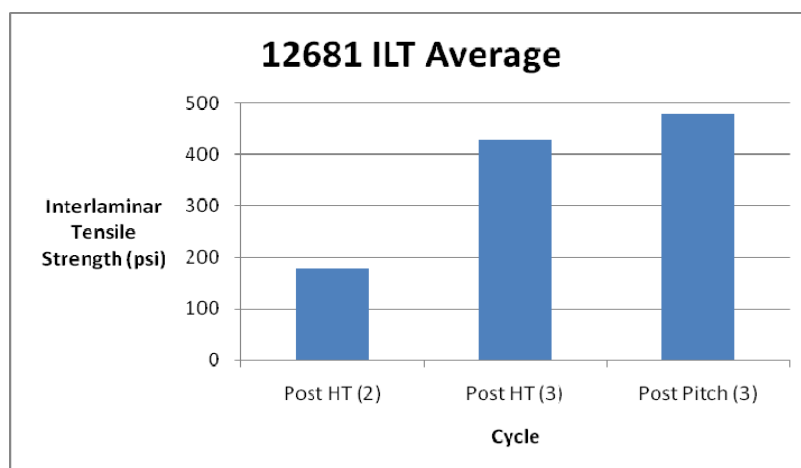**Figure 52: Graph of interlaminar tensile test results for panels 12680 and 12681.**

It was expected that the interlaminar strength of the composite would improve as the matrix was densified. Each time pitch is added to the composite, porosity decreases minimizing crack growth and propagation, and, therefore, increasing interlaminar properties. This hypothesis was verified by the interlaminar tensile test results displayed above. On average between the two panels, the interlaminar tensile strength increased by more than 100 psi over each densification cycle.

During heat treatment, partial graphitization of the matrix can occur. This should decrease interlaminar properties as the matrix realigns in a 2-dimensional molecular structure. Because of this, it was expected that the interlaminar strength would not increase significantly between Post HT (2) and Post HT (3). Although the results from panel 12680 follow this trend, allowing for this possibility, it was not supported by the results from panel 12681. This is due to the fact that graphitization does not fully occur at heat treatment temperatures of less than 1800° C. The *In-Situ* heat treatments only reach 1650° C. However, the heat treatment still densifies

and shrinks the matrix, which can potentially leave porosity increased or unchanged. For this

reason the change in interlaminar strength before and after a heat treatment cannot be precisely

predicted for this densification process. Below are the graphs of the individual results for panels

12680 and 12681. The increasing trend is slightly different for the two panels, which is most

likely caused by small variations within panels and also within each specially prepared sample.

In addition to the results for each individual sample, stress vs. strain curves are located in

Appendix D.
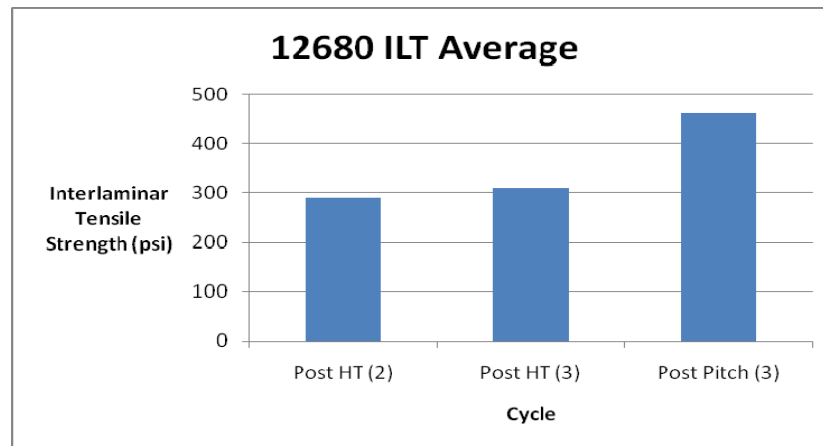
Figure 53: Graph of interlaminar tensile test results for panel 12680.

Figure 54: Graph of interlaminar tensile test results for panel 12681.

6. Task 2 Conclusions

Task 2 porosity testing resulted in a better understanding of density and porosity characteristics for a 2-D carbon-carbon composite panel throughout fabrication and densification. Data were gathered during the early stages of processing including cure and carbonization. These two initial heating steps greatly alter the composition of the composite. Once it is cured, the phenolic resin hardens and the matrix becomes rigid. Although there is very little porosity at this stage, the density is very low, which would result in inadequate mechanical and thermal properties. Once the composite undergoes carbonization, the matrix converts and densifies, restructuring its porosity. This results in densified matrix material, but it is filled with open voids and cracks, which formed when the matrix began to shrink separating from the reinforcing carbon fibers. The large, transverse, oval-shaped pores, which partially remain present throughout densification, are created during carbonization.

A large amount of closed porosity is created during carbonization and the first heat treatment also. This is best understood when comparing the bulk density trends with the skeletal density trends. The bulk density remains constant during the first heat treatment, which means there is not a significant loss of material. The skeletal density decreases during this same heat treatment, and since no material is lost, this means that closed porosity is created by the restructuring matrix.

During densification, porosity and density were monitored to assess the trends and find where improvements could be made. The trends found in Task 1 were verified by the Task 2 data. Porosity decreased from above 20% to 10% in the space of three densification cycles. Also skeletal density showed a steady increase, but only to about 1.71 g/cc.

The same data were gathered by means of mercury porosimetry. While this method provides similar trends with regards to decreasing porosity, there are some differences in the results which were noted. The two main causes of these dissimilar results are small porosity variation throughout a 12" by 12" panel and the inclusion of closed porosity measurements due to high pressure from the porosimeter.

Two panels were created for Task 2 to assess the possibility that there is slight variation in porosity formation within panels fabricated using the same methods and materials. The results varied between panels 12680 and 12681 by 1%-3% porosity in several cases indicating that some variation does exist. These differences were noted by both mercury porosimetry and water immersion.

The second explanation of the porosimeter results is a side effect of the high pressure used to force mercury into the sample. The porosimeter reaches 60,000 psi during each run in order to penetrate all the small open voids located in the matrix; however, this can also cause the structure to fracture, opening up closed porosity, which can then be included in the measurements. The results show that this is a likely explanation, although more concrete evidence is difficult to obtain. The porosity measurements taken by the porosimeter after each addition of pitch into the matrix showed a higher measured value than the results from water immersion. This is likely high pressure yielding a higher porosity value due to weaker points in the matrix. Once these differences were accounted for, the results from the two test methods became very similar.

The mechanical tests conducted during Task 2 successfully showed the correlation between matrix porosity and strength. As matrix porosity decreased and skeletal density increased, flexural strength of the composite increased from about 20 ksi to 23 ksi over two

densification cycles and one heat treatment cycle. Also interlaminar tensile tests showed a similar increasing trend. The tensile strength of the matrix more than doubled over the same cycles, increasing from 230 psi to 470 psi. The final values of flexural strength and interlaminar tensile strength are very respectable values that exceed requirements for many applications for carbon-carbon composites.

The *In-Situ* densification method has many advantages and disadvantages as determined by this porosity study. With only three densification cycles, it creates similar high performance composites to those produced commercially while keeping fabrication time and costs low. It also provides very simple processing methods, which require little man-power and cleanup. It can effectively decrease porosity by 50% over three densification cycles resulting in a skeletal density of over 1.7 g/cc. However, there are short-comings to be noted as well. The skeletal density increases only slightly throughout densification, and this might be inadequate when the highest thermal and mechanical properties are required. Also there is some slight variation in the porosity values throughout different panels. The root cause of these differences must be determined so the variation can be minimized.

7. Opportunities for Further Study

Although the current data describe the effectiveness of the *In-Situ* densification method and pore structure present throughout processing, there are still many areas for further study. These areas are mostly involved with improving the *In-Situ* short-comings, and better understanding the carbon matrix at high temperatures. While the water immersion and mercury porosimetry give detailed porosity measurements, density values, and even pore-size distribution plots, assumptions still need to be made concerning the exact behavior of the matrix during each stage of processing.

Throughout this study unexpected results were obtained that usually followed heat treatment to high temperatures. It would be beneficial to learn the behavior of this carbon matrix when it is brought to several different temperatures above 1200° C. A comparative study showing results after heat treatment to different temperatures at 100° increments with varying hold times would result in understanding the effects of temperature and the reasons for those effects.

The goal of other studies should be to further increase the skeletal density throughout the *In-Situ* method. It currently is producing composites with densities between 1.7 and 1.8 g/cc. These are reasonable values, but panels with consistent densities of 2.0 g/cc would provide better properties and would be more desirable for high-performance applications. One study would include optimizing the wicking ability of the pre-pitch matrix material during impregnation so the pores can be filled more effectively. Another would involve improving the strength of the matrix-fiber bond during heat treatment. This would result in more composite shrinkage in the z-direction minimizing the formation of more cracks and pores throughout the matrix.

One more area of further study would be a detailed analysis of the effect of the mercury porosimeter on undensified 2-D carbon-carbon composite samples. This was an area of speculation throughout testing, and more concrete data would be very beneficial when analyzing the results. There are much data comparing the accuracy of different porosity test methods, but the types of samples vary. This specific case was unique as the matrix structure was weaker than most because final processing was not yet complete. This caused the samples to be more susceptible to damage from the porosimeter's application of high pressure. This type of study would require a lot of time and a large number of samples to be tested in order to evaluate the averages and effectively compare the different test methods.

References

[1]   *Auto Pore IV General Operating Instructions.* (2000).

[2]   Brassell, G. W., Horak, J. A., & Butler, B. L. (1975). Effects of porosity on strength of carbon-carbon composites. *Journal of Composite Materials , 9*, 288-296.

[3]   Buckley, J. D., & Edie, D. D. (Eds.). (1992). *Carbon-Carbon Materials and Composites.* Langley, VA: NASA Reference Publication.

[4]   Butyrin, G. M., & Demin, A. V. (1996). Evaluation of density and open porosity of carbonplastic and carbon/carbon composites by nondestructive techniques. *International Conference on Advanced Materials*, (pp. 12-15). Beijing, China.

[5]   Chlopek, J., Blazewicz, S., & Powroznik, A. (1993). Mechanical properties of carbon-carbon composties. *Ceramics International , 19*, 251-257.

[6]   Delmonte, J. (1981). *Technology of Carbon and Graphite Fiber Composites.* New York, NY: Van Nostrand Reinhold Company.

[7]   Figueiredo, J. L., Bernardo, C. A., Baker, R. K., & Huttinger, K. J. (Eds.). (1989). *Carbon Fiber Filaments and Composites.* Dordrecht, Netherlands: Kluwer Academic Publishers.

[8]   Fitzer, E., & Manocha, L. M. (1998). *Carbon Reinforcements and Carbon/Carbon Composites.* Berlin, Germany: Springer-Verlag.

[9]   Hu, Y., Luo, R., Zhang, Y., Zhang, J., & Li, J. (2010). Effect of preform density on densification rate and mechanical properties of carbon-carbon composites. *Materials Science and Engineering , A* (527), 797-801.

[10] Klucakova, M. (2004). Rheological properties of phenolic resin as a liquid matrix precursor for impregnation of carbon-carbon composites with respect to the conditions of the densification process. *Composites Science and Technology* (64), 1041-1047.

[11] Marsh, H., & Rodriguez-Reinoso, F. (Eds.). (2000). *Sciences of Carbon Materials.* Universidad de Aliconte: Secretariado de Publicaciones.

[12] Oh, S., & Park, Y. (1994). An analysis of densification process of carbon/carbon composites. *Novel Forms of Carbon II*, (pp. 93-97). San Francisco, CA.

[13] Oya, M., Takahashi, M., Iwata, Y., Jono, K., Hotta, T., & Yamamoto, H. (2002). Mercury Intrusion Porosimetry. *American ceramic Society Bulletin , 81* (3), 52-56.

[14] Rellick, G. (1990). Densification efficiency of carbon-carbon composites. *Carbon , 28* (4), 589-594.

[15] Ritter, H. L., & Drake, L. C. (1945). Macropore-size distributions in some typical porous substances. *Industrial and Engineering Chemistry, Analytical Edition , 17* (12), 787-791.

[16] Ritter, H. L., & Drake, L. C. (1945). Pore-size distribution in porous materials-pressure porosimeter and determination of complete macropore-size distributions. *Industrial and Engineering Chemistry, Analytical Edition , 17* (12), 782-786.

[17] Safiuddin, M., & Hearn, N. (2004). Comparison of ASTM saturation techniques for measuring the permeable porosity of concrete. *Cement and Concrete Research , 35* (2005), 1008-1013.

[18] Schmidt, D. L. (1996). *Carbon-Carbon Composites-A Historical Perspective.* Wright-Patterson AFB, OH: Materials Directorate, Wright Laboratory.

[19] Tzeng, S., & Pan, J. (2001). Densification of two-dimensional carbn/carbon composites by pitch impregnation. *Materials Science and Engineering , A* (316), 127-134.

[20] Weber, E., Fernandez, M., Wapner, P., & Hoffman, W. (2010). Comparison of X-ray micro-tomography measurements of densities and porosity principally to values measured by mercury porosimetry for carbon-carbon composites. *Carbon , 48* (8), 2151-2158.

[21] White, J. L., & Sheaffer, P. M. (1983). *Mesophase behavior fundamental to the processing of carbon-carbon composites.* El Segundo, CA: Materials Sciences Laboratory.

[22] www.fibermaterialsinc.com. 2005. Fiber Materials Inc. 2010.

Appendix A: Task 1 Microstructure Photos
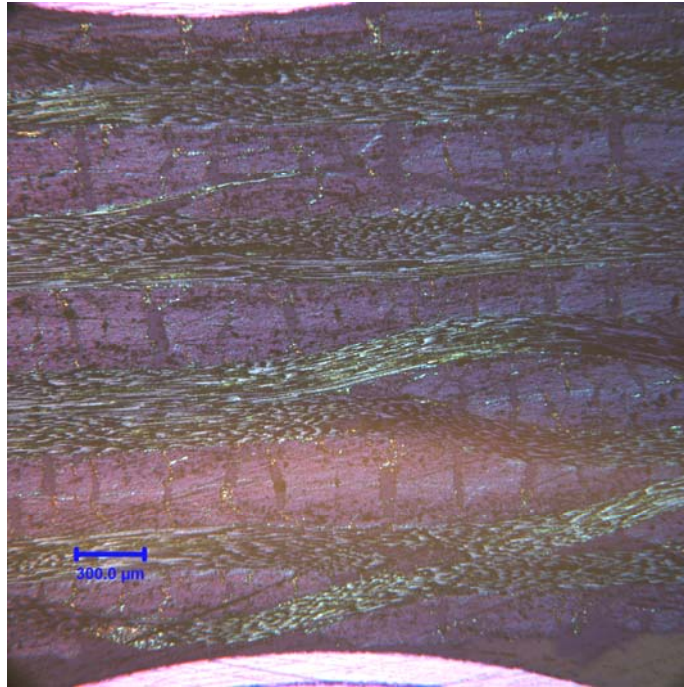
Figure A-1: Panel 12656-4, Post Pitch (1) at 50x magnification.
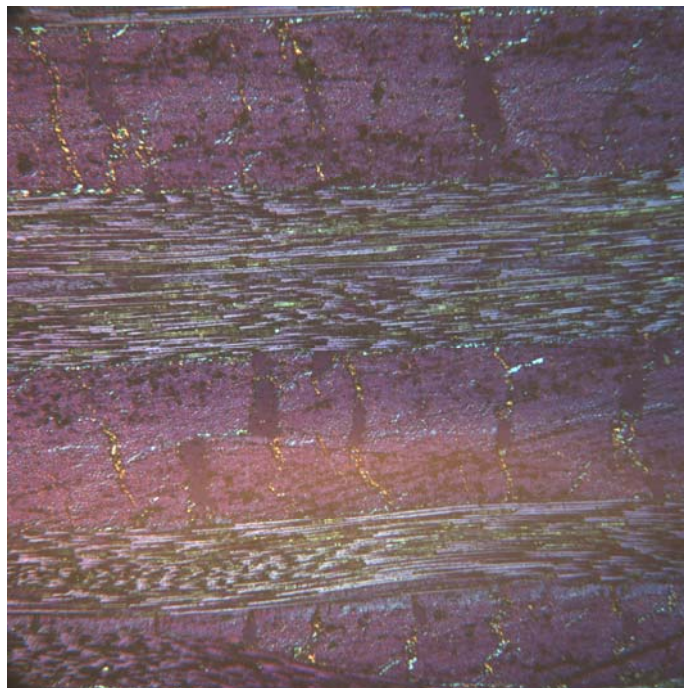
Figure A-2: Panel 12656-4, Post Pitch (1) at 100x magnification.
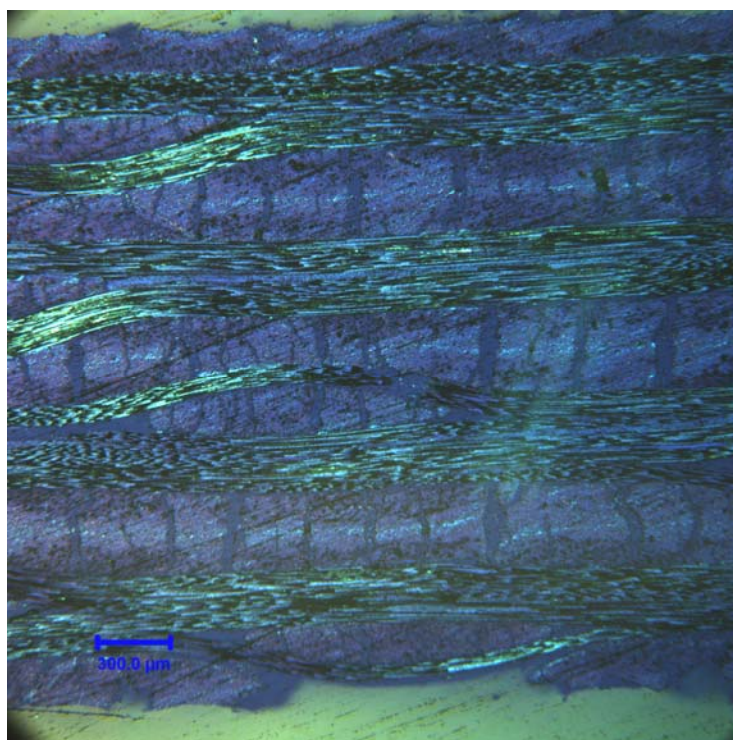
Figure A-3: Panel 12656-4, Post HT (1) at 50x magnification.
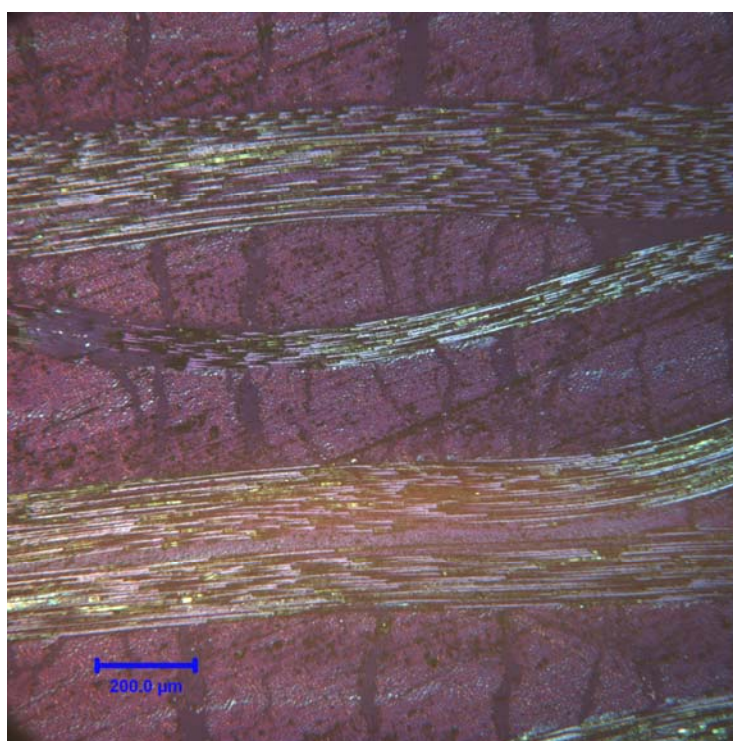
Figure A-4: Panel 12656-4, Post HT (1) at 100x magnification.
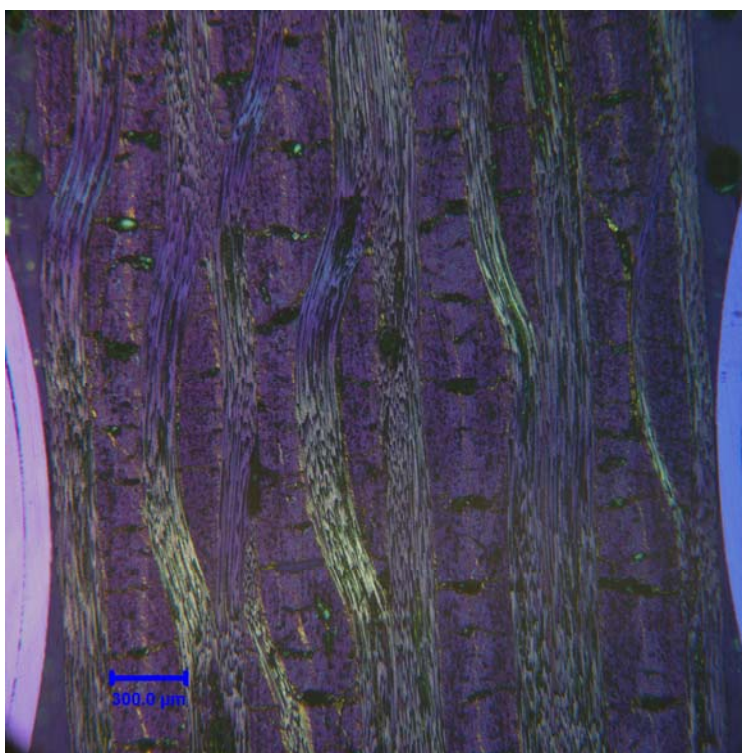
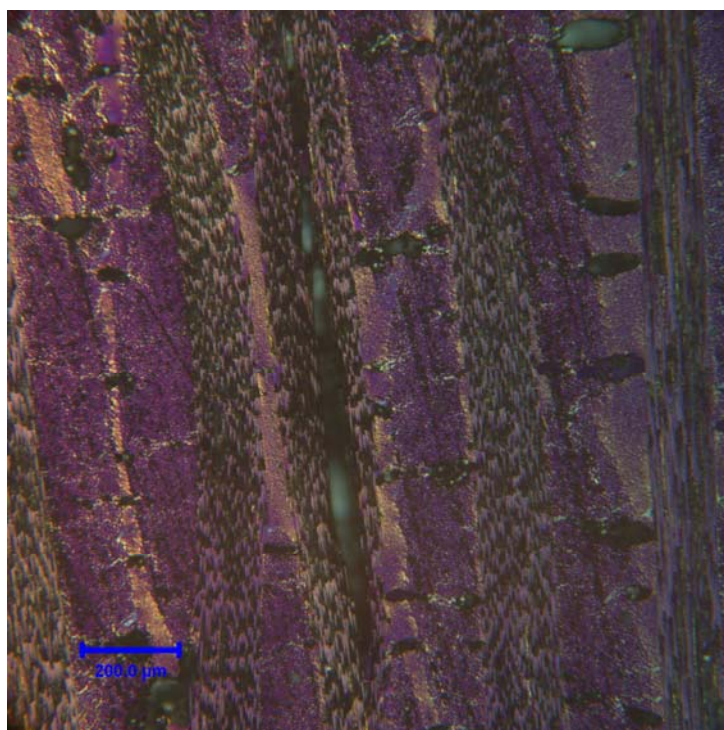**Figure A-5: Panel 12656-4, Post Pitch (3) at 50x magnification.**
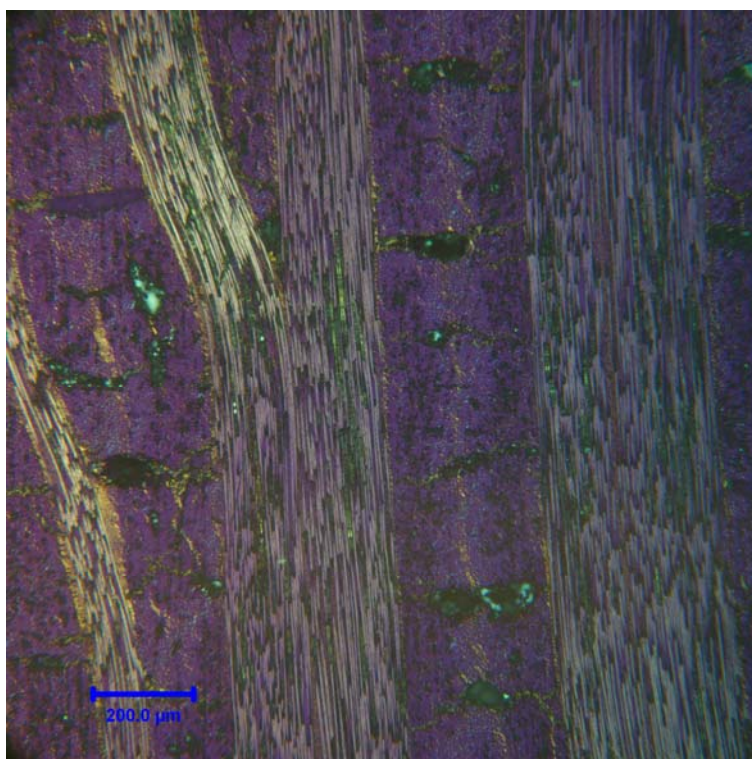
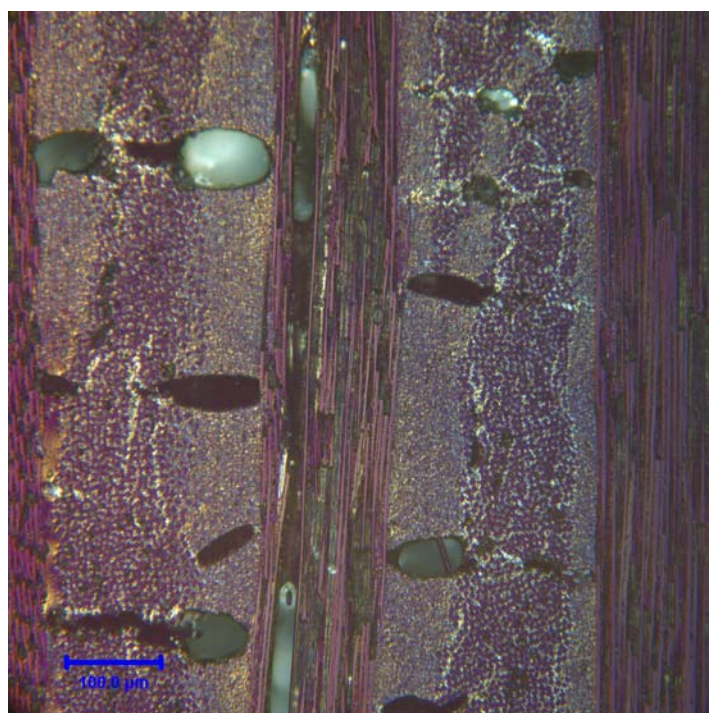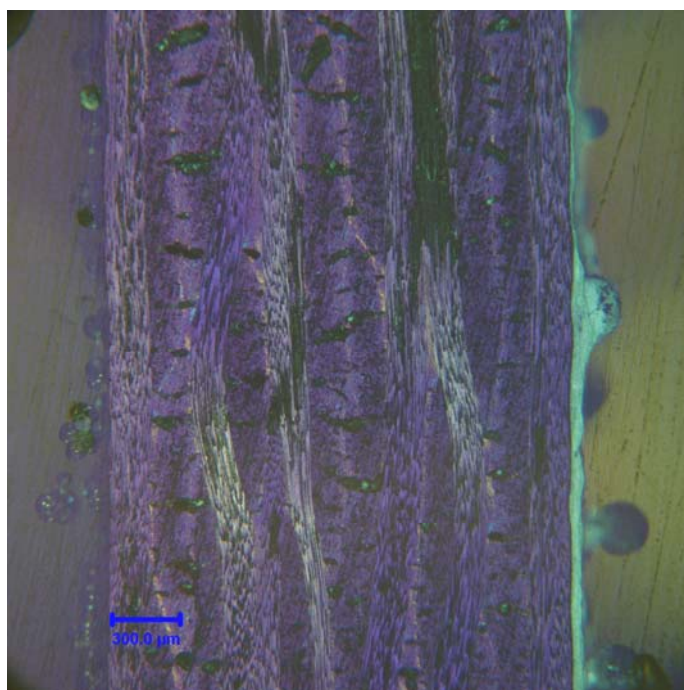**Figure A-6: Panel 12656-4, Post Pitch (3) at 100x magnification.**
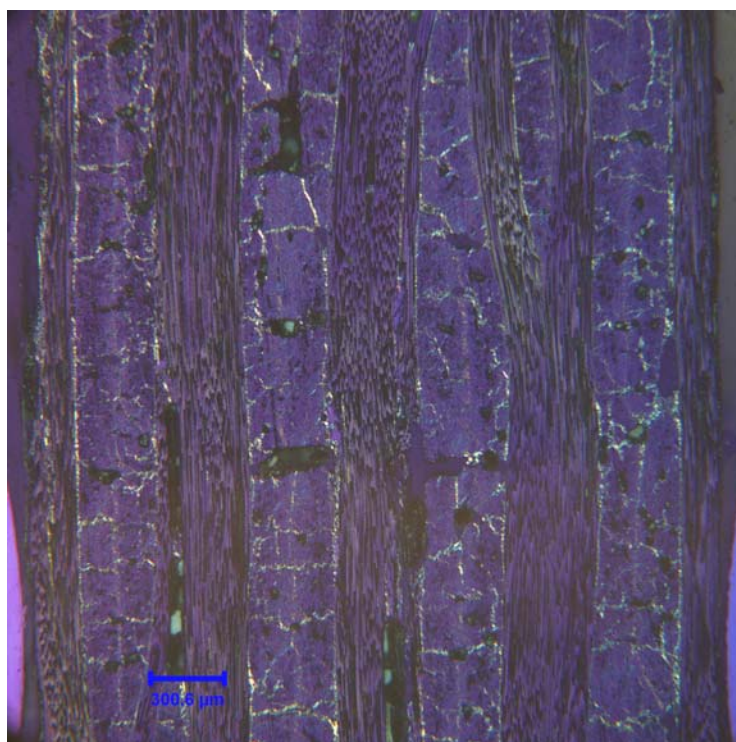
Figure A-7: Panel 12656-3, at 50x magnification.
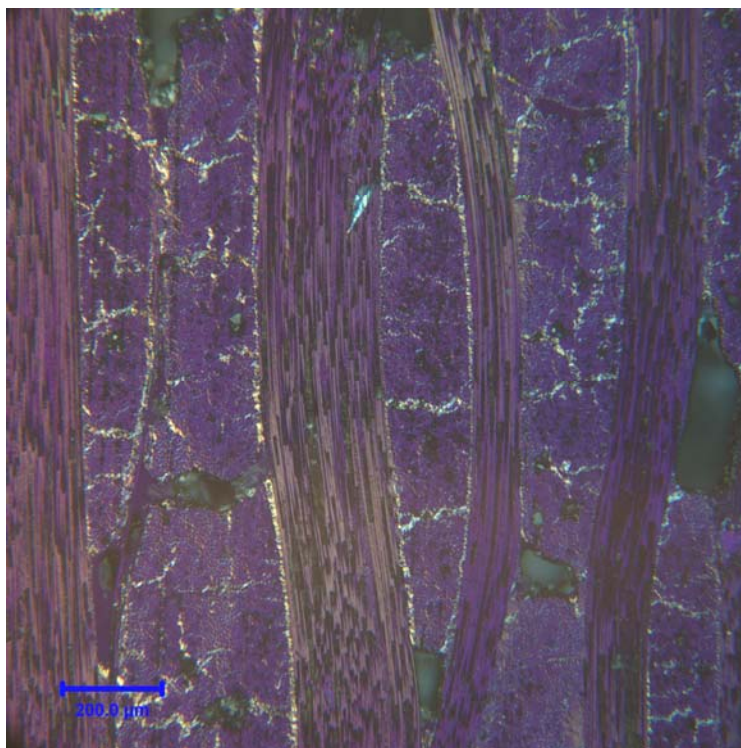
Figure A-8: Panel 12656-3, at 100x magnification.

Figure A-9: FMC 41, at 50x magnification.

Figure A-10: FMC 41, at 100x magnification.

Figure A-11: 12473, at 50x magnification.
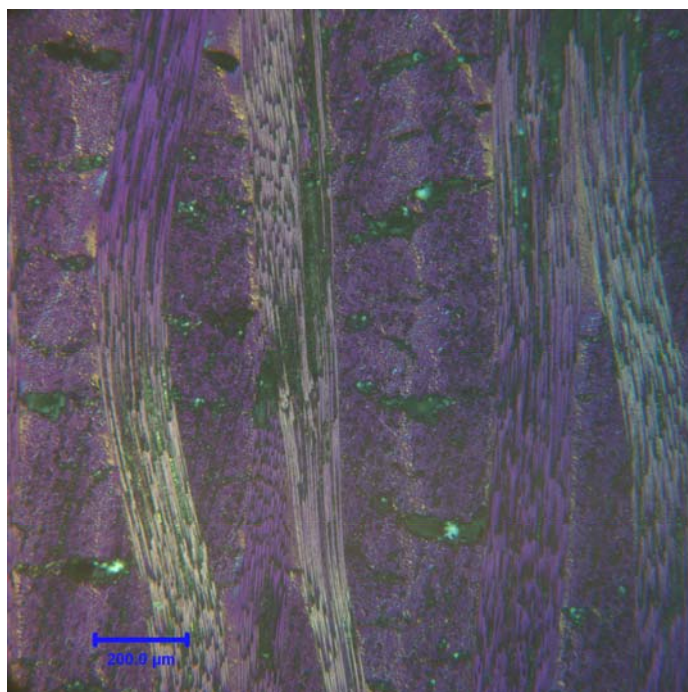
Figure A-12: 12473, at 100x magnification.
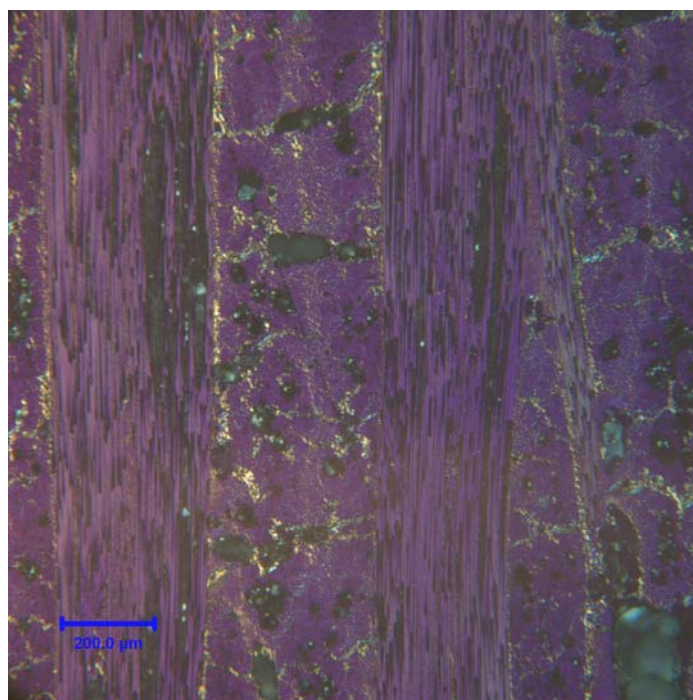
Figure A-13: H5-3, at 100x magnification.

Appendix B: Task 2 Microstructure Photos
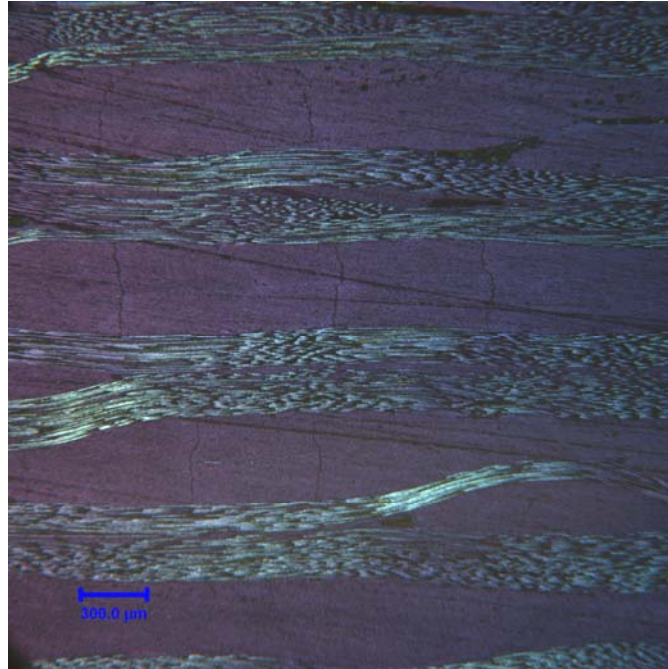
Figure B-1: Panel 12680, Post Cure at 50x magnification.
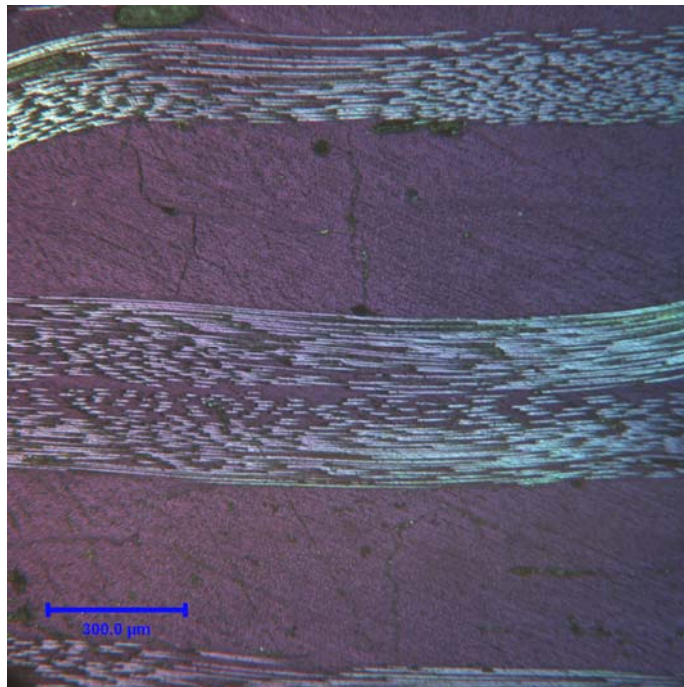
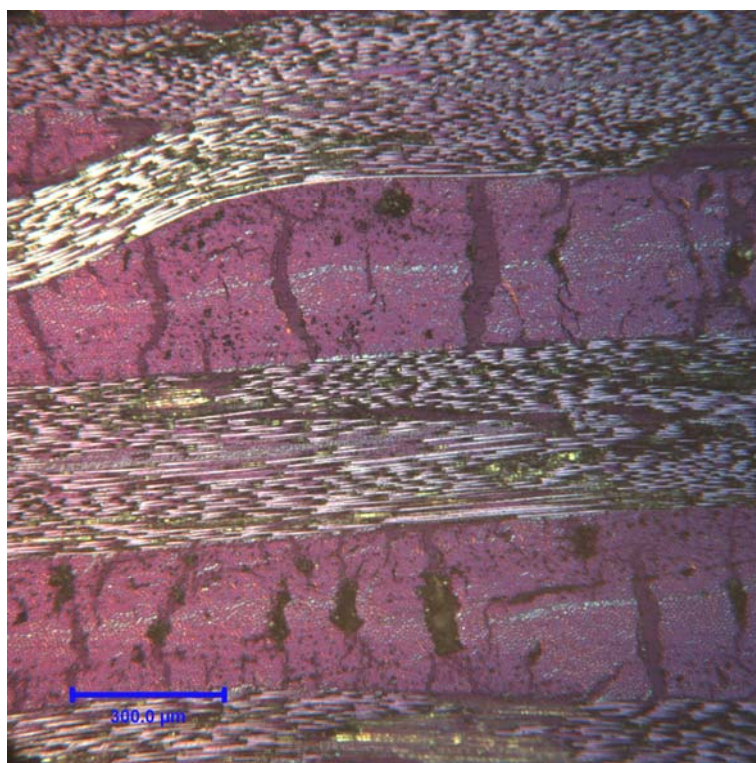**Figure B-2: Panel 12680, Post Cure at 100x magnification.**
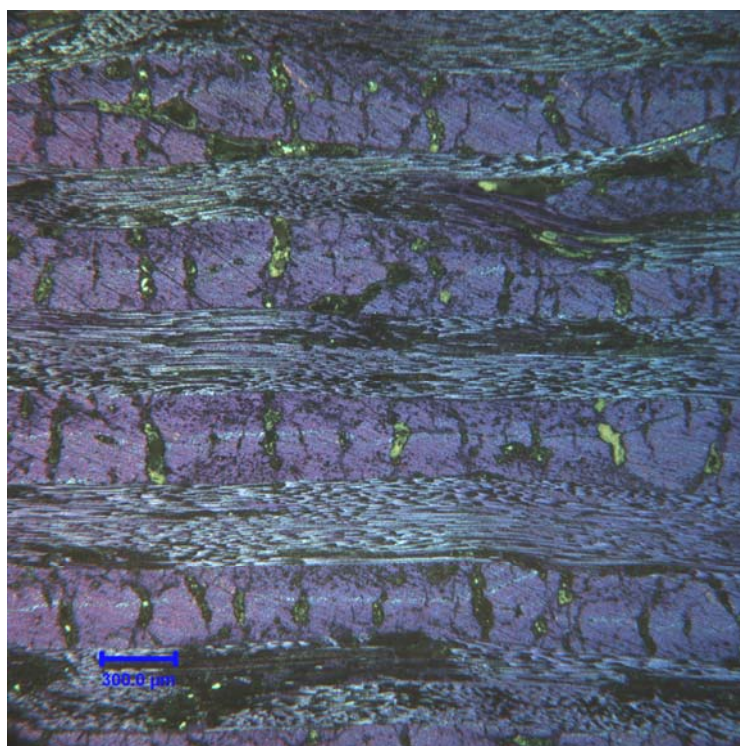
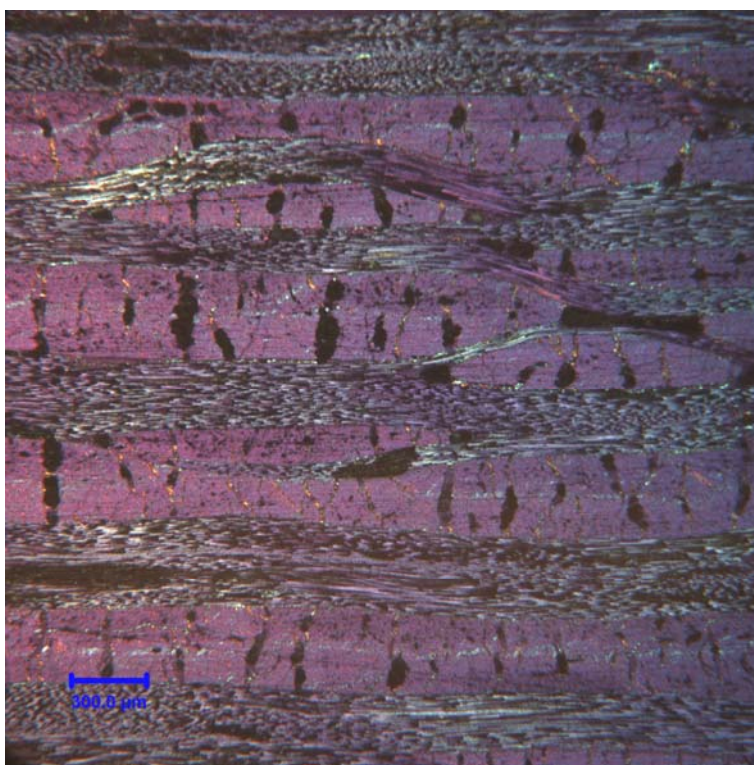**Figure B-3: Panel 12680, Post Carbonization at 50x magnification.**
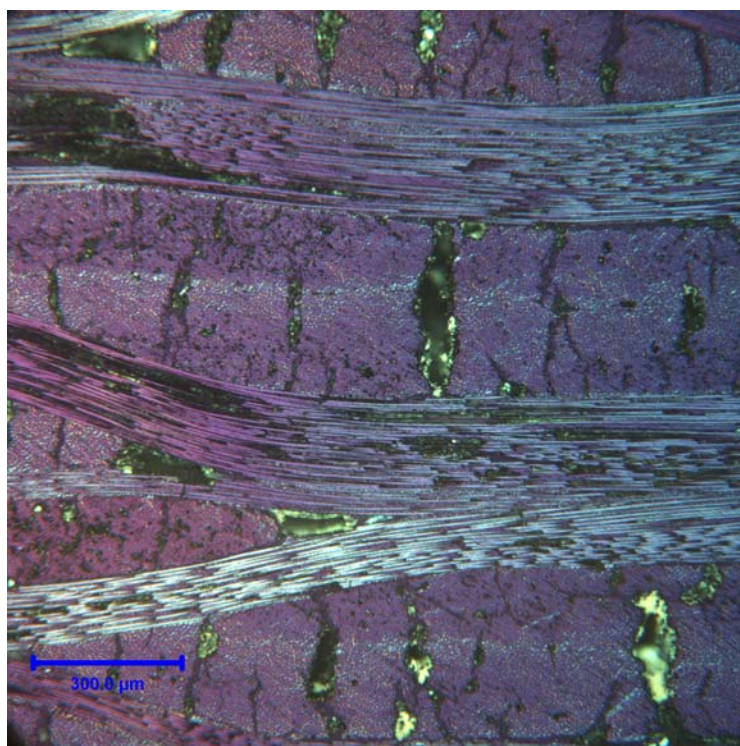
Figure B-4: Panel 12680, Post Carbonization at 100x magnification.
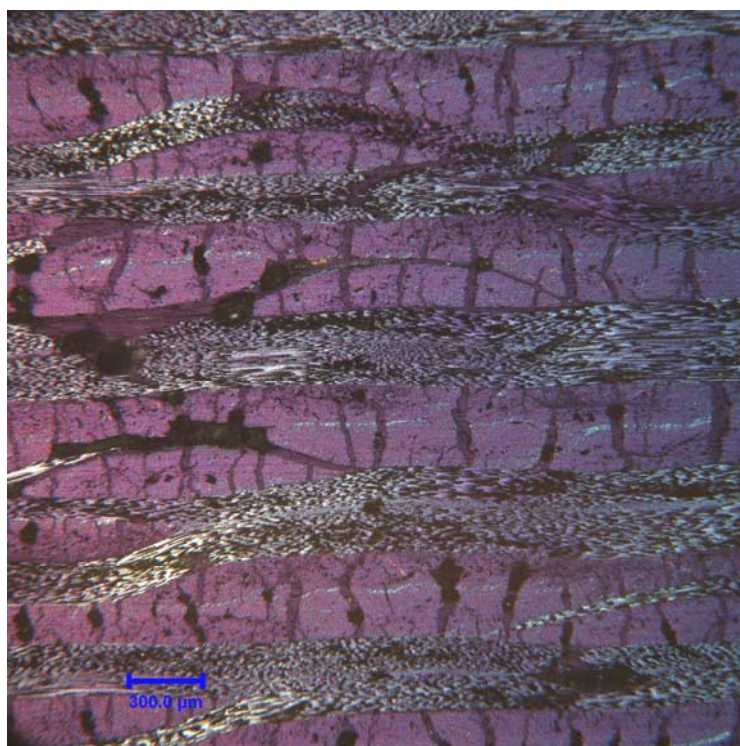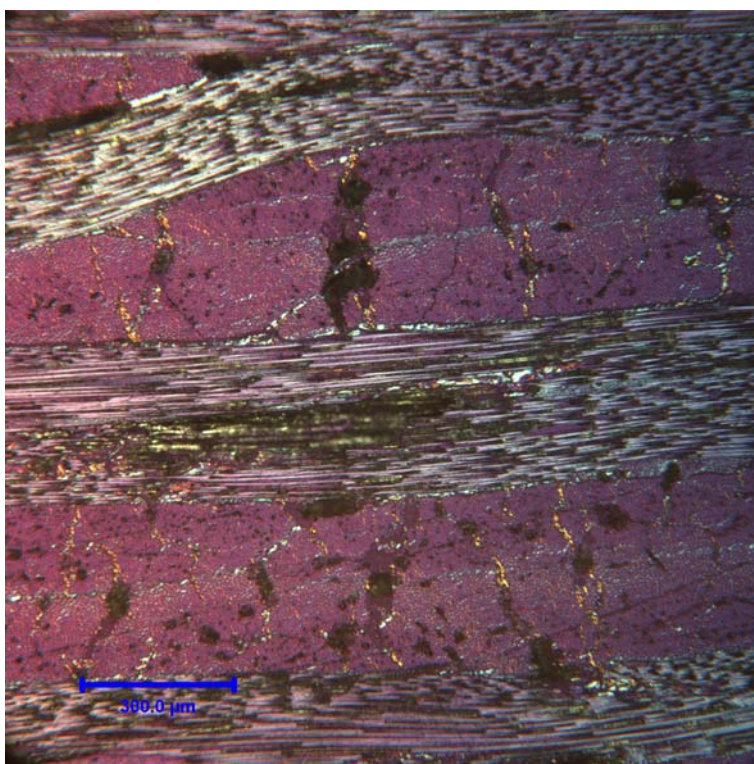
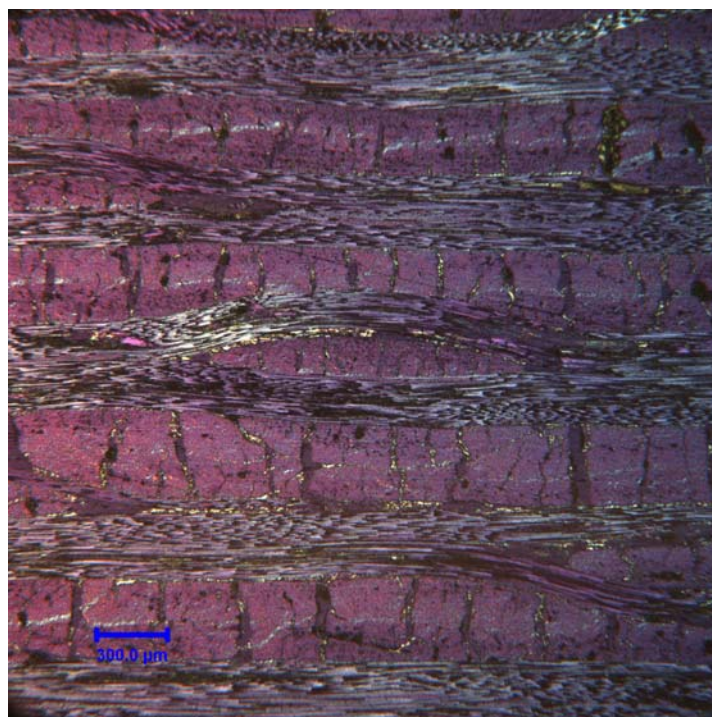**Figure B-5: Panel 12680, Post HT (1) at 50x magnification.**

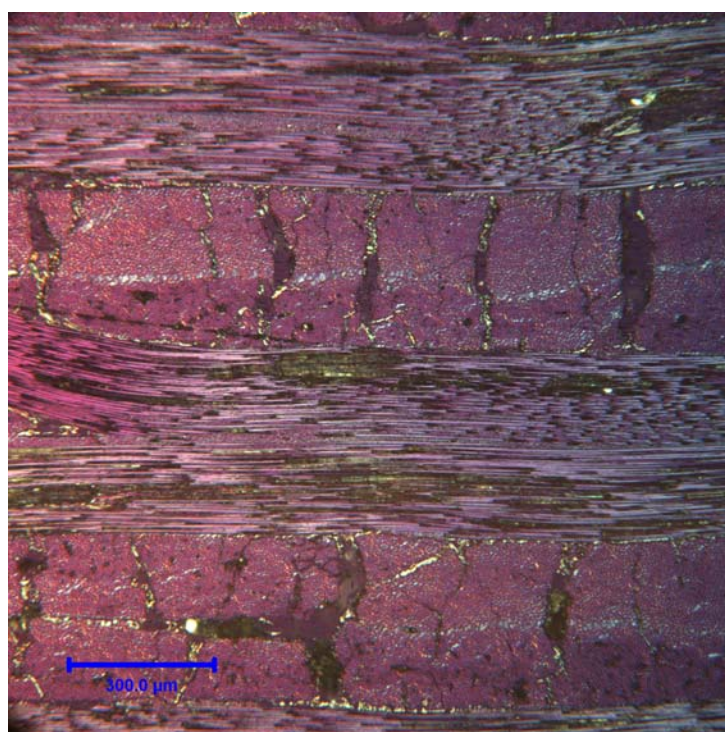**Figure B-6: Panel 12680, Post HT (1) at 100x magnification.**

Figure B-7: Panel 12680, Post Pitch (1) at 50x magnification.
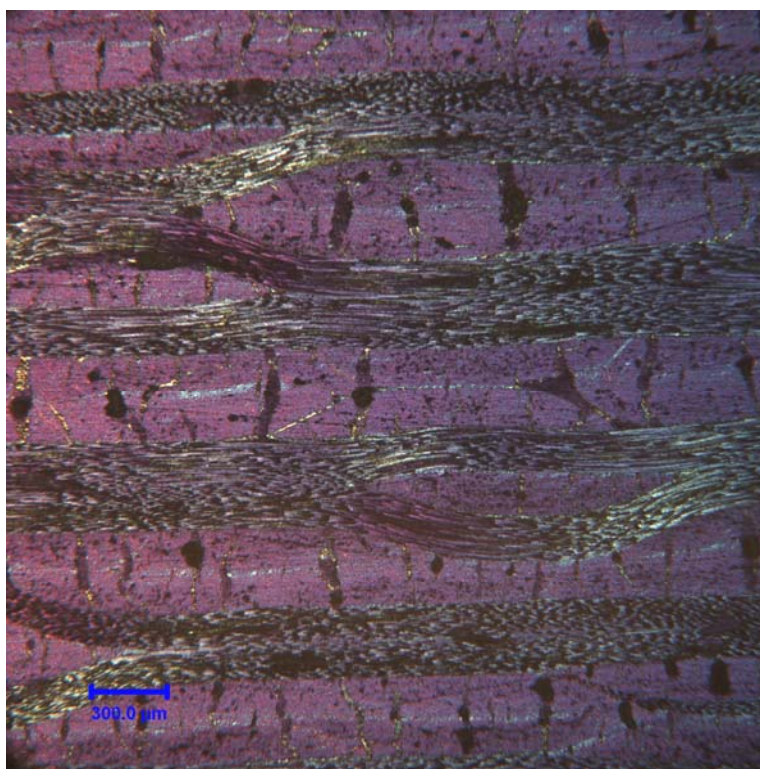

Figure B-8: Panel 12680, Post Pitch (1) at 100x magnification.

Figure B-9: Panel 12680, Post HT (2) at 50x magnification.

Figure B-10: Panel 12680, Post HT (2) at 100x magnification.

Figure B-11: Panel 12680, Post Pitch (2) at 50x magnification.

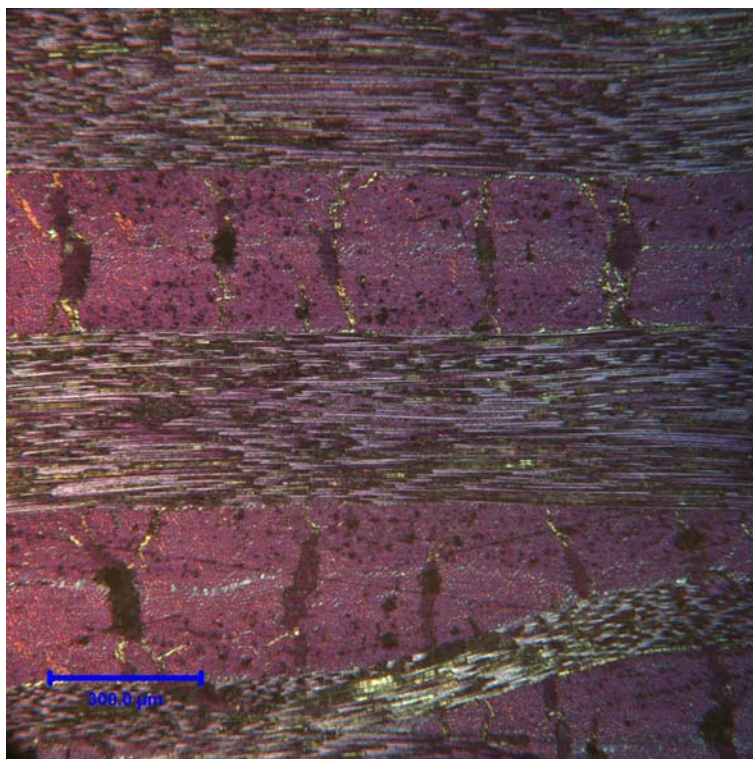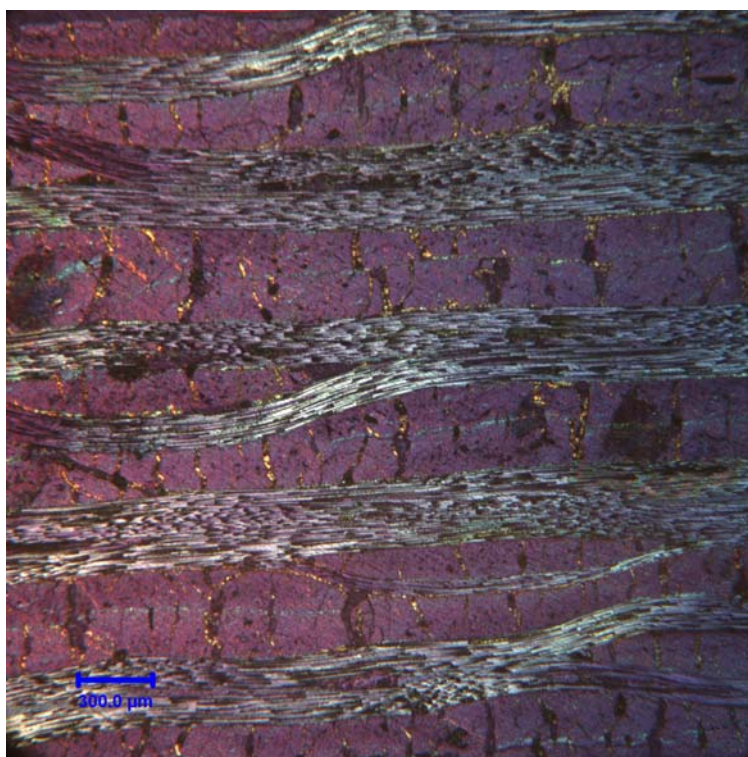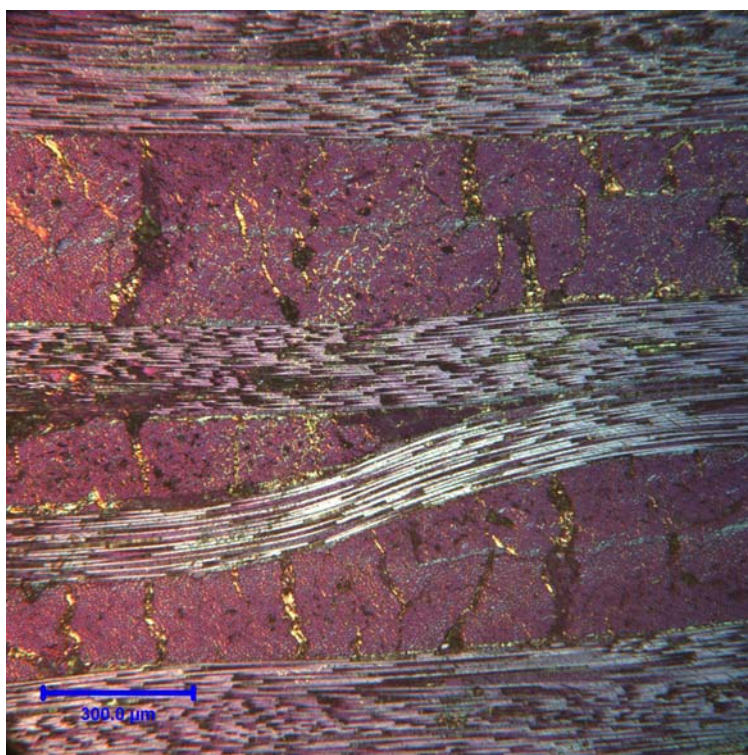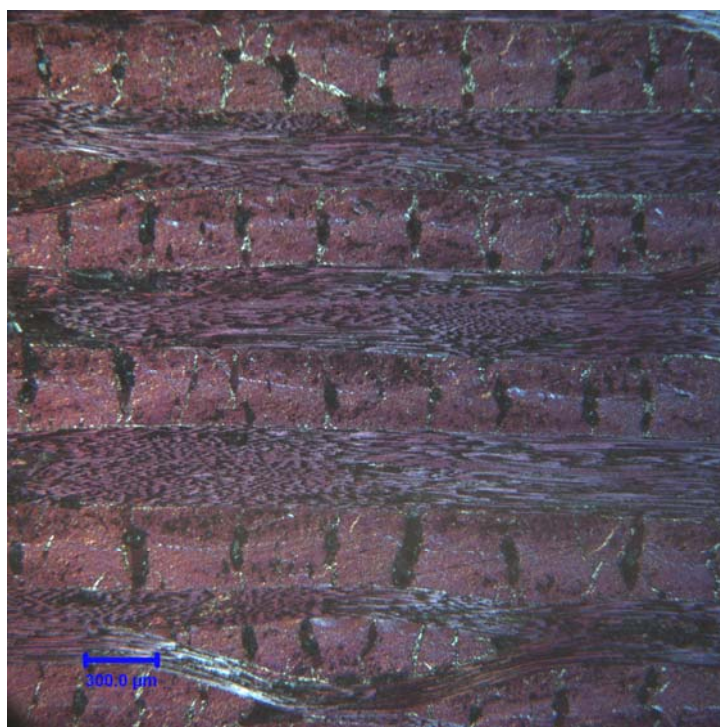**Figure B-12: Panel 12680, Post Pitch (2) at 100x magnification.**

Figure B-13: Panel 12680, Post HT (3) at 50x magnification.

**Figure B-14: Panel 12680, Post HT (3) at 100x magnification.**

Figure B-15: Panel 12680, Post Pitch (3) at 50x magnification.

Appendix C: Flexure Test Data

Table C-1: Flexure Test Results for Panels 12680 and 12681 after the second heat treatment.

Sample	Cycle	Max Force (lbf)	Max Deflection (in)	Flexural Strength (psi)	Bending Modulus (psi)
12680-1	HT (2)	42.712	0.070	19522.209	8278217.718
12680-2	HT (2)	42.112	0.069	19109.952	8212354.947
12680-3	HT (2)	43.761	0.071	19858.097	8334297.836
12680-4	HT (2)	42.038	0.078	19038.320	7233103.202
12680-5	HT (2)	43.087	0.070	19863.101	8555965.683
	Average	**42.742**	**0.072**	**19478.336**	**8122787.877**
12681-1	HT (2)	47.208	0.074	22834.491	9451526.282
12681-2	HT (2)	46.309	0.069	22299.974	9855952.428
12681-3	HT (2)	35.368	0.073	16577.921	6914066.507
12681-4	HT (2)	45.560	0.073	21713.061	9012004.959
12681-5	HT (2)	41.064	0.064	19882.046	9584069.257
12681-6	HT (2)	45.560	0.069	22080.727	9767518.520
	Average	**43.511**	**0.070**	**20898.037**	**9097522.992**
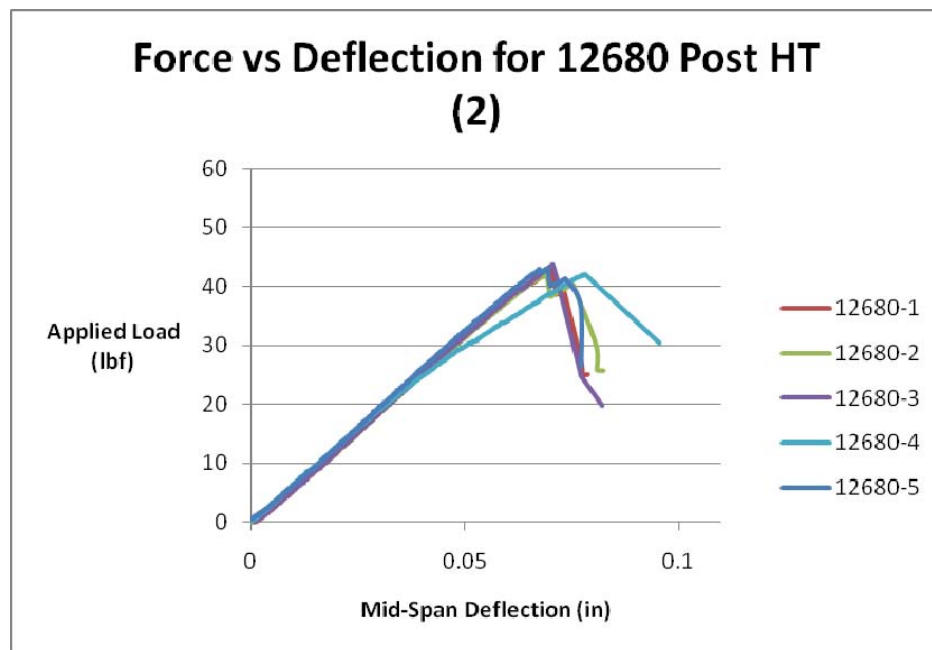
Figure C-1: Force vs. deflection graph for each sample cut from panel 12680 following the second heat treatment.
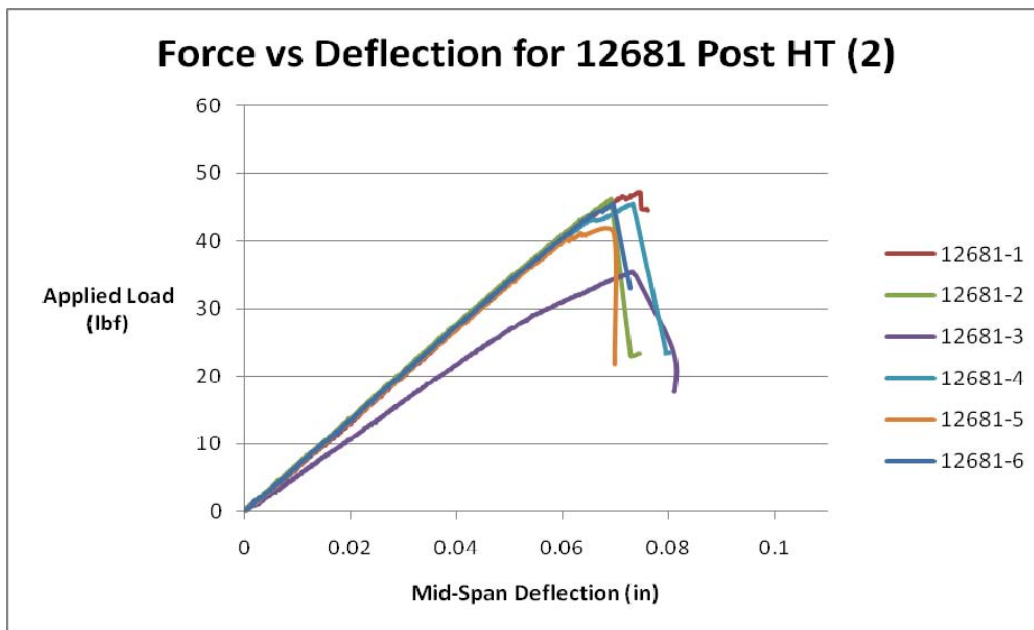
Figure C-2: Force vs. deflection graph for each sample cut from panel 12681 following the second heat treatment.

Table C-2: Flexure test results for panels 12680 and 12681 after the third heat treatment.

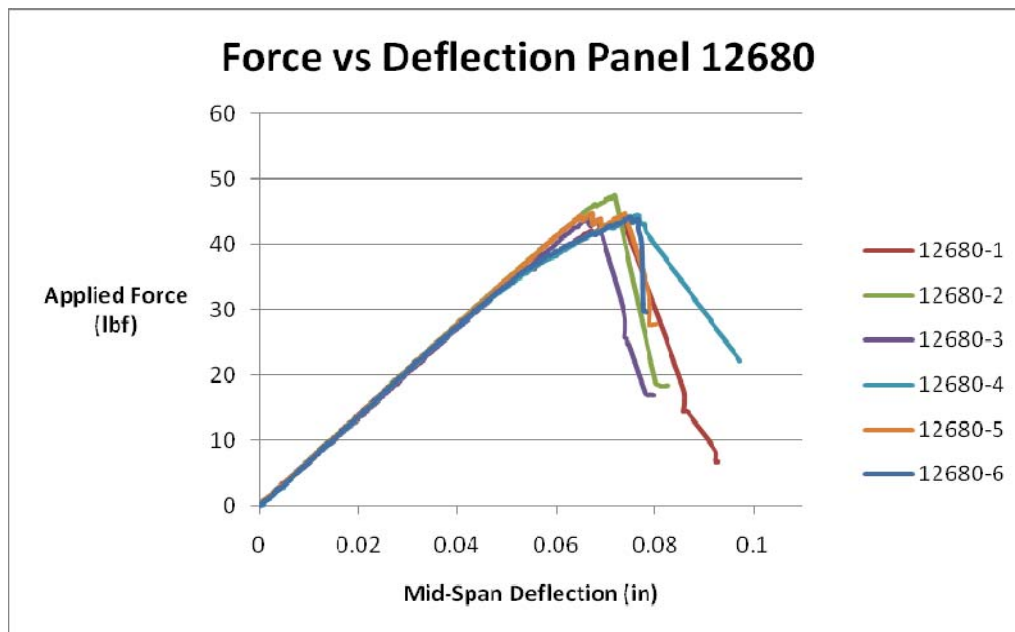| Sample	Cycle	Max Force (lbf)	Max Deflection (in)	Flexural Strength (psi)	Bending Modulus (psi)
12680-1	HT (3)	44.360	0.073	19966.266	8066697.335
12680-2	HT (3)	47.583	0.072	21035.242	8611836.807
12680-3	HT (3)	43.986	0.066	19388.321	8626580.835
12680-4	HT (3)	44.436	0.076	19701.713	7596314.307
12680-5	HT (3)	44.735	0.074	19699.383	7850214.198
12680-6	HT(3)	44.211	0.075	19577.938	7675958.566
	Average	**44.885**	**0.073**	**19894.810**	**8071267.008**
12681-1	HT (3)	53.502	0.075	24723.559	9983043.286
12681-2	HT (3)	50.580	0.071	23976.158	10238979.495
12681-3	HT (3)	51.854	0.076	24008.787	9498834.242
12681-4	HT (3)	50.130	0.072	23142.707	9624193.977
12681-5	HT (3)	51.629	0.075	24033.026	9739761.941
12681-6	HT (3)	50.730	0.072	23488.366	9767940.873
	Average	**51.404**	**0.074**	**23895.434**	**9808792.302**

Figure C-3: Force vs. deflection graph for each sample cut from panel 12680 following the third heat treatment.
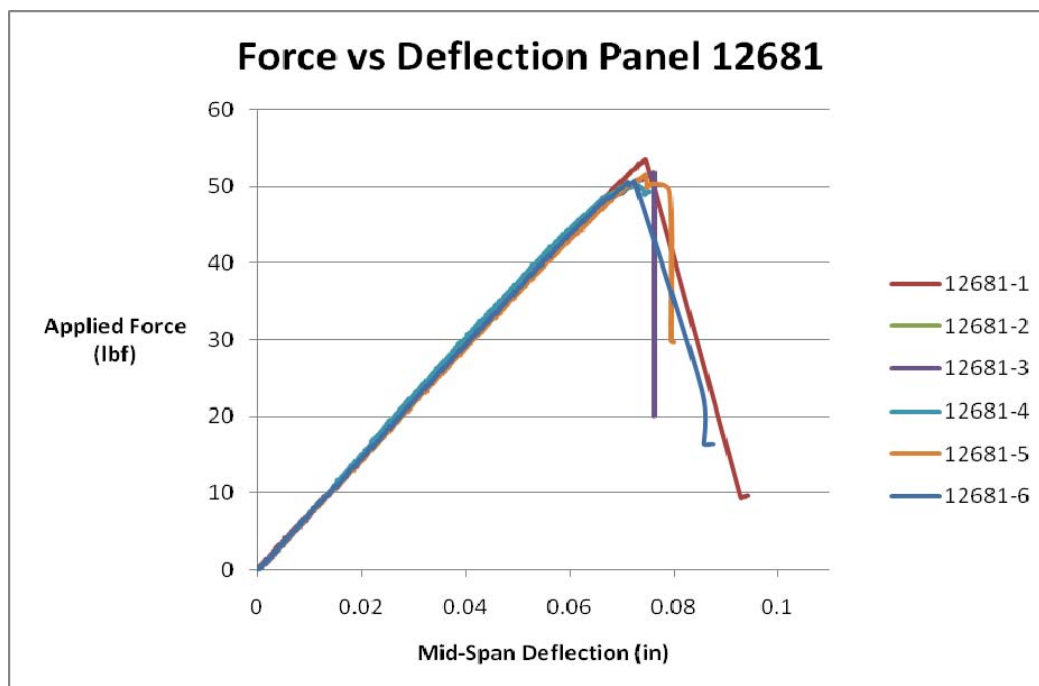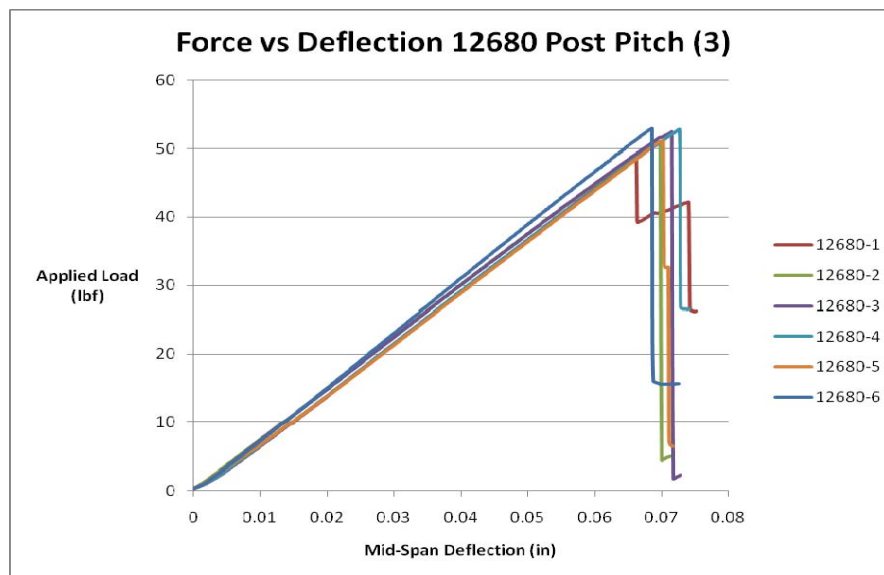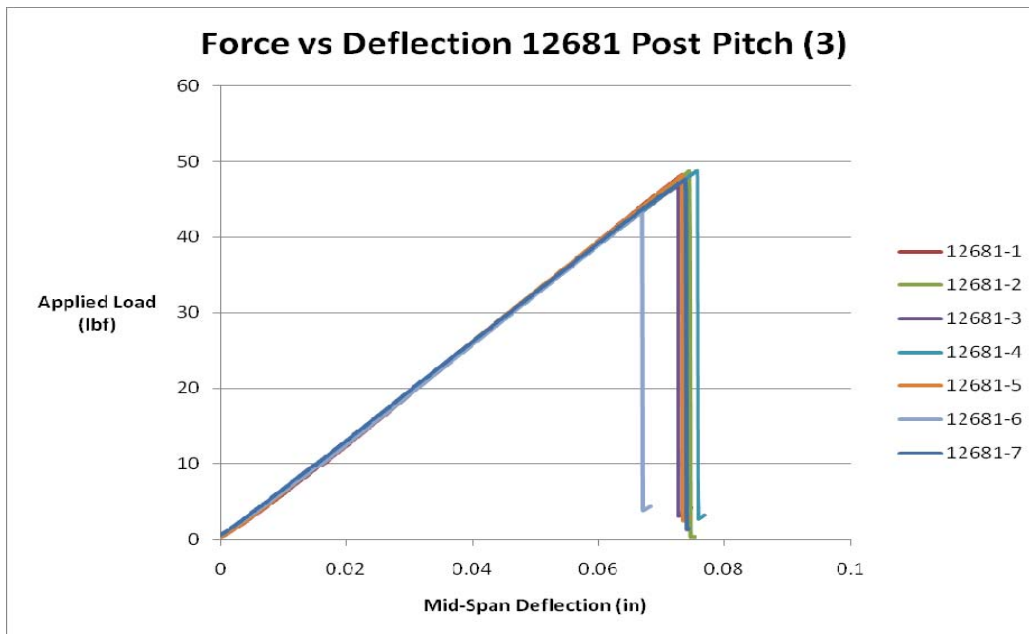

Figure C-4: Force vs. deflection graph for each sample cut from panel 12681 following the third heat treatment.

Table C-3: Flexure test results for panels 12680 and 12681 after final densification.

Sample	Cycle	Max Force (lbf)	Max Deflection (in)	Flexural Strength (psi)	Bending Modulus (psi)
12680-1	PP (3)	48.782	0.066	20966.970	9241074.616
12680-2	PP (3)	51.030	0.069	21659.814	9097006.101
12680-3	PP (3)	52.528	0.072	22533.614	9182734.075
12680-4	PP (3)	52.828	0.073	22531.167	9052205.884
12680-5	PP (3)	51.180	0.070	21849.148	9063425.254
12680-6	PP (3)	52.903	0.069	22390.527	9517266.829
	Average	**51.542**	**0.070**	**21988.540**	**9192285.460**
12681-1	PP (3)	48.182	0.073	23136.984	9557438.439
12681-2	PP (3)	48.707	0.074	23625.666	9645522.741
12681-3	PP (3)	46.983	0.073	23284.561	9706880.634
12681-4	PP (3)	48.782	0.076	24026.756	9630644.552
12681-5	PP (3)	48.182	0.073	23300.413	9650821.611
12681-6	PP (3)	43.461	0.067	21450.380	9726469.410
12681-7	PP (3)	47.658	0.074	23667.740	9740125.375
	Average	**47.422**	**0.073**	**23213.214**	**9665414.680**

Figure C-5: Force vs. deflection graph for each sample cut from panel 12680 after final densification.

Figure C-6: Force vs. deflection graph for each sample cut from panel 12681 after final densification.

Appendix D: Interlaminar Tensile Test Data

Table D-1: Interlaminar Tensile Test Results for panel 12680 at three different times during the densification process.

Panel	Cycle	Sample #	Max Stress (psi)	Max Strain (in/in)
12680	Post HT (2)	1	336.9518655	0.181779035
12680	Post HT (2)	2	324.6472576	0.107652559
12680	Post HT (2)	3	207.2821287	0.160248524
		Average	**289.6270839**	**0.149893373**
12680	Post HT (3)	1	188.3521593	0.09552585
12680	Post HT (3)	2	373.8651213	0.15503876
12680	Post HT (3)	3	367.2394758	0.211194531
		Average	**309.8189188**	**0.153919714**
12680	Post Pitch (3)	1	538.5550318	0.112356148
12680	Post Pitch (3)	2	447.6916329	0.066929134
12680	Post Pitch (3)	3	405.0994147	0.126892792
		Average	**463.7820265**	**0.102059358**

Table D-2: Interlaminar Tensile Test Results for panel 12680 at three different times during the densification process.

| Panel	Cycle	Sample #	Max Stress (psi)	Max Strain (in/in)
12681	Post HT (2)	1	179.8337156	0.069654755
12681	Post HT (2)	2	158.064549	0.088431254
12681	Post HT (2)	3	196.8706029	0.155966081
		Average	**178.2562892**	**0.10468403**
12681	Post HT (3)	1	434.4406259	0.137795276
12681	Post HT (3)	2	417.4037386	0.105390672
12681	Post HT (3)	3	439.1731893	0.146274985
		Average	**430.3391846**	**0.129820311**
12681	Post Pitch (3)	1	547.0734754	0.128104179
12681	Post Pitch (3)	2	434.4406259	0.113567535
12681	Post Pitch (3)	3	456.2100765	0.112356148
		Average	**479.2413926**	**0.118009287**
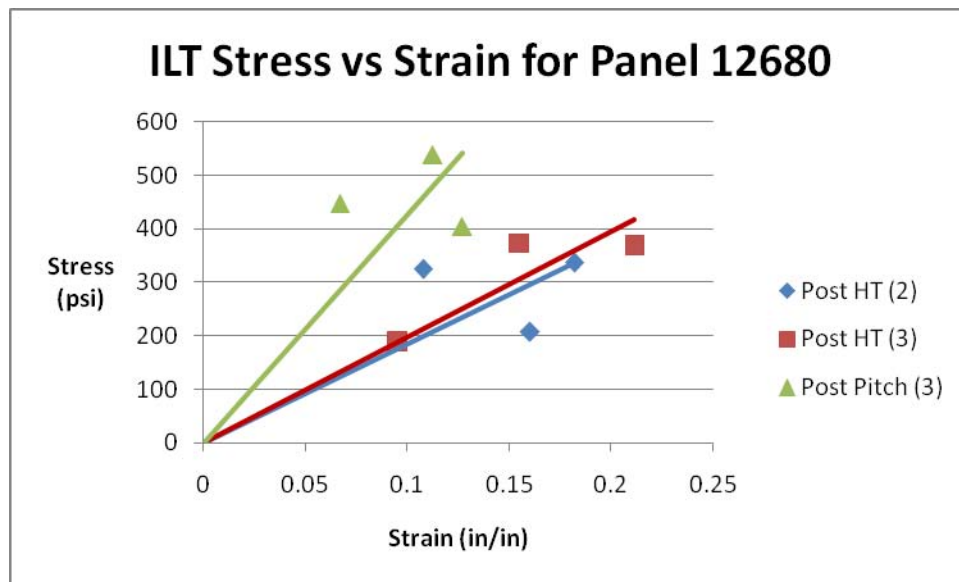
Figure D-1: Stress vs. strain curve for panel 12680.
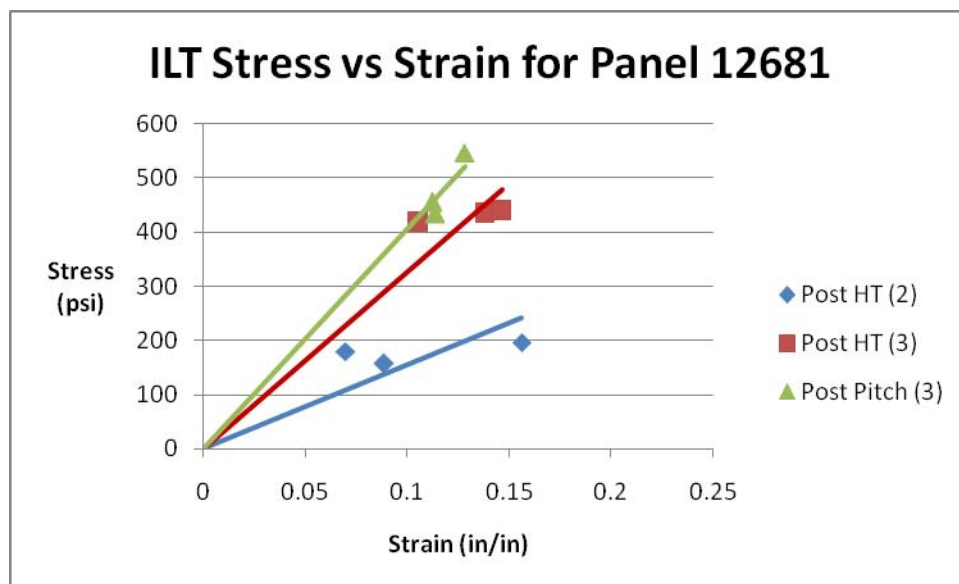
Figure D-2: Stress vs. strain curve for panel 12681.